Stability of the Climate System and Extreme Climates in Model Experiments

Stabilität des Klimasystems und extreme Klimate in Modellexperimenten

---

Vanya Romanova

Ber. Polarforsch. Meeresforsch. 510 (2005)
ISSN 1618 - 3193

Vanya Romanova

Universität Bremen
Fachbereich Geowissenschaften
Klagenfurterstr.
28334 Bremen
Deutschland

Alfred-Wegener-Institut für Polar- und Meeresforschung
Bussestraße 24
27570 Bremerhaven
Deutschland

Die vorliegende Arbeit ist die inhaltlich unveränderte Fassung einer Dissertation, die dem Fachbereich Geowissenschaften der Universität Bremen vorgelegt wurde.
http://elib.suub.uni-bremen.de/publications/dissertations/E-Diss1125_diss.pdf

Contents

Abstract

The present thesis examines the ocean and atmospheric dynamics of present-day climate and Last Glacial Maximum (LGM) through Ocean and Atmosphere General Circulation models. Simulating the glacial climate different LGM reconstructions of sea surface temperatures (SST) and sea-ice margins are used as forcing fields for the models: CLIMAP (1981), a modification of CLIMAP (1981), with additional cooling in the tropics, and reconstructions as produced from Weinelt et al. (1996) and GLAMAP 2000, which show seasonally ice free conditions in the Nordic seas. The stability of the thermohaline circulations (THC) under different reconstructions is investigated together with the corresponding atmospheric dynamics. The stability analysis, by means of freshwater flux hysteresis maps reveals monostability for each glacial background state, which appears to be a robust feature of the glacial ocean. The impact of the changed orography in North America together with the ice-albedo feedback due to the largely expanded Laurentide Ice Sheet and the reduction of the CO_2 concentration are assessed. The results show a strong dependence of the glacial Northern Hemisphere circulation pattern to the changed orography. The Laurentide Ice Sheet forces a deflection of the westerlies, their enhancement and a southward displacement. The oceanic heating contributes only 20-40% to the North Atlantic cooling. Motivated by the extreme climates in the Earth's history, namely the full earth glaciation in the Neoproterozoic era (600-800 million years ago), known as "snowball" Earth, the atmospheric model is forced with extreme boundary and initial conditions. The impact of land albedo, oceanic heat transport, CO_2 concentration, initial temperature conditions on the extreme climates are examined. Changing only one boundary or initial condition, the model produces open ice free tropical oceans. Using a proper combination of the varied forcing parameters a full 'Earth glaciation' results. Oceanic heat transport and orography have only a minor influence on the climate instability.

Zusammenfassung

Die vorliegende Arbeit untersucht Ozean- und Atmosphärendynamik des heutigen Klimas sowie des Letzten Glazialen Maximums (LGM) mit Hilfe von Allgemeinen Zirkulationsmodellen. Verschiedene LGM-Rekonstruktionen der Meeresoberflächentemperaturen und Meereisbedeckungen werden als Antriebsfelder für die Modelle zur glazialen Simulation verwendet: CLIMAP (1981), eine Modifikation von CLIMAP (1981) mit verstärkter Abkühlung in den Tropen, eine Rekonstruktion von Weinelt et al. (1996) sowie GLAMAP 2000. Letztere zeigen jahreszeitlich eisfreie Bedingungen im Europäischen Nordmeer. Die Stabilität der thermohalinen Zirkulation bezüglich der verschiedenen Antriebsfelder wird zusammen mit der dazugehörigen Atmosphärendynamik untersucht. Stabilitätsanalysen (Süßwasser-Hysteresekurven) offenbaren Mono-Stabilität für sämtliche glazialen Hintergrundzustände. Die Einflüsse einer veränderten Orographie in Nordamerika, des Eis-Albedo-Feedbacks aufgrund eines wesentlich ausgedehnten laurentischen Eisschildes sowie der Reduktion der CO_2-Konzentration werden bewertet. Der Ergebnisse zeigen eine starke Abhängigkeit der glazialen, nordhemisphärischen Atmosphärenzirkulation von der veränderten Orographie. Der laurentische Eisschild bewirkt eine Ablenkung, Verstärkung und südwärtige Verlagerung der Westwinde. Der ozeanische Wärmetransport trägt lediglich 20–40% zur nordatlantischen Abkühlung bei.

Motiviert durch ein extremes Klima in der erdgeschichtlichen Vergangenheit, nämlich der Vollvereisung im Neoproterozoikum ("Schneeballerde" vor 600–800 Millionen Jahren), wird das Atmosphärenmodell mit extremen Rand- und Anfangsbedingungen angetrieben. Die Einflüsse von Landalbedo, ozeanischem Wärmetransport, CO_2-Konzentration und Anfangstemperaturen werden untersucht. Nach Veränderung von nur einer Rand- oder Anfangsbedingung produziert das Modell offene, eisfreie tropische Ozeane. Eine geeignete Kombination von Antriebsparametern resultiert in einer vollen Erdvereisung. Ozeanische Wärmetransporte und Orographie üben nur einen kleinen Einfluss auf die Klimainstabilität aus.

CHAPTER I

INTRODUCTION

I.1 Abrupt climate changes

During the last decades the interest in modelling the glacial climate increased, with the goal to better understand the ocean and atmospheric processes that are responsible for large climate changes. Investigating the past alterations of climate states by models could also provide confidence in simulation of future climate changes (e.g. IPCC, 2001).

The paleoclimatic records from Greenland ice cores reveal a number of dramatic climate changes, which occurred in very short time periods. The past climate of the Earth has fluctuated between long glacial and short interglacial states in 'sawtooth' pattern of a 100 ky time period. This is probably associated with the variation of the eccentricity of the Earth's orbit, obliquity and precession of the Earth (Milankovitch, 1941). However, astronomical forcing cannot explain the abrupt climatic events, as registered in the proxies (Fig. I.1). The rapid temperature changes could also be caused by events associated with the change of the Laurentide Ice Sheet, atmospheric and oceanic circulation, and thus count as "internal variability". One idea is to search for mechanisms which amplify the response to insolation forcing or internal variations through positive or negative feedbacks in the interacting ocean-

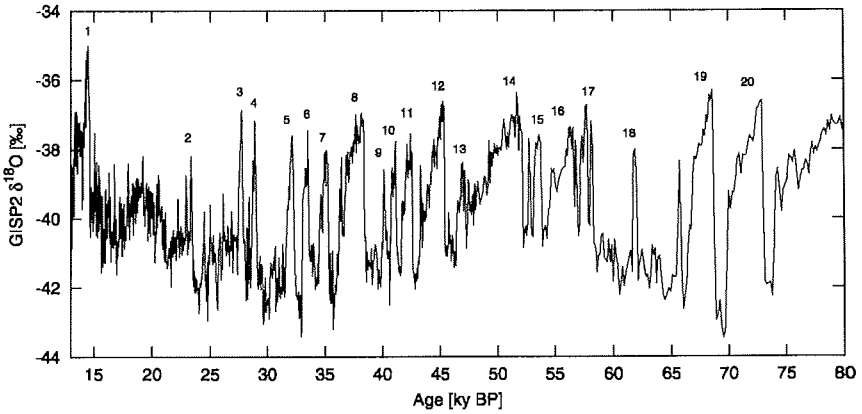

Fig. I.1.: *$\delta^{18}O$ record from Greenland - GISP2 ice core (Grootes and Stuiver, 1997), the numbers denote the 'Dansgaard-Oeschger' interstadial events (Dansgaard et al., 1993; the plot is taken from Schulz, 2002).*

atmosphere-cryosphere system of the Earth. The smooth response of the climate system to gradually varying parameters, e.g. the hydrological cycle, may drastically change into an abrupt one at a given point and the climate system could be set at a completely new state. Such abrupt climate events are the Quaternary transitions from glacial to interglacial conditions or vice versa, the Dansgaard-Oeschger cycles (Dansgaard et al. 1993; Grootes et al. 1993), or the Heinrich events (Heinrich, 1988; Broecker et al., 1992) and are of interest to many modelers (e.g. Sakai and Peltier, 1997; Schulz et al., 2002, Sima et al., 2004).

The abrupt climate changes involve a mechanism by which the treshold is reached, after that qualitative changes in the climate system are triggered. Using models of various complexity, the sensitivity of the climate system is investigated with respect to changes in the Earth's hydrology, continental ice sheets, carbon dioxide, solar insolation and other climatic parameters. Transporting heat over large distances, the ocean plays a pivotal role for the climate on the planet. The intensification or reduction of the strength of the ocean thermohaline circulation (THC) (Alley and Clark, 1999; Mc Manus et al., 2004) triggers switches of the climate system from one state to another.

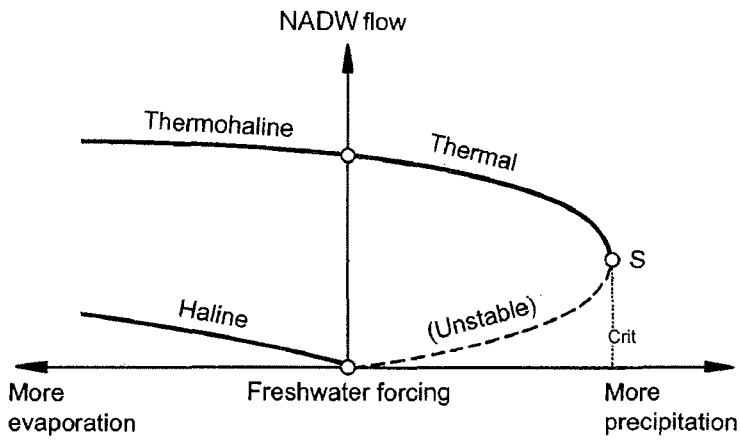

Fig. I.2.: *The three flow regimes of a simple 4 box model of cross-hemispheric thermohaline flow. The dashed line is an unconditionally unstable solution. S is the saddle-node bifurcation point (from Rahmstorf, 1996).*

I.2 Stability of THC and the existence of multiple equilibria

Stommel (1961) was the first to use a simple 2-box model to investigate the existence of multiple equilibria in the ocean circulation. He found two stable equilibria - one mode with cold water sinking at high latitudes and a thermally driven circulation and another mode with sinking of warm saline waters at low-latitudes and salinity driven circulation. The existence of multiple equilibrium states of the Atlantic THC was further examined by Rooth (1982) and Marotzke (1990), who have used box models with extended geometrical configurations to include two hemispheres and cross-equatorial heat transport. One representation of the existence of multiple equilibria and the nonlinear (hysteresis) behavior of the ocean is shown by a simple 4 box model of the thermohaline flow (Fig. I.2). With respect to freshwater forcing, three dynamical regimes are detected: 1) thermohaline regime, in which the temperature and salinity gradients work together to drive the flow; 2) thermal regime, in which the salinity gradients oppose the flow, the state can reach a critical point (point S in Fig. I.2) and the circulation may break down; 3) haline regime, in which the flow is driven only by salinity gradients. In the thermal flow regime the Atlantic THC is a self-sustaining phenomenon and thus prone to instability. If the northward

flow of saline tropical waters decreases, the density of the high latitude waters is reduced and the circulation collapses. Thus the THC can exhibit more than one stable equilibrium.

Bryan (1986) demonstarted the existence of multiple equilibrium states of the THC in a three-dimensional model. He pointed out the importance of the high latitude convection, which increases the sensitivity of the circulation. Manabe and Stouffer (1988) found two stable equilibrium states in a coupled ocean-atmosphere model: one with active THC and the other with weak reverse THC without any deep water formation in the northern North Atlantic Ocean. The transition of the Atlantic conveyor with respect to freshwater perturbations was investigated by many scientists (e.g. Stocker and Wright, 1991; Manabe and Stouffer, 1995; Lohmann et al., 1996; Rahmstorf, 1996; Ganopolski et al., 2001; Schmittner et al., 2002; Lohmann, 2003). A hysteresis like response of the NADW, as predicted by conceptual models (for example the one shown above) is found in both present-day and glacial simulations (e.g. Stocker and Wright, 1991; Rahmstorf, 1996; Ganopolski et al., 2001, Schmittner et al, 2002). Rahmstorf (1996) stated that the location of the equilibrium state on the hysteresis curve depends on the freshwater balance of the conveyor belt, South Atlantic wind driven subtropical gyre and net precipitation over the Atlantic catchment area. Ganopolski et al. (2001) constructed hysteresis maps for the present-day and glacial Atlantic and reported distinct differences in the shape of the hysteresis curves. The present-day hysteresis is wide and only a large freshwater perturbation is able to shut down the conveyor. On contrast to this, the hysteresis curve for the glacial simulation is much narrower. Moreover, Ganopolski et al. (2002) suggested that the present-day equilibrium is located in the 'thermal' flow regime, where multiple equilibria exist. The equilibrium glacial climate is situated on the 'thermohaline' branch of the hysteresis map, where only one stable solution exists (discussed in Chapter 1).

Different glacial climate equilibrium states, obtained through different SST and sea-ice forcings, could possess their own background hydrological cycle. Lohmann and Lorenz (2000) suggested that during glacial times the hydrology is associated

with increased water vapor transport from the Atlantic to the Pacific Oceans and enhanced net evaporation over the Atlantic catchment area. Chapter 2 focusses on the stability of the glacial THC and its dependence on the hydrological cycle.

I.3 LGM reconstructions of SST and sea-ice margins

The CLIMAP (1981) SST and sea-ice extent reconstruction for the Last Glacial Maximum, based on foraminiferal assemblages, is taken as a boundary condition to simulate glacial conditions. This reconstruction uses samples for a time interval between 24 and 14 ^{14}C ka B.P., in which a climatic stability is assumed (Mix et al., 2001). It is characterised by far to the south reaching sea-ice margins in the Northern Hemisphere and general cooling of the surface waters, except for some areas in the tropical Pacific Ocean, where sea temperatures are higher than present-day values. The validity of CLIMAP reconstruction is strongly discussed, especially in the tropical areas (e.g. Farrera et al., 1999; Mix et al., 1999; Bard, 1999) indicating too warm SSTs. An additional reduction of CLIMAP SSTs in the tropics (Lohmann and Lorenz, 2000) can provide for the consistency with more recent paleo-data (Farrera et al., 1999) and snowlines (Lorenz and Lohmann, 2004). To reduce the temperature discrepancies between marine and terrestrial proxy data for the LGM, an additional cooling of 3°C can be applied in the tropics.

Another LGM reconstruction is given by Weinelt et al. (1996). It represents a reconstruction of the SSTs for the Nordic Seas and is combined with the CLIMAP data set (Schäfer-Neth and Paul, 2001). This reconstruction assumes LGM to be a period of climatic stability and characterized by a minimum meltwater flux for the time interval between 18 and 15 ^{14}C ka B.P. The data set shows seasonally ice-free conditions in most parts of the Nordic Seas along with higher summer SST than in the CLIMAP (1981) reconstruction.

The new LGM reconstruction, GLAMAP 2000 (German Glacial Atlantic Ocean

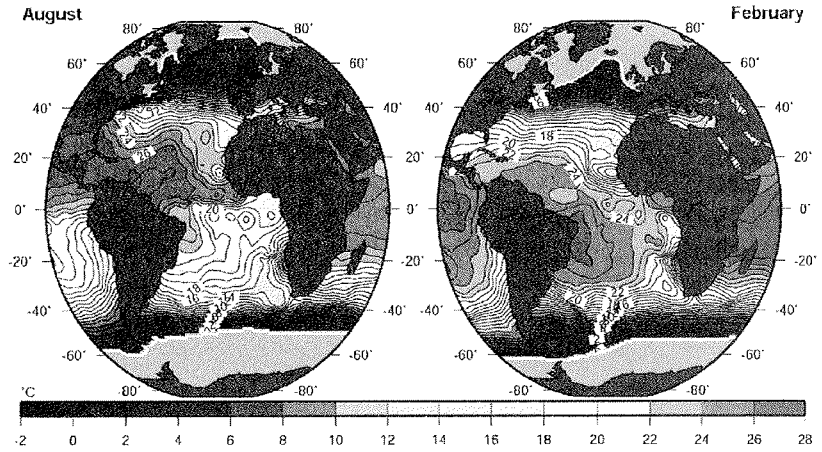

Fig. I.3.: *August and February sea surface temperatures and the sea-ice cover in the GLAMAP reconstruction (from Schäfer-Neth and Paul, 2003).*

Mapping Project), provides SSTs and sea-ice margins for another set of boundary condition. It comprises the North, Central and South Atlantic Ocean using joint definitions of the LGM time slice as the overlap of the Last Isotope Maximum (18-15 ^{14}C ka B.P.) and the EPILOG Level-1 (19-16 ^{14}C ka B.P.) time span, sedimentation rates and resolution (Paul and Schäfer-Neth, 2003). A detailed description of the choice of the LGM slice and age control is given in Sarnthein et al. (2003). It uses 275 sediment cores and the SST estimates are based on a new set of more than 1000 reference samples of planktonic foraminifera, radiolarians and diatoms, and on improved transfer-function techniques. In this reconstruction, the winter sea ice is similar to the CLIMAP summer sea ice margin and the Nordic Seas are ice-free during summer months (Fig. I.3). The average surface temperatures are significantly higher in the northern North Atlantic than in the CLIMAP reconstruction.

The described LGM reconstruction are used to force an ocean general circulation model, different background states are obtained. The CLIMAP (1981) reconstruction with applied additional tropical cooling at the surface boundary of an ocean model, provoke weakening of the overturning circulation. The GLAMAP 2000 and Weinelt et al. (1996) SST reconstructions, taken as boundary conditions to an ocean general circulation model (OGCM), cause an even intensified overturning strength

compared to the present-day simulation, in which the warm temperatures in the Nordic Seas are maintained. To examine the atmospheric response to different glacial oceanic background conditions (Chapter 4), we use the corresponding heat transports, as obtained from an OGCM, to force an atmospheric general circulation model (AGCM) and investigate the circulation patterns.

I.4 Glacial atmospheric circulation

Several scientific groups have been involved in modeling the glacial atmospheric circulation (e.g., Kutzbach and Guetter, 1986; Manabe and Broccoli, 1985; Rind and Peteet, 1985; Cook and Held, 1988; Marsiat and Valdes, 1999; Broccoli, 2000; Lohmann and Lorenz 2000; Shin et al., 2003; Chiang and Biasutti, 2003; Kim, 2004) using different model approaches - atmosphere only models and AGCMs coupled to a mixed layer ocean model or to an ocean general circulation model. The highly elevated Laurentide Ice Sheet (Peltier, 1996) is shown to have a significant effect on the atmospheric circulation first of all due to the blocking effect of the midlatitude circulation and, secondly, due to the high ice albedo leading to a positive ice-albedo feedback. The GCM experiments indicate a split of the jet stream (Fig. I.4), with one branch following around the northern edge of the Ice Sheet and another, stronger one, flowing around the southern edge of the ice front. Splitting of the jet was caused by ice sheet orography and midtropospheric cooling, and the ice sheet orography seems to dominate. However, Crowley and North (1991), proposed a reexamination of the jet stream split using an ice sheet of lower elevation.

Together with the changed Northern Hemispheric orography during the last glacial maximum, some models suggest that the oceanic heat transport was drastically reduced (e.g., Winguth et al, 1999), due to changed rates of the overturning circulation in the North Atlantic Ocean. This, also, contributes to the cooling of the midlatitudes in the Northern Hemisphere. Therefore, we investigate the dominance of each factor in each Northern Hemispherical latitudinal belt - the glacial orography or

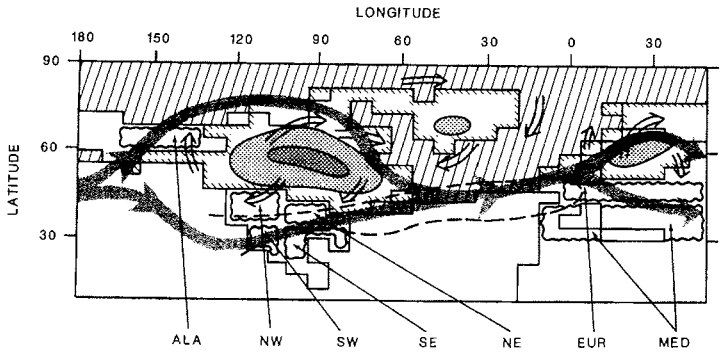

Fig. I.4.: *NCAR climate model simulation in Northern midlatitudes at 18,000 B.P. (from Kutzbach and Wright, 1985; Crowley and North, 1991). Stippled arrows show the winds aloft and double-shafted arrows show the winds at the surface.*

the oceanic heat transport. Moreover, in Chapter 4 the isolated effect of the CO_2 reduction is presented.

I.5 Extreme events in the Earth's history: 'snowball' Earth scenarios

Recent geological studies of the Neoproterozoic era (around 600-800 million years ago), have suggested that the Earth has experienced global glaciation events, termed 'snowball' Earth (Hoffman and Schrag 2002). Paleomagnetic studies of equatorial carbonate deposits, the prolonged drop in biological activity and the formation of rich of iron rocks, which are formed in the absence of oxygen, indicate widespread glaciation (Kirschvink, 1992; Hoffman et al., 1998; Kirschvink et al., 2000; Hoffman and Schrag, 2002). Based on the magnetic orientation of mineral grains in glacial deposits, it is hypothesized that the continents were clustered together near the equator during that time. The Neoproterozoic era is also characterized by a reduced solar insolation of 6%, due to the Faint Young Sun (Sagan and Chyba, 1997). Still, the question exists, whether the Earth was completely ice covered ('hard snowball'

Earth) or some ocean areas remained ice free ('slushball' Earth), and what was the mechanism that forced the climate system to escape from the glaciated state (Hyde et al., 2000).

The geological findings and the enigmas connected with this time period provoke climate modelers to test their models under extreme boundary conditions, to produce a global earth glaciation (e.g. Crowley and Baum, 1993; Jenkins and Frakes, 1998; Hyde et al., 2000; Crowley et al., 2001; Poulsen et al., 2001; Donnadieu et al., 2002; Lewis et al., 2003; Donnadieu et al., 2004). Using different types of models, the authors investigate the role of changed solar insolation, Earth's rotation rate and high obliquity, the contribution of the changed paleogeography and continental geometries, and the sensitivity of the earth climate system to CO_2 levels.

Such extreme climates in the Earth's history are a motivation also to investigate the possibility of a 'snowball' Earth at present-day solar insolation and continental distribution and to examine the existence of multiple steady states of the atmosphere as it has been shown by Budyko (1969) and Sellers (1969). Therefore, in Chapter 5, it is searched for an appropriate combination of the boundary and initial conditions for a 'snowball' Earth simulation and a thorough analysis is performed how the climate responses to those parameters that have been shown to be important for the climate system.

I.6 Objectives of the study

This subsection outlines the major research objectives on how the present-day and the glacial ocean and atmosphere systems function and how the climate responds to a large set of boundary and initial conditions, which to a certain extent could represent human and natural forcings. The specific topics addressed include:

- To test the stability of the present-day and glacial thermohaline circulation with respect to transient and pulse meltwater numerical experiments.
- To elucidate the relation between the hydrological balance and stability characteristics of the conveyor belt.
- To qualify the atmospheric response to the glacial thermohaline circulation.
- To investigate the role of orography and oceanic heat transport for the North Atlantic cooling.
- To study extreme forcings and extreme climates. analysis of the atmosphere.

CHAPTER II

THE GLACIAL THERMOHALINE CIRCULATION: STABLE OR UNSTABLE?

Matthias Prange[1,2], Vanya Romanova[1], Gerrit Lohmann[1,2]

[1]Geoscience Department, University of Bremen, Klagenfurterstr., 28334 Bremen, Germany

[2]DFG Research Center Ocean Margins (RCOM), University of Bremen, 28334 Bremen, Germany

Abstract[1]

The stability of the glacial thermohaline circulation (THC) with respect to North Atlantic freshwater input is examined using a global ocean general circulation model. It is found that the quasi-equilibrium hysteresis behaviour is much less pronounced under glacial conditions than under present-day conditions, and the existence of multiple equilibria requires an anomalous freshwater inflow. The results may help to assess the effect of iceberg invasions and meltwater events, suggesting that the THC is prone to instability during a deglaciation phase when the Atlantic meridional overturning is weakened. Under full glacial conditions, however, the THC is mono-stable and even extreme freshwater pulses are unable to exert a persistent effect on the conveyor.

[1]Received: 16 April 2002/Accepted: 3 July 2002/Published: 12 November 2002 in Geophysical Research Letters, 21, 2028 doi:/10.1029/2002GL0153337

II.1 Introduction

The waxing and waning of continent-sized ice sheets was an important source for variability of the North Atlantic freshwater budget during the last glacial period (~100–10 kyr ago). Massive surges and melting of icebergs (e.g., Heinrich, 1988; Broecker et al., 1992), so-called Heinrich events, caused abrupt changes in the freshwater budget (e.g., Keigwin and Lehman, 1994; Bard et al., 2000). There is clear geological evidence of a strong interconnection between ice-rafting events, fluctuations in the thermohaline circulation (THC), and climatic changes in the Atlantic realm (e.g., Chapman and Shackleton, 1999; Broecker and Hemming, 2001; Clark et al., 2002). Understanding the stability properties of the THC during glacial times is therefore of utmost importance for a proper interpretation of the geological record. Here, we study the sensitivity of the glacial THC with respect to variable North Atlantic freshwater input in a global ocean general circulation model (GCM), examining both the quasi-equilibrium hysteresis behaviour and the response to sudden freshwater pulses.

II.2 Model design and forcing

The ocean model is based on the Hamburg large-scale geostrophic ocean model LSG (Maier-Reimer et al., 1993). The resolution is 3.5° with 11 levels. A third-order QUICK scheme (Leonard, 1979; Schäfer-Neth and Paul, 2001) for the advection of temperature and salinity has been implemented as described in Prange et al. (2002). Depth-dependent horizontal and vertical diffusivities are employed ranging from 10^7 cm^2 s^{-1} at the surface to 5x10^6 cm^2 s^{-1} at the bottom, and from 0.6 cm^2 s^{-1} to 1.3 cm^2 s^{-1}, respectively.

The model is driven by monthly fields of wind stress, surface air temperature and freshwater flux provided by a Last Glacial Maximum (LGM) simulation of the atmo-

spheric GCM ECHAM3/T42. Forcing of the atmosphere comprises orbital changes, reduced concentration of CO_2 (200 ppm), and CLIMAP (1981) sea ice and surface temperatures with an additional cooling in the tropics (30°S–30°N) of 3 K. For a detailed description of the model run we refer to Lohmann and Lorenz (2000). In order to close the hydrological cycle, a runoff scheme transports freshwater from the continents to the ocean. For the heat flux Q into the ocean we apply a boundary condition of the form $Q = (\lambda_1 - \lambda_2 \nabla^2)(T_a - T_s)$, where T_a and T_s denote air and sea surface temperatures, respectively. This thermal boundary condition allows an adjustment of surface temperatures to changes in the ocean circulation, based on an atmospheric energy balance model with diffusive lateral heat transports (Rahmstorf and Willebrand, 1995). For λ_1 and λ_2 we choose 15 W m^{-2} K^{-1} and $2 \cdot 10^{12}$ W K^{-1}, respectively. In all model components the ice age paleotopography of Peltier (1994) is applied and a global sea level drop of 120 m is taken into account.

II.3 Glacial THC and hydrographic fields

Starting from a present-day hydrography with a salinity anomaly of +1 psu imposed globally, the ocean model is integrated under glacial forcing for 5500 years to obtain an equilibrium circulation (Fig. II.1a). The simulated glacial Atlantic THC is weaker than the modern one, consistent with proxy data (e.g., Boyle, 1995; Rutberg et al., 2000)and previous modelling studies (e.g., Ganopolski et al., 1998; Weaver et al., 1998). The total volume flux of sinking water masses in the glacial North Atlantic amounts to 12 Sv, while 7 Sv are exported to the Southern Ocean. Compared to a present-day simulation with the same model (Prange et al., 2002), this corresponds to a ~20% decrease of NADW flux into the circumpolar deep water. Due to an expanded sea ice cover in the North Atlantic, convection sites are shifted southward compared to the present-day circulation. Hence, the sinking branch of the glacial Atlantic meridional overturning circulation is located between 40°N and 60°N, and contributions from the Nordic Seas to North Atlantic Deep Water (NADW) are negligible (Fig. II.1a).

In low latitudes, sea surface temperatures (Fig. II.1c) are about 4 K below modern values. Mean temperatures in the core of NADW are shown in Fig. II.1e. Salinities at that depth are relatively high (Fig. II.1d), exceeding mean surface salinities (Fig. II.1b) in mid and high latitudes. Similarly high deep water salinities were found in the LGM simulation of an Earth system model of intermediate complexity (Ganopolski et al., 1998).

II.4 Hysteresis behaviour

Applying a slowly varying surface freshwater flux anomaly uniformly between 20°N and 50°N to the Atlantic Ocean, we analyse the quasi-equilibrium hysteresis behaviour of the glacial THC. The stability diagram is shown in Fig. II.2. For comparison, the hysteresis loop of the model with present-day forcing (Prange et al., 2002) is displayed in the same figure. The present-day THC exhibits a pronounced hysteresis behaviour around the region of zero perturbation. For anomalous freshwater fluxes between -0.1 Sv and $+0.1$ Sv we identify two equilibrium modes of operation. By way of contrast, the stability diagram of the glacial THC reveals that multiple equilibria exist only in a narrow range in the area of positive anomalous freshwater input.

II.5 Freshwater pulse experiments

In order to examine the destabilizing impact of abrupt meltwater perturbations in the glacial North Atlantic, we perform a series of freshwater pulse experiments (Fig. II.3). The pulses have a duration of 50 years and are uniformly applied to the North Atlantic between 20°N and 50°N. A first set of experiments deals with the stability of the glacial equilibrium circulation at point A in Fig. II.2. Freshwater fluxes of 0.2 Sv and 0.5 Sv cause a temporary weakening of the THC, while a

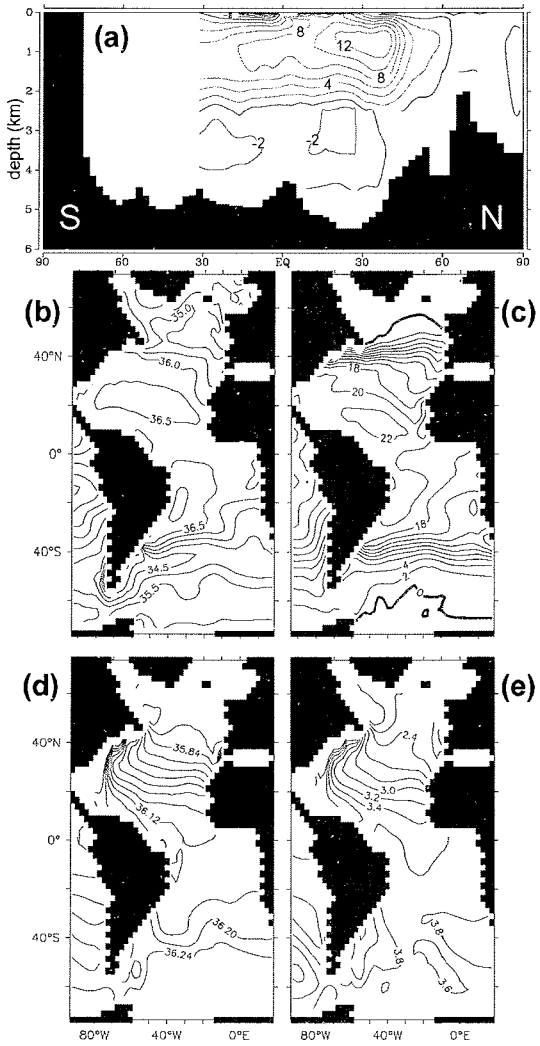

Fig.II.1: *Glacial Atlantic Ocean in equilibrium: (a) meridional overturning streamfunction (Sv); (b) surface salinity; (c) surface temperature (°C); (d) salinity at 2000 m depth; (e) temperature at 2000 m depth (°C). 40 yr means are shown.*

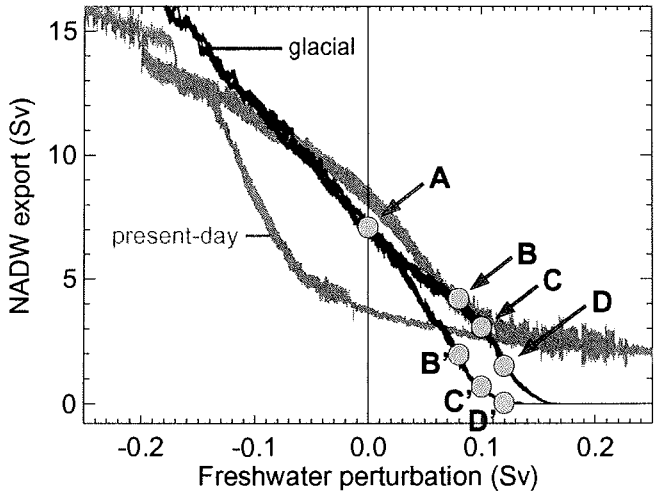

Fig.II.2: *Maximum meridional Atlantic overturning streamfunction at 30° S (i.e., NADW export across 30° S) against North Atlantic surface freshwater flux anomaly for the last glacial and the present. Hysteresis loops are obtained as follows: Integration starts at the upper branch with zero freshwater perturbation. The freshwater input is then slowly increased until* 0.3 *Sv. The integration proceeds on the lower branch with freshwater input decreasing until* -0.3 *Sv. Then the freshwater input increases again to close the loop. Due to the slowly-varying nature of the surface forcing* ($5{\cdot}10^{-5}$ *Sv* yr^{-1}) *the model is in quasi-equilibrium during the integration (Rahmstorf, 1995). Curves are smoothed by a one-year boxcar-average. The stability of the states A, B, C, and D is examined in freshwater pulse experiments (see Fig. II.3).*

perturbation of 1 Sv leads to zero overturning (Fig. II.3a). However, the THC recovers spontaneously after the perturbation, regaining its initial strength after about 1000 years. Due to the THC's mono-stability, freshwater pulses are unable to exert a persistent effect on the glacial conveyor, regardless of their magnitudes.

Upper-ocean flow field and temperature distribution respond immediately to freshwater perturbations in the Atlantic Ocean (Fig. II.4). After 50 years of 1 Sv freshwater input, when the overturning is zero (see Fig. II.3a), a modified circulation is directly linked to changes in oceanic heat transports and hence temperature distribution. In the upper ocean, the breakdown of the conveyor is reflected in an overall anomalous southward flow (Fig. II.4b), the main effect of which is a general warming in the South Atlantic and a cooling in the North Atlantic (Fig. II.4c), well-known as the "seesaw-effect" (e.g., Stocker, 1998; Clark et al., 2002). In addition to the north-south contrast, pronounced zonal differences in temperature change arise. For instance, an anomalous southward flow in the northeastern Atlantic (Fig. II.4b) causes particularly strong cooling off Southern Europe (Fig. II.4c). Similar North Atlantic temperature patterns, characterized by extreme coolings off France and Portugal, can be inferred from marine proxy data during Heinrich events (Bard et al., 2000; Broecker and Hemming, 2001; Clark et al., 2002). In a second set of pulse experiments, we investigate the stability of equilibrium states that reside within the hysteresis loop (states B, C, and D in Fig. II.2). A freshwater pulse of 1 Sv applied to state B causes the conveyor to collapse (Fig. II.3b). After 250 years some convection sites become reactivated, while others remain shut down (not shown) – the overturning restarts, but settles into a new equilibrium with low NADW formation. This equilibrium state corresponds to point B' on the lower branch of the hysteresis loop in Fig. II.2. Applying a perturbation of 1 Sv to state C, the THC behaves in a similar way and ends up in point C'. State D is much more vulnerable: a smooth transition to D' can be induced by a weak perturbation of 0.05 Sv, while an abrupt change is triggered by a 0.2 Sv-pulse. The experiments reveal that the THC becomes increasingly unstable with reduced initial overturning strength.

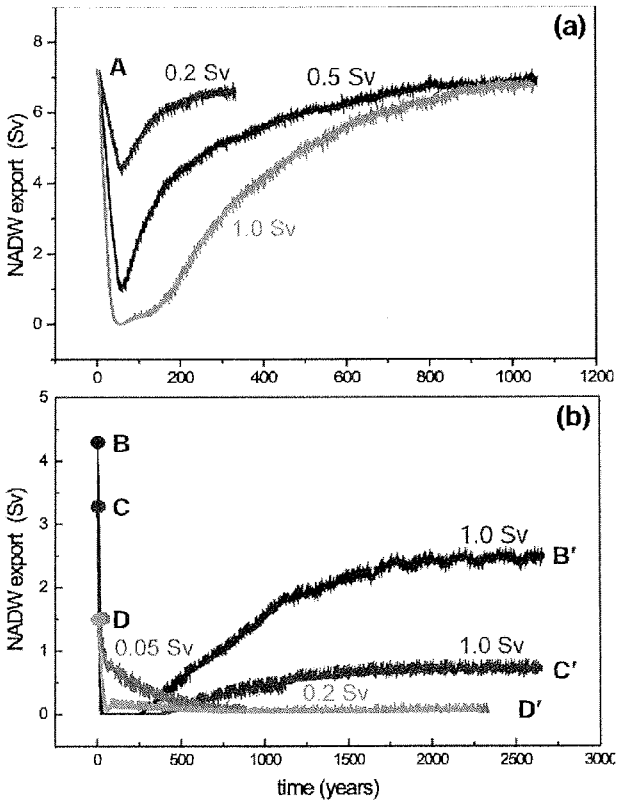

Fig.II.3: *Temporal changes of the maximum Atlantic overturning streamfunction at 30° S (i.e., NADW export across 30° S) in consequence of 50 years-freshwater perturbations with different magnitudes: (a) perturbations of the glacial equilibrium at point A in Fig. II.2; (b) perturbations of the equilibrium states B, C, and D in Fig. II.2.*

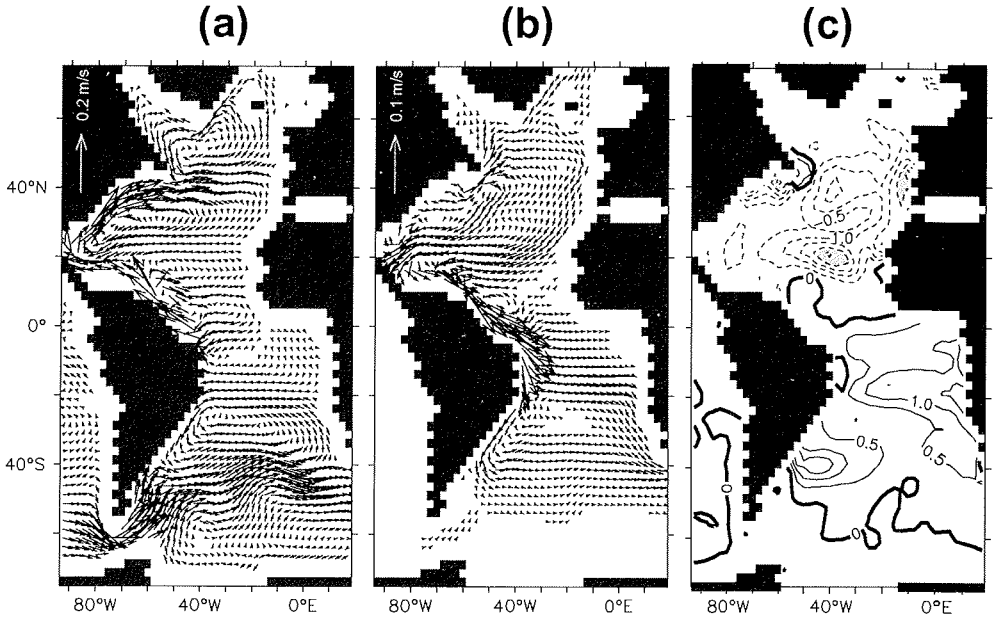

Fig.II.4: *Response of the upper ocean to a 1 Sv-freshwater perturbation after 50 years of anomalous freshwater input when the overturning is zero: (a) unperturbed mean flow field of the glacial equilibrium (point A in Fig. II.2) averaged over the top 150 m; (b) annual mean velocity anomalies induced by the perturbation (averaged over the top 150 m); (c) annual mean sea surface temperature anomalies (K) induced by the perturbation; areas with temperature differences below −2 K are shaded.*

II.6 Discussion and conclusions

Utilizing an oceanic GCM, we examined the stability of the glacial THC with respect to North Atlantic freshwater forcing. We found that the quasi-equilibrium hysteresis behaviour is much less pronounced than under present-day conditions, and multiple equilibria exist only when an anomalous freshwater input is applied. These results are consistent with a recent study of Ganopolski and Rahmstorf (2001), in spite of very different modelling approaches, i.e. one-way coupling of GCMs, as applied here, versus interactive coupling using a zonally averaged ocean model. In a model of intermediate complexity which employs a three-dimensional ocean GCM, a computationally inexpensive energy-moisture balance model of the atmosphere, and an ice sheet component, the glacial THC possesses different stability properties (Schmittner et al., 2002). In the absence of anomalous freshwater fluxes, the only stable glacial mode in that model is characterized by a conveyor shutdown, and the regime of bi-stability is shifted to the range of negative freshwater anomalies.

How can the stability behaviour be understood? Rahmstorf (1996) pointed out that the stability properties of the Atlantic THC are linked to its freshwater budget. In our model set-up, the atmospheric moisture export out of the Atlantic catchment area ($> 30°$S, Arctic Ocean included) is enhanced under glacial conditions by 0.08 Sv relative to the present. An important process that contributes to the changed freshwater budget of the glacial Atlantic is a decrease of water vapour transport from the Pacific Ocean into the Arctic and into the northern Atlantic via Canada (Lohmann and Lorenz, 2000). The lack of a low-saline Bering Strait throughflow, owing to a lowered sea level, lead to further reductions in the freshwater supply to the polar seas and hence to the convective regions in the glacial North Atlantic. Taking a reference salinity of 35 psu, this freshwater supply amounts to 0.05 Sv in our present-day simulation, which is in good agreement with observations (Aagaard and Carmack, 1989). The reduced freshwater input to the glacial North Atlantic results in relatively high salinities of deep water masses formed there during winter. High salinities in glacial NADW relative to the upper layers (Figs. II.1b, II.1d) indicate

a "thermohaline flow regime" of the THC (Rahmstorf, 1996). In this regime, freshwater is carried northward by the conveyor's upper limb into the regions of deep water formation. Consequently, a circulation with reduced overturning is unstable, since net evaporation and/or wind-driven oceanic salt transports would inevitably enhance North Atlantic surface salinities, driving NADW formation and the THC. By way of contrast, the present-day conveyor is driven by heat loss with freshwater forcing braking the overturning ("thermal flow regime"). As a result, multiple equilibria exist (Stommel, 1961; Rahmstorf, 1996).

The results of our study may help to assess the effect of massive iceberg invasions and meltwater events documented in sediment records from the North Atlantic, suggesting the following conclusions: During a deglaciation phase, anomalous freshwater inflow may shift the THC into the regime of bi-stability (points B, C, D in Fig. II.2) where the conveyor is prone to instability and mode transitions. A mode transition results in a persistent slow-down of the THC, and the overturning does not recover until substantial changes in the North Atlantic freshwater budget occur. In the mono-stable regime of "full glacial conditions" (point A), even extreme freshwater pulses are unable to exert a persistent effect on the conveyor. As soon as the freshwater influx comes to an end the THC starts to recover spontaneously.

The present study highlights the importance of the hydrological cycle for the stability properties of the THC. A correct representation of atmospheric moisture transports is crucial. A logical next step would be the inclusion of other climate components which may be important for the hydrological cycle, in particular land ice processes and the motion of sea ice.

Acknowledgements *We are grateful to A. Paul and C. Schäfer-Neth for stimulating discussions. Many useful comments by A. Ganopolski and an anonymous reviewer helped to improve the manuscript. We thank K. Herterich for his support. The study was funded by grants from DEKLIM and KIHZ (BMBF).*

CHAPTER III

STABILITY OF THE GLACIAL THERMOHALINE CIRCULATION AND ITS DEPENDENCE ON THE BACKGROUND HYDROLOGICAL CYCLE

Vanya Romanova[1], Matthias Prange[1,2], Gerrit Lohmann[1,2]

[1]Geoscience Department, University of Bremen, Klagenfurterstr., 28334 Bremen, Germany
[2]DFG Research Center Ocean Margins (RCOM), University of Bremen, 28334 Bremen, Germany

---

Abstract[1]

Different reconstructions of glacial sea-surface temperatures (SST) are used to force a hybrid coupled atmosphere-ocean model. The resulting glacial states differ in global salinity and temperature distributions, and consequently in the strength of the thermohaline circulation. Stability analysis of

[1]Received: 10 April 2003/Accepted: 29 December 2003/Published online: 24 March 2004 in Climate Dynamics (2004) 22, 527-538

the Atlantic ocean circulation, by means of freshwater-flux hysteresis maps, reveals mono-stability for each glacial background state, which appears to be a robust feature of the glacial ocean. We show that this behaviour is directly linked to the hydrological cycle. A monotonic relation between the freshwater input necessary for reaching the off-mode and the hydrological budget in the Atlantic catchment area, accounts for the sensitivity of the ocean's circulation. The most sensitive part of the hydrological balance appears to be in the tropical and subtropical regions suggesting that the 'Achilles heel' of the global conveyor belt circulation is not restricted to the northern North Atlantic where convection occurs.

III.1 Introduction

Transporting heat over large distances, the thermohaline circulation (THC) plays a pivotal role in the climate system. Geological records from the Last Glaciation indicate that greater abundances of ice-rafted debris in the North Atlantic (Heinrich Events) were associated with global-scale climatic changes (Broecker and Hemming, 2001), probably resulting from a THC slowdown (Boyle and Keigwin, 1987; Clark et al., 2002). The concept of THC fluctuations with global impact has motivated a large number of researchers to study the sensitivity of the circulation to North Atlantic meltwater inflow, utilizing numerical climate models (e.g., Bryan, 1986; Maier-Reimer and Mikolajewicz, 1989; Stocker and Wright, 1991; Mikolajewicz and Maier-Reimer, 1994; Manabe and Stouffer, 1995; Rahmstorf, 1995; Lohmann et al., 1996a; Rahmstorf, 1996; Fanning and Weaver, 1997; Schiller et al., 1997; Rind et al., 2001). In many of these models, the THC possesses multiple equilibria, and transitions from one mode of operation to another can be triggered by a sufficiently strong freshwater perturbation. Consequently, a short-term meltwater influx can have a persistent effect on the THC by inducing a transition from a mode with intense North Atlantic Deep Water (NADW) formation to a mode with weak or ceased convective activity.

In model experiments, meltwater perturbations were usually applied to present-day

states of the THC. The suitability of such experiments for glacial conditions has been challenged by results from box models, suggesting that the weaker overturning circulation of the ice age was more vulnerable than the modern one (Lohmann et al., 1996b; Prange et al., 1997). A recent study by Ganopolski and Rahmstorf (2001) provides a new perspective on the stability properties of glacial climate. Utilizing an earth system model of intermediate complexity, the authors suggested that the glacial THC possesses only one equilibrium. This mono-stable behaviour of the THC may explain the conveyor's recovery after a meltwater-induced shutdown associated with a Heinrich Event. The results of Ganopolski and Rahmstorf (2001) were corroborated by Prange et al. (2002), who demonstrated the mono-stability of the THC in a hybrid-coupled model with a three-dimensional ocean under glacial conditions. In their modelling approach, the authors used CLIMAP (1981) surface temperatures with an additional cooling in the tropics to force the atmospheric circulation (Lohmann and Lorenz, 2000) as background climate state. This reconstruction is characterized by an extensive North Atlantic sea ice cover: the Nordic Seas are ice-covered the whole year round, and the winter ice cover advances southward to almost 45°N. More recent reconstructions, however, provide evidence for a substantially reduced ice coverage with vast ice-free areas in the Nordic Seas during summer (Weinelt et al., 1996; Paul and Schäfer-Neth, 2003).

Extending the work of Prange et al. (2002), this study applies the surface temperature reconstructions of Weinelt et al. (1996) and GLAMAP 2000 (Paul and Schäfer-Neth, 2003) in a hybrid-coupled climate model. We shall examine the effects of different glacial sea surface temperature fields on the hydrologic cycle, salinity distributions and the oceanic circulation. In particular, we focus on the stability of the glacial THC and its dependence on the background hydrological cycle. The paper is organized as follows: In Sect. 2, the model and experimental set-up is described. The results are presented in the third section and they are discussed in Sect. 4. Conclusions are drawn in the fifth section.

III.2 Model Description and Experimental Set-up

III.2.1 Atmospheric Model

We use the three-dimensional atmospheric general circulation model (AGCM) ECHAM3/T42 (Roeckner et al., 1992). It is based on the primitive equations and includes radiation and hydrological cycle. It has 19 levels and a resolution of 128 x 64 points on a Gaussian grid. The forcing is given by insolation, following the astronomical theory of Milankovic and CO_2 concentration. The orbital parameters for 21,000 y B.P. are taken to calculate the insolation pattern, which remains unchanged during the experiments. The CO_2 concentration is fixed to 200 ppm for the glacial simulations and to 345 ppm for the control run (Lohmann and Lorenz, 2000). The bottom boundary conditions are given by the Earth's orography, including ice sheets (Peltier, 1994), albedo, sea ice cover and sea surface temperatures. The last two parameters are taken from three different reconstruction sets. As yet, the model has no dynamic ice sheets. The model output comprises the monthly averaged surface freshwater fluxes, surface air temperatures and wind stresses. The model is run for 15 years of model integration and averaged years are constructed from the last 10 years of the simulations.

III.2.2 Oceanic Model

The ocean model is based on the LSG ocean circulation model. It integrates the primitive equations, including all terms except the nonlinear advection of momentum, using a time step of 1 month (Maier-Reimer et al., 1993). It has a horizontal resolution of 3.5°x3.5° and 11 vertical levels on a semi-staggered grid type 'E'. Parametrization of the density is given by the UNESCO formula. A new numerical scheme for the advection of temperature and salinity has been implemented (Schäfer-Neth and Paul, 2001; Prange et al., 2003). It uses a predictor-corrector method,

as the predictor step is centered differences and the corrector step is a third-order QUICK scheme (Leonard, 1979). The advantage of this scheme is the reduced numerical diffusion in comparison with the previously used upstream scheme. The vertical diffusivity is prescribed ranging from 0.6 cm^2s^{-1} at the surface up to 1.3 cm^2s^{-1} in the abyssal ocean. The sea level is reduced by 120 m, accounting for the water stored in the land ice, thus the Bering Strait is closed.

III.2.3 Hybrid coupling

The monthly averaged surface freshwater fluxes, surface air temperatures and wind stresses calculated with the AGCM are applied to the upper boundary conditions of the OGCM . The coupling is made by including a run-off scheme. The boundary heat flux Q at the ocean surface is formulated as suggested by Rahmstorf and Willebrand (1995):

$$Q = (\lambda_1 - \lambda_2 \nabla^2)(T_a - T_s)$$

allowing for scale-selective damping of temperature anomalies. Here, T_a is the prescribed air temperature, and T_s denotes the ocean surface temperature (λ_1 and λ_2 are chosen to be 15 $Wm^{-2}K^{-1}$ and $2x10^{12}WK^{-1}$). In the model, sea surface salinity (SSS) can freely evolve. When the grid cells are covered by sea-ice the surface temperatures are set to the freezing point.

An extensive parameter study of this hybrid-coupled model approach has been carried out by Prange et al. (2003). It has been shown that this model approach is able to simulate variable sea surface temperatures and salinities and it has been applied to deglaciation scenarios (Knorr and Lohmann, 2003; Rühlemann et al., 2004; Prange et al., 2004). The model set-up neglects feedbacks connected with atmospheric dynamics, vegetation and cryosphere.

III.2.4 Experimental Set-up

The control run is forced with present-day SSTs used in AMIP (Atmospheric Model Intercomparison Project) and is discussed in Prange et al. (2003). For the glacial we use three different SST and sea-ice reconstruction data sets. Experiment C, the reference experiment, employs CLIMAP (1981) SST and sea ice. This reconstruction uses samples for a time interval between 24 and 14 ^{14}C ka B.P., in which a climatic stability is assumed (Mix et al., 2001). An additional tropical cooling of 3°C is applied in the tropics. It has been shown that this provides for a consistency with terrestrial and marine proxy data during the Last Glacial Maximum (LGM) (Farrera et al., 1999; Lohmann and Lorenz, 2000). The second experiment W is forced with SST reconstructions of Weinelt et al. (1996) for the Nordic Seas, combined with the CLIMAP data set (Schäfer-Neth and Paul, 2001). This reconstruction assumes LGM as a period of climatic stability and minimum meltwater flux for the time interval between 18 and 15 ^{14}C ka B.P. The data set shows seasonally ice-free conditions in most parts of the Nordic Seas (see Fig. III.3b) along with higher summer SST than in the CLIMAP (1981) reconstruction. A recent reconstruction, GLAMAP 2000 (German Glacial Atlantic Ocean Mapping Project), comprises the North, Central and South Atlantic Ocean using joint definitions of the LGM time slice as the overlap of the Last Isotope Maximum (18-15 ^{14}C ka B.P.) and the EPILOG Level-1 (19-16 ^{14}C ka B.P.) time span, sedimentation rates and resolution (Paul and Schäfer-Neth, 2003). A detailed description of the choice of the LGM slice and age control is given in Sarnthein et al. (2003). It uses 275 sediment cores and the SST estimates are based on a new set of more than 1000 reference samples of planktonic foraminifera, radiolarians and diatoms, and on improved transfer-function techniques. The winter sea ice in the GLAMAP 2000 reconstruction is similar to the CLIMAP summer sea ice boundary and the Nordic Seas are ice-free during the summer months (see Fig. III.4). The whole year round, the SSTs are significantly higher in the North Atlantic compared with the CLIMAP reconstruction. The summer SSTs are considerably higher around Newfoundland and the Nordic Seas. The simulation using the SSTs provided by GLAMAP 2000 is indicated by the abbreviation G. The experiments described above are called 'glacial experiments' hereafter.

III.3 Results

III.3.1 Glacial Surface Air Temperature Anomalies

Using different forcings, the AGCM simulates three different states of the glacial climate. Fig. III.1 shows the North Atlantic anomalous near-surface air temperature relative to present-day temperatures for the LGM. A particularly strong cooling in high northern latitudes is found in all cases, caused by the increase of the albedo due to the vast ice-sheets over the continents (Peltier, 1996), the expanded sea ice cover and advection of cold air from the ice sheets. Experiment C yields a temperature reduction of more than 10°Cover northern Europe, Greenland and the Nordic Seas, which are ice-covered the whole year round (Fig. III.1). Experiments W and G show the strongest cooling over the continents and smaller temperature anomalies over the Nordic Seas due to the heat exchange between the atmosphere and the surface waters. The strongest cooling in the tropics (of 5°C) occurs in experiment C.

III.3.2 The Oceanic Equilibrium States

The oceanic equilibrium states are obtained after 5500 years of model integration, starting from the present-day hydrography with a global salinity increase of 1 psu. The results are shown as a 40 years mean. The results for different oceanic equilibrium states are displayed in Figs. 2, 3, and 4, respectively. The sea ice conditions strongly vary for the different cases. In the Figs. 2a, 3a and 4a, the grey fill shows the winter sea-ice cover and in 2b, 3b and 4b the summer sea-ice cover. The summer sea ice margin in experiment C is situated south of Iceland at about 60°N, while in W and G it is north of Iceland, and the Labrador Sea is partly ice-free.

The anomalous salinity field, averaged over the top 150 m for experiment C is shown in Fig. III.2a relative to present-day. Taking the global salinity elevation of 1 psu

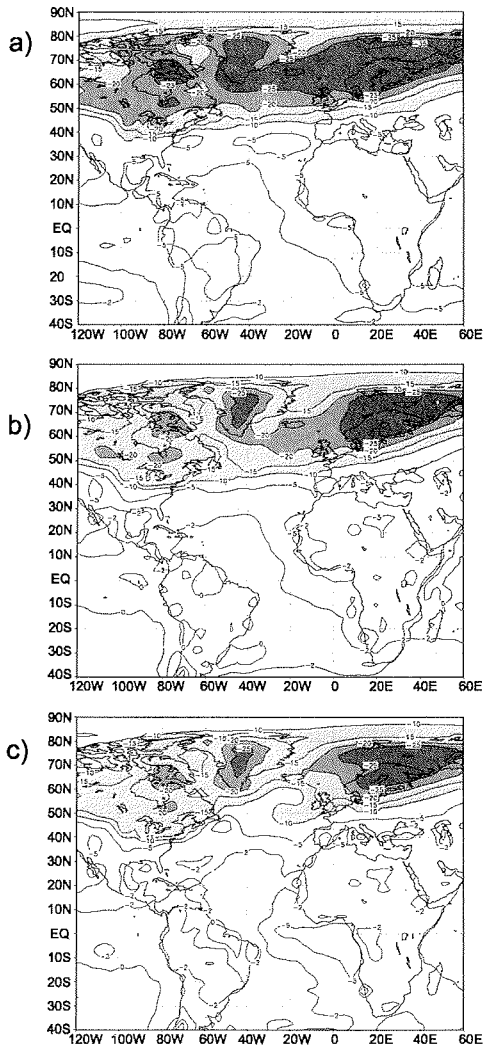

Fig.III.1: *Differences between the glacial and present-day annual mean air temperatures for different reconstructions: a) CLIMAP (1981) with tropical cooling (Lohmann and Lorenz, 2000); b) Weinelt et al. (1996); c) GLAMAP 2000 (Paul and Schäfer-Neth, 2003)*

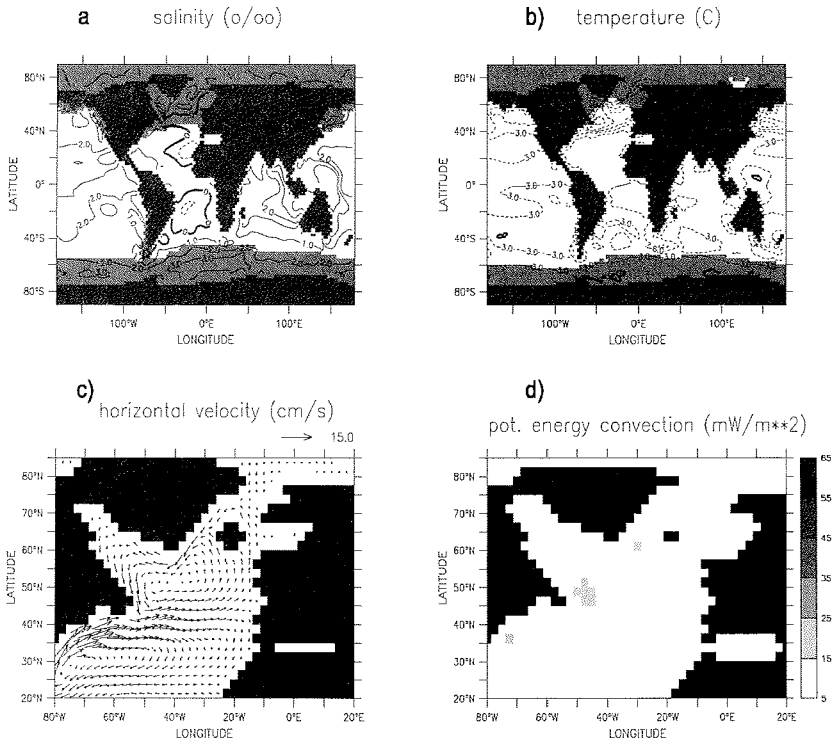

Fig.III.2: *Differences of the equilibrium states (as a 40 years mean) of experiment C and present-day for: a) global salinity (contour interval 1.0 psu), the shading indicates the winter sea-ice cover; b) global temperature (contour interval 3° C), the shading indicates the summer sea-ice cover and c) absolute horizontal velocities and d) the convection sites in the North Atlantic. Salinity, temperature and velocity fields are averaged over the top 150 m.*

into account, the glacial upper ocean appears relatively fresh. The salinity of the surface waters decreases gradually from the tropics to the North up to 45°N and further. A salty tongue of 35.0 psu spreads southward of Iceland up to the summer sea ice margin (not shown). The salinity differences of W and G relative to C are shown in Figs. 3a and 4a. A slight salinity increase occurs at 60°N in the southern vicinities of Iceland, favouring NADW formation in these regions. Experiment G shows positive salinity anomalies (around +1 psu) in the Northern Hemisphere and negative anomalies (around −1 psu) in the Southern Hemisphere in the Atlantic relative to experiment C. This enhanced north-south salinity contrast is not representative for experiment W, where the anomalies are positive in the whole Atlantic. In the South Pacific we find a highly saline subtropical gyre (maximum salinity 37.0 psu), and an area of freshwater in the North Pacific (of around 33.0 psu). Therefore, it has formed a bipolar saline-fresh structure opposite to the Atlantic structure, a configuration similar to the present-day distribution. The salinity anomalies W–C and G–C (Figs. 3a and Fig. III.4a) show fresher conditions in the Pacific. The model simulates an Indonesian salinity maximum in the Indian Ocean and the Western Pacific.

Fig. III.2b shows annual mean temperature anomalies relative to present-day values, averaged over the uppermost 150 m, for experiment C. Very strong temperature gradients (not shown) are located in the Atlantic between 35°N and 55°N. The temperature front, which is zonal in C (Fig. III.2b), is turned to a more meridional direction in experiment W (Fig. III.3b) and G (Fig. III.4b). Strong anomalies are found near Newfoundland (up to 10°C) in experiment G.

In all three experiments, the subtropical and subpolar Atlantic gyres are well simulated (Figs. 2c, 3c and 4c). The warm North Atlantic Current divides into three parts. The first part flows into the Nordic Seas, circulating around Iceland and, after cooling, the waters head southward through the cold East Greenland Current. This horizontal circulation appears to be stronger for G and W. The second part of North Atlantic waters is advected southwards, to the eastern branch of the subtropical gyre. The third part of the current system circulates cyclonically in the latitudes south of Iceland forming the subpolar gyre. The last type of circulation

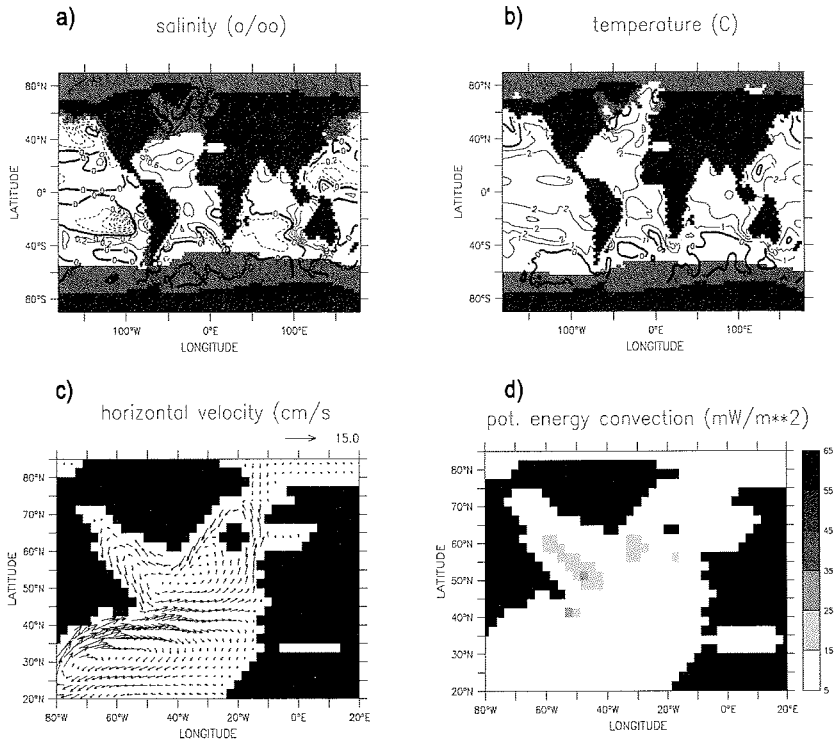

Fig.III.3: *As in Fig. III.2, differences between experiments W and C. The contour intervals for a) are 0.2 psu and for b) are 1° C.*

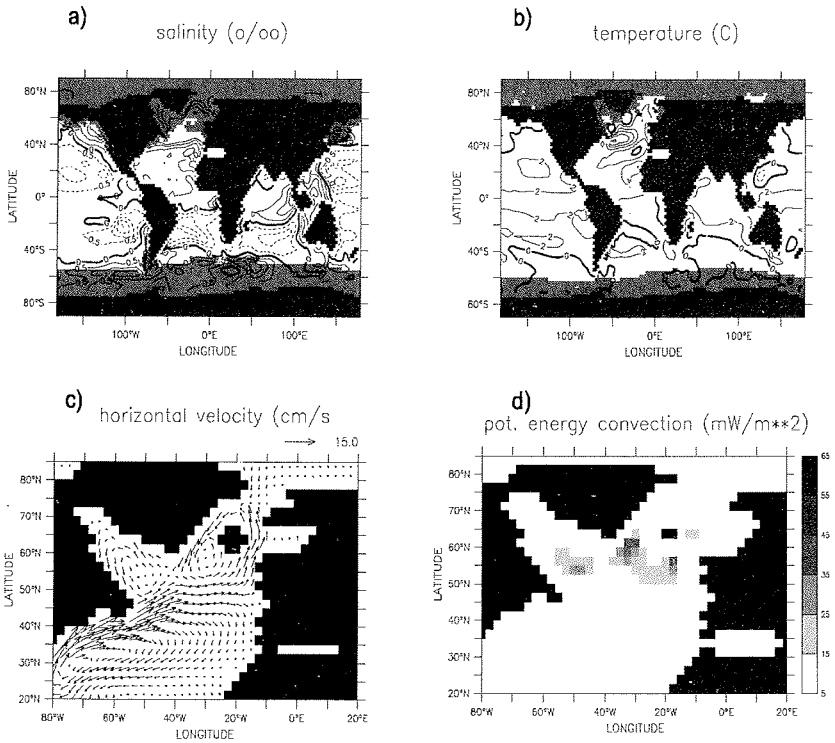

Fig.III.4: *As in Fig. III.2, differences between experiments G and C. The contour intervals for a) are 0.5 psu and for b) are 2°C.*

is particularly strong in C. In conclusion the horizontal circulation for the climates with warm glacial conditions appear more meridionally than in experiment C.

The North Atlantic convection sites (Figs. 2d, 3d, 4d) in the glacial simulations are located near the North American coast, in the Labrador Sea and in the Irminger Sea. The convective areas are between 40°N and 65°N in all cases. This differs from the present-day pattern, simulated with the same model, where the regions of convection are situated mainly in the Nordic Seas and in the Labrador Sea (Prange et al. 2003). The southward displacement of the convection sites in the glacial simulations is associated with a southward shift of NADW formation. In spite of this common general feature, the three experiments differ in convection strength and geographical details in the convective patterns. Convective activity is strongest in experiment G and weakest in experiment C. Investigating the seasonality of the convection, the maximum activity in C is found in autumn, when the temperatures of the surface waters are low enough to form denser waters for convection to start. The required cooling for maximum convection occurs in the early autumn, rather than in winter, due to the low summer temperatures. In experiment G, maximum convection occurs in January, several months later than in C, as a result of the longer time for the necessary surface water cooling. In experiment W, the maximum convection is found in late autumn, as the summer surface waters are warmer than in C, but cooler than in G. Experiment C yields a North Atlantic overturning cell down to 2500 m (Fig. III.5a). The net NADW export at 30°S amounts to 7 Sv (1 Sv = 10^6 m^3s^{-1}). The maximum North Atlantic meridional overturning is 12 Sv. Below 3500 m, AABW (Antarctic Bottom Water) enters the Atlantic with a volume flux of 3 Sv. In experiment W, the North Atlantic overturning cell is much deeper, occupying almost the whole Atlantic basin. The maximum overturning is 20 Sv and the net export of NADW at 30°S is about 15 Sv. In experiment G the meridional overturning is even stronger (more than 20 Sv) with a greater export at 30°S (around 16 Sv). The values of maximum North Atlantic overturning in both experiments G and W are about 70% greater than in experiment C. Moreover, the meridional heat transport into the Atlantic basin also differs significantly for the three experiments. Its maximum is found in all experiments around 30°N with values of 0.83 PW, 1.23

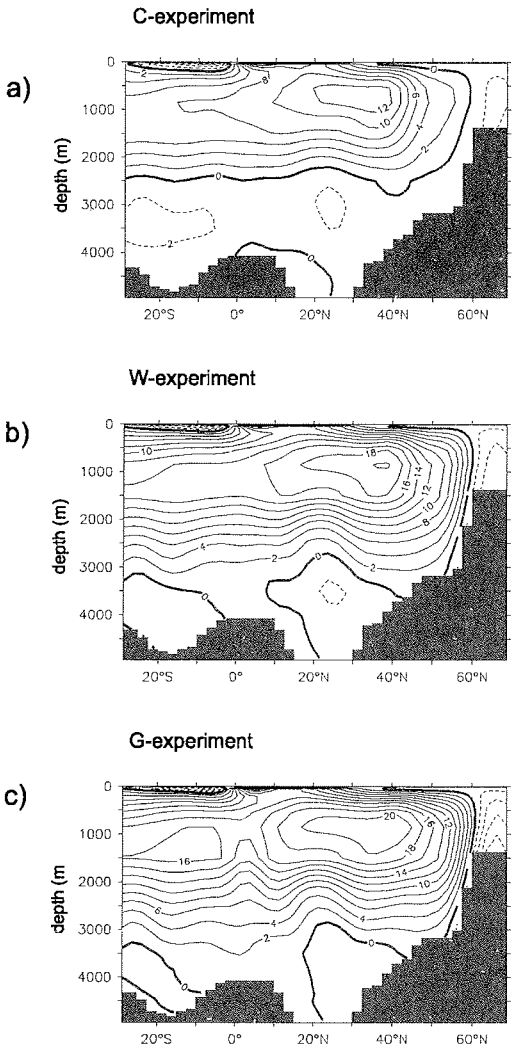

Fig.III.5: *Atlantic meridional overturning streamfunction in Sv for experiments a) C, b) W and c) G. All panels represent a 40 years mean.*

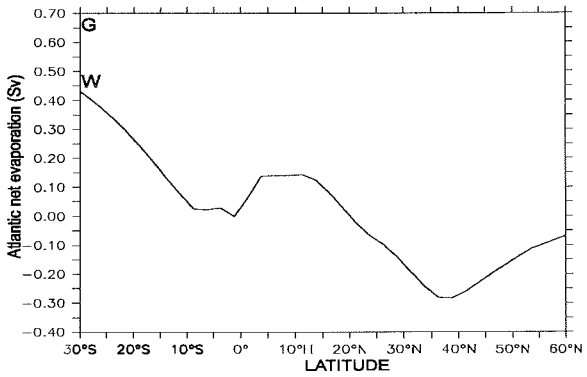

Fig.III.6: *Northward freshwater transport in the Atlantic for experiments C, W and G in equilibrium.*

PW and 1.42 PW for experiments C, W and G, respectively.

III.3.3 Atlantic Freshwater Budgets and Hystereses

To assess the role of the hydrological balance for the stability of the THC, we integrated the surface freshwater fluxes over the Atlantic Ocean (including the Arctic). The calculations reveal a net freshwater loss for the ocean in all three experiments (Fig. III.6), i.e. a predominant evaporative regime. The lowest value of the balancing oceanic freshwater import at 30°S is found in experiment C and the highest value in experiment G. A plot of the zonal mean precipitation (P), evaporation (E) and P–E over the Atlantic basin for the three experiments is shown in Fig. III.7. The precipitation follows a similar structure in all experiments (Fig. III.7a) - maximum in the tropical and mid-latitude regions and minimum in the subtropical and polar latitudes - as the values increase from experiments C to W and G. The evaporation rates are at a maximum between 30°S and 30°N and are highest for the warmer climates (Fig. III.7b). Enhanced evaporation is also found in the northern mid-latitudes for experiment W and even more pronounced for experiment

G, due to the ice-free Nordic Seas and warmer conditions in this region. A weaker hydrological cycle is found in experiment C compared with W and G. The main difference between the hydrology in the experiments appears in the tropical and subtropical latitudes (Fig. III.7c). The differences in spatial patterns of the surface freshwater flux (P–E) between experiments G and W and the experiment C, are shown in Fig. III.8. In subequatorial and tropical latitudes, anomalous negative freshwater fluxes (experiment C refers to the experiment LGM.N in Lohmann and Lorenz, 2000) are associated with large water vapour transport from the Atlantic to the Pacific. The same general trends are found in the G and W simulations, as the strengths of the negative centers are stronger in the same tropical areas. Positive anomalies relative to C are situated along the thermal equator and in mid-latitudes. Thus the three different experiments provide for three different hydrological cycles. The contribution of the overturning component of the Atlantic freshwater transport is calculated through: $F_{ot} = -\frac{1}{S_0} \int \bar{v}\bar{S}dz$ (Prange et al., 2003; Lohmann, 2003). The integral is calculated over the depth, $\bar{S}$ is the zonally averaged salinity, $\bar{v}$ is the zonally integrated meridional velocity and $S_0 = 35$ psu is a reference salinity. At 30°S, the lowest value of the freshwater transport due to the overturning is found in experiment C ($F_{ot} = 0.034$ Sv), followed by experiment W ($F_{ot} = 0.054$ Sv), and the largest value is found in experiment G ($F_{ot} = 0.072$ Sv). When comparing these numbers with the total freshwater loss, it is concluded that the overturning component of the freshwater transport is only a minor part of the net evaporation over the Atlantic.

Aiming to find a link between hydrology and stability of the glacial THC, we calculate hysteresis stability diagrams. A slowly varying freshwater flux perturbation (10^{-4} Sv/yr) is applied to the North Atlantic between 20°N and 50°N. The sequence of quasi-equilibrium states is reflected by the upper branch of the hysteresis, down to the 'critical point' where the freshwater input causes a complete shutdown of the THC. Then the freshwater input is decreased so that the circulation recovers. Afterwards, the freshwater input is increased again in order to return to the initial state. The resulting hysteresis diagrams for experiments C, W and G are displayed in Fig. III.9. In experiment C, an anomalous ('critical') freshwater flux of 0.16 Sv

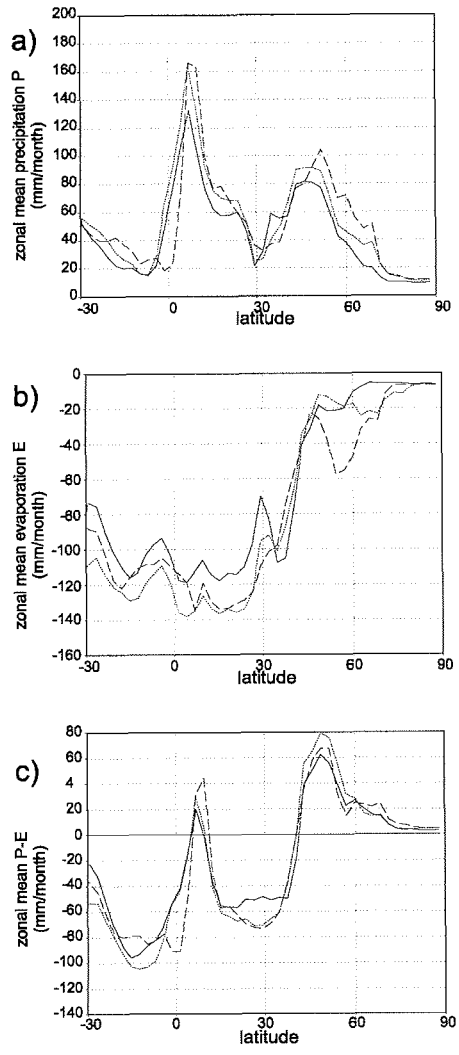

Fig.III.7: *a) Zonal mean precipitation P, b) zonal mean evaporation E, and c) zonal mean P–E over the Atlantic basin for experiments C (solid line), W (short dashed line) and G (long dashed line). The units are mm/month.*

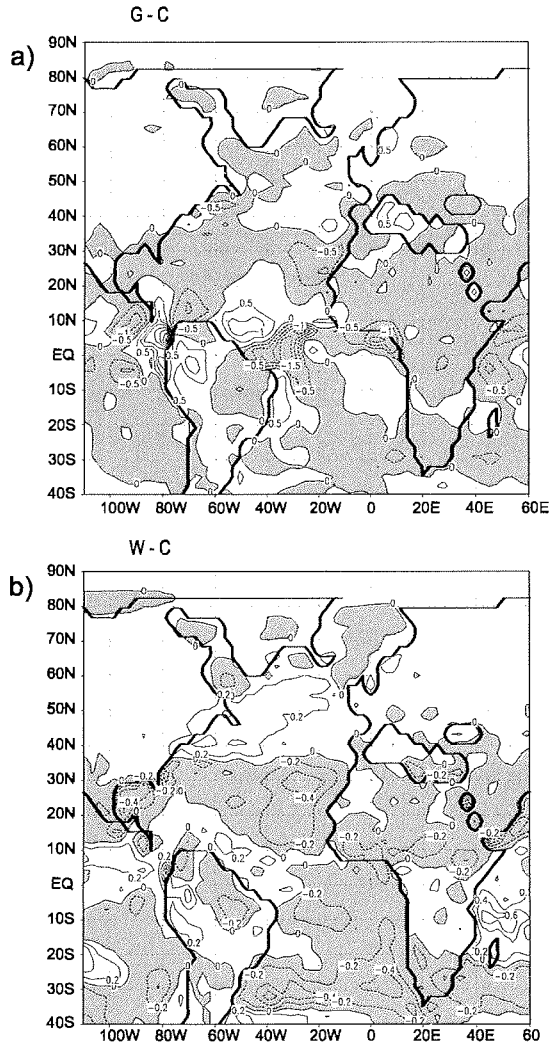

Fig.III.8: *Surface freshwater flux (P–E) differences in the Atlantic area: a) between G and C; b) between W and C. The grey fill shows the areas of negative anomalies. Units are m/year.*

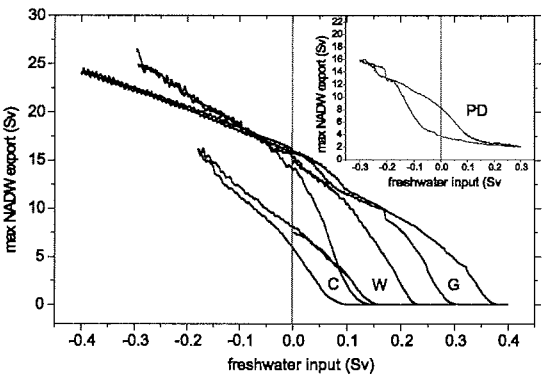

Fig.III.9: *The hysteresis loops for the experiments C, W and G. The equilibrium states of the experiments C, W and G are situated on the zero line of the freshwater input. In the upper right corner of the plot the present-day (control run) hysteresis is shown (Prange et al., 2002).*

is required for a THC shutdown. The 'critical' freshwater input increases for W and G (0.24 Sv and 0.36 Sv, respectively). In Fig. III.10 the dependence of the 'critical' freshwater perturbation on the net evaporation rate is displayed. The graph suggests a monotonic relationship between the stability of the ocean circulation and the hydrological budget in the Atlantic Ocean.

III.4 Discussion

One could pose the question whether the glacial THC was weaker than the present-day circulation. In our cold glacial simulation (experiment C) we find a reduction of 20% of the Atlantic meridional overturning circulation relative to the present-day simulation (Prange et al., 2003). Utilizing different kinds of coupled models, Weaver et al. (1998), Ganopolski and Rahmstorf (2001), and Shin et al. (2003) simulated a similar weakening of the conveyor during the glacial maximum, which is consistent with geological findings of Rutberg et al. (2000), who, based on ratios of neodymium

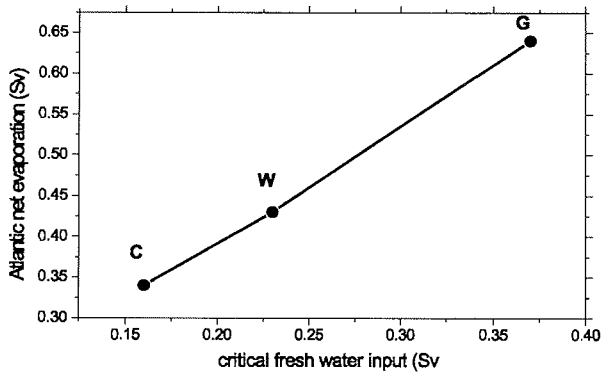

Fig.III.10: *The freshwater export at 30°S versus the 'critical' freshwater input for reaching the 'off-mode'.*

isotopes, reported weakening of NADW export to the Southern Ocean during the full glacial stages (e.g., LGM), and almost no change during the warm glacial intervals. A weaker circulation is also consistent with assimilated paleonutrient tracer distribution in an ocean circulation model (Winguth et al., 1999). Furthermore, benthic foraminifera $\delta^{13}C$, Cd/Ca and Ba/Ca ratios suggest that the deep Atlantic circulation during the LGM was influenced by the deep penetration of AABW and consequent reduction of NADW (Boyle and Keigwin, 1987; Duplessy et al., 1988; Boyle, 1992; Marchitto et al., 2002). A shallower overturning cell, approximately 1000 m less than present-day, is also indicated by the shoaling of the sedimentary lysocline, which gives the interface between NADW and AABW (Volbers and Henrich, 2003; Frenz and Henrich, 2003). However, the strength of the overturning remains a controversial topic. No change of the overturning rate is inferred from sedimentary records of $^{231}Pa/^{230}Th$ (Yu et al., 1996) and a new reconstruction combining 55 benthic foraminiferal stable carbon isotopes suggests no considerable difference to the present-day circulation strength (Bickert and Mackensen, 2003). On the other hand, three-dimensional coupled models obtained even intensification of the LGM ocean circulation (Hewitt et al., 2001; Kitoh et al., 2001). Our simulations with warm glacial background conditions (W and G) also exhibit stronger (around 50%) overturning compared to the present-day simulation in Prange et al.

(2003).

Using different SST reconstructions, we are able to detect different glacial salinity distributions at the surface and in the depth. In experiment C, the SSS field shows a tongue of salty waters deeply penetrating from the subtropics to the southern vicinities of Iceland, a feature consistent with the reconstructions of Duplessy et al. (1991). For warm background conditions (W and G) a salinity increase in the Irminger Sea is responsible for the stronger convection and NADW formation. The modeled salinities in the North Atlantic are more consistent with the reconstructions of Duplessy et al. (1991) for both types of experiments with warm (W and G) and cold (C) conditions, and they differ substantially (by more than 1.5 psu) from the values suggested by de Vernal et al. (2000). The mean surface salinity of the glacial ocean appears relatively fresh compared to the present one in our model. The salinity excess of the glacial ocean (+1 psu) is mainly stored in the abyssal ocean, consistent with geological evidence (Adkins et al., 2002).

All experiments for the glacial ocean yield an Atlantic Ocean saltier than the Pacific, similar to the present-day configuration. However, the model study of Lautenschlager et al. (1992) finds the opposite contrast with the Pacific Ocean being saltier than the Atlantic. The simulations of the present-day climate with reduced greenhouse gases, performed by Shin et al. (2003), show also the opposite contrast, but their coupled LGM simulation reveals a fresher Pacific and a saltier Atlantic Ocean relative to present day. An intensification of the salinity contrast between the Atlantic and Pacific Oceans is found in experiments G and W relative to C, which originates from strongly increased moisture export out of the Atlantic to the Pacific Ocean. In experiment C, Lohmann and Lorenz (2000) attributed this to enhanced water vapour transport over Panama, less water input over the dry African continent and less water vapour import over the North American continent. The latter effect is linked to the presence of the large continental ice-sheets.

Perturbations of the glacial THC with different climatic background states result in different hysteresis maps. At zero freshwater input, the glacial THC has one

stable equilibrium only. This can be directly inferred from the hysteresis curves for experiments W and G (Fig. III.9). The weak bistability at zero freshwater input in experiment C is caused by the relative high freshwater flux perturbation rate of 10^{-4} Sv/yr compared to our previous work where we found a strict monostability at the zero point (Prange et al., 2002). In each experiment, the freshwater budget reveals a net evaporation over the Atlantic (including Arctic) catchment area with different strengths. The experiments show that higher net evaporation tends to shift the equilibrium to a more stable state. The hystereses show that the coldest climate is more sensitive to freshwater changes than the warm glacial climates. The salinity enhancement along the conveyor route through the subtropics induces a northward freshwater transport across 30°S compensating the freshwater loss from the evaporation. It may be splitted into an overturning component, a component related to the gyre circulation, and a term related to diffusion. The small values, which are found for the overturning component, suggest that gyre and diffusive transports play an important role for the stability of the THC. Consistent with Saenko et al. (2002), F_{ot} is a poor measure for the stability of the conveyor. During glacial times, the salinity and temperature induced density gradients between the North and South Atlantic act in one direction driving the conveyor, which corresponds to the thermo-haline regime of the ocean system according to Rahmstorf's (1996) definition. The strong salinity contrast between the South Atlantic and the North Atlantic in experiment G is associated with a more haline driven ocean circulation. The haline factor is weaker in experiment W, which is partly compensated by the thermal forcing. The predomination of the haline mechanism induces a stabilizing effect on the THC, which allows only one stable state of the circulation, namely an on-mode with NADW formation.

We relate the 'critical' freshwater input, which causes the collapse of the circulation, to the hydrological background conditions. The lower evaporation rates over the Atlantic basin in the cold glacial climate of experiment C results in a less stable circulation, while the warmer climates with higher Atlantic net evaporation are more stable. In this sense, the stability parameters depend explicitly on the background hydrology with a monotonic (almost linear) relation between the Atlantic

evaporation rates and the 'critical' perturbation.

The glacial THCs substantially differ from the present-day circulation. Using present-day forcing, our model produces a THC with two stable equilibria (Prange et al., 2003), like many other models. Freshwater perturbations can shut down the overturning irrevocably. In the present-day ocean, the THC is driven by SST gradients, while salinity gradients across the Atlantic Ocean tend to weaken the overturning, which allows multiple equilibria of the ocean circulation in the thermal flow regime (Stommel, 1961; Rahmstorf, 1996). In a coupled three-dimensional OGCM with an energy-moisture balance model for the atmosphere including an ice sheet component, the glacial THC possesses different stability properties (Schmittner et al., 2002). As the ice sheet component in this model set-up does not permit the system to settle into equilibrium, this glacial ocean is characterized by a mode different than the one studied here. In the absence of anomalous freshwater fluxes, their experiments showed only one stable glacial mode, namely the off-mode.

III.5 Conclusions

In this study we performed three glacial simulations using three different reconstructions of SST and sea-ice margin as forcing fields for an AGCM. One reconstruction, based on CLIMAP (1981) with additional tropical cooling generates a cold glacial climate equilibrium, whereas the Weinelt et al. (1996) and GLAMAP 2000 (Paul and Schäfer-Neth, 2003) reconstructions produce relatively warm glacial climate backgrounds in the North Atlantic realm. In contrast to the present-day THC, all equilibrium states of the simulated LGM climates show a mono-stable behaviour, which can serve as an explanation for the recovery of the THC after meltwater-induced shutdowns (Ganopolski and Rahmstorf, 2001; Prange et al., 2002).

In the differing glacial climate backgrounds, the warm climates show higher stability than the cold climate. Analysing the hydrological balance in the Atlantic catchment

area, we find a monotonic dependence between the Atlantic net evaporation and the 'critical' freshwater input in the hysteresis causing a complete collapse of the THC. We conclude that the background hydrological balance plays a crucial role for the stability of the ocean circulation and, hence, of the glacial climate. Since THC changes sensitively depend on the climatic background state with its associated hydrological cycle, our modeling strategy, employing an AGCM in T42 resolution with explicitly resolved hydrological cycle seems to be appropriate. This suggests an important role of the low-latitude hydrological cycle for the branching and sensitivity of the THC. Such a hydrological bridge and its changes have been attributed to changes of interannual variability in the tropical Pacific Ocean (Latif et al., 2000; Schmittner and Clement, 2002) as well as to times of weak overturning causing enhanced water vapour transport over the Isthmus of Panama (Lohmann, 2003). Moreover, changes in the South Atlantic, connected with the cold and warm water routes of the global ocean circulation (Gordon, 1986) may strongly determine the regime of the THC (Knorr and Lohmann, 2003).

In our model set-up, we have neglected feedbacks connected with atmosphere dynamics, vegetation and the cryosphere. Changes in the hydrological balance are estimated to be in the order of 0.15 Sv, when comparing the climate state of the on and off mode in a coupled atmosphere-ocean general circulation model (Lohmann, 2003). The cryosphere provides a great uncertainty. Iceberg discharge has been estimated to be of order 0.15 Sv for 500-1000 years (Calov et al., 2002; Chappell, 2002). The effect of vegetation cover on the interocean basin water vapour transport has not been analysed so far.

In this study, we have not addressed the question, to which extent the climatic templates represent real glacial climate states. One could speculate that the modeled THC states may possess features of stadial and interstadial circulations, respectively. The different hydrological budgets during relatively cold and warm background conditions would then imply different sensitivities with respect to Heinrich Events (cold conditions) and the Younger Dryas (about 13,000-11,500 years B.P.), a cold phase which directly followed the warm Bølling-Allerød. Our study emphasizes the impor-

tance of the tropical hydrological cycle, which may provide a possible link between the low latitudes and the ocean circulation on paleoclimatic time scales. In order to understand these linkages, more geological data of the tropical regions is required.

Acknowledgements *We gratefully acknowledge the comments and suggestions of Andre Paul and Christian Schäfer-Neth and Klaus Grosfeld, and Andreas Manschke and Silke Schubert for technical support. We also thank the reviewers for constructive comments. The study was funded by the BMBF through DEKLIM project Climate transitions and by the Deutsche Forschungsgemeinschaft as a part of the DFG Research Centre 'Ocean Margins' of the University of Bremen (No. RCOMO 127).*

Chapter IV

Modelling tempo-spatial signatures of Heinrich Events: Influence of the climatic background state

Matthias Prange[1,2], Gerrit Lohmann[1,2], Vanya Romanova[1], Martin Butzin[1]

[1]Geoscience Department, University of Bremen, Klagenfurterstr., 28334 Bremen, Germany
[2]DFG Research Center Ocean Margins (RCOM), University of Bremen, 28334 Bremen, Germany

---

Abstract[1]

Different sea surface temperature (SST) reconstructions for the Last Glacial Maximum are applied to a hybrid-coupled climate model. The resulting oceanic states are perturbed by North Atlantic meltwater inputs in order to simulate the effect of Heinrich Events on the Atlantic thermohaline

[1]Received: 2 September 2003/Accepted: 10 November 2003/Published in Quaternary Science Reviews (2004) 23, 521-527

circulation (THC) and SST. The experiments show that both the Atlantic SST signature of the meltwater event and the time span of THC recovery strongly depend on the climatic background state. Data-model comparison reveals that the overall spatial signature of SST anomalies is captured much better in the glacial meltwater experiments than in an analogous experiment under present-day conditions. In particular, a breakdown of the modern THC would induce a much stronger temperature drop in high northern latitudes than did Heinrich Events during the ice age. Moreover, our results suggest that the present-day circulation can settle into a stable 'off' mode, whereas the glacial THC was mono-stable. Mono-stability may serve as an explanation for the recovery of the THC after Heinrich Event shutdowns during the last glaciation.

IV.1 Introduction

Transporting heat over large distances, the Atlantic thermohaline circulation (THC) plays a key role in the climate system. Geological records from the last glacial period suggest that enhanced abundances of ice-rafted debris in the North Atlantic (Heinrich Events) were associated with shutdowns of the THC and global-scale climatic changes (e.g., Broecker and Hemming, 2001; Clark et al., 2002). The concept of THC fluctuations with global impact has motivated a large number of ocean and climate modellers to simulate THC disruptions by injecting freshwater to the North Atlantic (e.g., Bryan, 1986; Maier-Reimer and Mikolajewicz, 1989; Stocker and Wright, 1991; Manabe and Stouffer, 1995; Rahmstorf, 1995; Lohmann et al., 1996; Schiller et al., 1997; Crucifix et al., 2001; Ganopolski and Rahmstorf, 2001; Rind et al., 2001; Lohmann, 2003). These model results suggest that the THC is highly sensitive to changes in the North Atlantic freshwater budget, such that anomalous freshwater inputs can trigger a collapse of the circulation, thereby causing an abrupt temperature drop in the order of 5-10°C in the North Atlantic realm.

Even though the combined efforts of palaeoceanographers and climate modellers are well on the way to providing a consistent picture about the climatic impact of Heinrich Events and the important role of the THC, a closer inspection still reveals

a number of discrepancies between geological data and model results. Here, we highlight the importance of the climatic background state for the spatial pattern of sea surface temperature (SST) change in response to a THC shutdown. In the model studies mentioned above, freshwater perturbations were applied either to non-glacial states or to highly simplified, zonally averaged models of the ocean. Utilizing an atmosphere general circulation model (AGCM) in combination with an ocean general circulation model (OGCM) in a hybrid-coupled framework, we demonstrate that important features of the Heinrich Event tempo-spatial signature in the Atlantic Ocean can only be simulated by perturbing a *glacial* state of the ocean.

IV.2 Glacial climate simulations with an AGCM

We employ three different SST reconstructions for the Last Glacial Maximum to force the AGCM ECHAM3/T42 (Roeckner et al., 1992): 1) The CLIMAP (1981) reconstruction with an additional cooling of 3°C in the tropics (Lohmann and Lorenz, 2000), 2) the North Atlantic reconstruction by Weinelt et al. (1996) merged with CLIMAP (Schäfer-Neth and Paul, 2001), and 3) the new GLAMAP 2000 Atlantic reconstruction (Sarnthein et al., 2003) combined with CLIMAP as described by Paul and Schäfer-Neth (2003). As compared to CLIMAP, the North Atlantic sea-ice cover is substantially reduced in the newer reconstructions. The GLAMAP winter sea-ice margin is similar to CLIMAP's summer sea-ice boundary, and the Nordic Seas are ice-free during summer. Consistent with the reduced sea-ice extent, the new reconstructions provide higher SSTs in the northern North Atlantic than CLIMAP.

The three glacial experiments are denoted as experiments C ('C'LIMAP), W ('W'einelt) and G ('G'LAMAP). Orbital forcing, reduced concentration of carbon dioxide (200 ppm), and topographic changes (Peltier, 1994) are taken into account (cf. Lohmann and Lorenz, 2000). A fourth experiment, PD, is carried out with present-day SSTs. Fig. IV.1 shows simulated North Atlantic surface air temperatures for the three glacial experiments relative to experiment PD. As a result of the

excessive sea-ice cover and the additional tropical cooling, experiment C provides the coldest climate. For a detailed description of the simulated glacial climates, including analysis of the hydrologic cycle, we refer to Lohmann and Lorenz (2000) and Romanova et al. (2003).

IV.3 Modelling the glacial ocean with an OGCM

Monthly outputs of the atmosphere model (wind stress, air temperature, net precipitation) from experiments C, W, G and PD are applied to an improved version of the three-dimensional ocean model LSG (Maier-Reimer et al., 1993), including a third-order QUICK advection scheme (Leonard, 1979; Schäfer-Neth and Paul, 2001; Prange et al., 2003). The model has 11 vertical levels and a horizontal resolution of 3.5° on a semi-staggered grid type 'E'. Forcing of the ocean model involves a runoff scheme and a surface heat flux formulation that allows for scale-selective damping of temperature anomalies (Rahmstorf and Willebrand, 1995). It has been demonstrated by Prange et al. (2003) that this hybrid-coupled model approach enables the simulation of observed/reconstructed SSTs as well as the maintenance of large-scale temperature anomalies during freshwater perturbation experiments.

The oceanic equilibrium circulations and hydrographies for the different glacial SST forcings are analysed and discussed in Romanova et al. (2003). Compared to the present-day meridional overturning circulation of the Atlantic Ocean (experiment PD), the glacial equilibrium is about 20% weaker in experiment C, but stronger in the experiments W and G (see Fig. IV.3 prior to year 0). In the simulation of the present climate, the major northern hemisphere convection sites are located in the Nordic Seas and in the Labrador Sea (Prange et al., 2003). Due to expanded winter sea-ice covers and more zonal wind stresses, convection sites are shifted southward in the glacial experiments, thus deep water is entirely formed in the North Atlantic south of 65°N (Romanova et al., 2003). Consequently, the 'conveyor' extends further to the north in experiment PD than in the glacial experiments. Fig. IV.2a shows

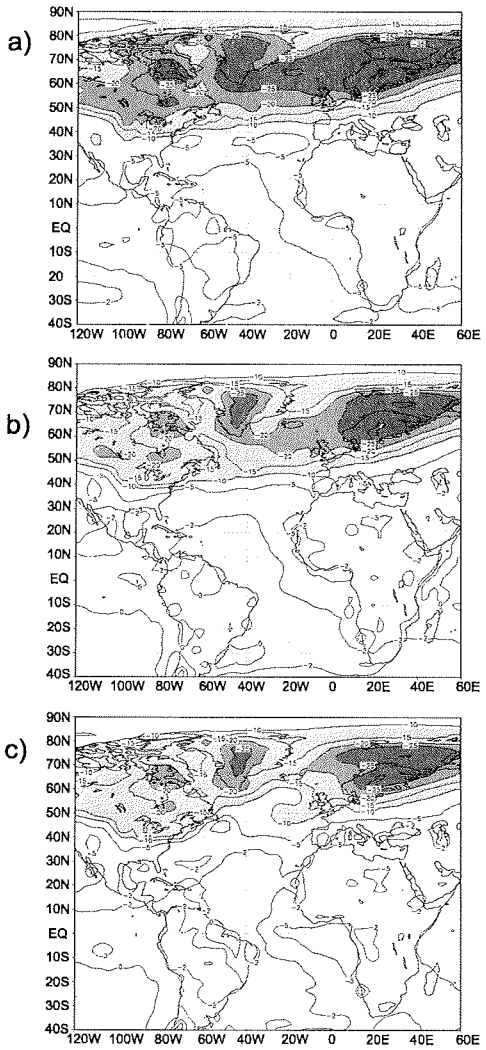

Fig.IV.1: *Differences between glacial and present-day (experiment PD) mean surface air temperatures for experiments a) C, b) W and c) G in the Atlantic realm. Units are* $^{\circ}C$.

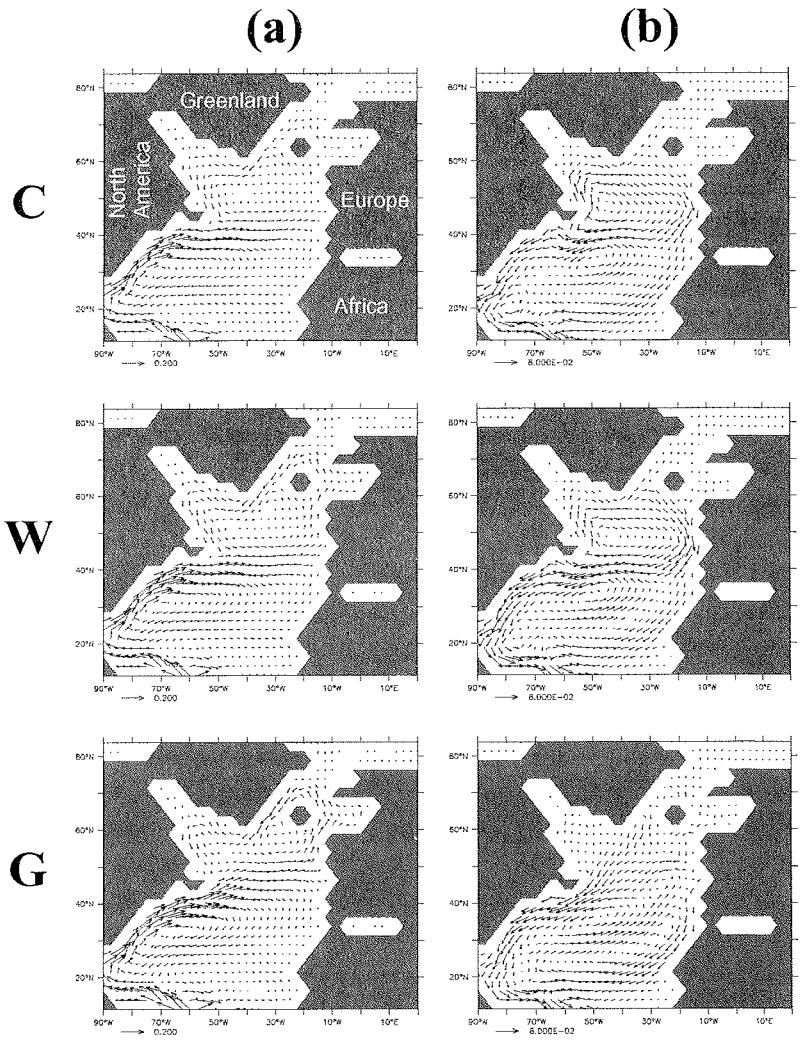

Fig.IV.2: *(a) Equilibrium upper ocean circulation (averaged over 0-100 m) in the North Atlantic for the glacial experiments C, W and G; (b) annual mean velocity anomalies (averaged over 0-100 m) induced by the meltwater perturbation in experiments C, W and G at year 500 (cf. Fig. IV.3). Units are* ms^{-1}.

the surface circulation in the North Atlantic/Nordic Seas for the glacial climates. In experiment C, meridional velocities are very small north of 40°N and the North Atlantic Current (NAC) turns out to be a zonal stream. The subpolar gyre is more vigorous in experiment W with a significant inflow to the Nordic Seas. The surface circulation in experiment G resembles the present-day flow pattern, including a strong northward component of the NAC.

IV.4 Meltwater perturbation experiments

The equilibrium states are perturbed by a sudden 500-year freshwater input to the North Atlantic, uniformely applied between 40°N and 55°N. A relatively high freshwater influx of 0.5 Sv (0.5×10^6 $m^3 s^{-1}$) has been chosen to ensure a complete and rapid shutdown of the THC in all experiments, making direct comparison of the resulting temperature anomaly fields easier. The temporal response of the Atlantic THC to the freshwater input is plotted in Fig. IV.3. After termination of the anomalous freshwater forcing, the present-day circulation remains in the 'off' mode, whereas the glacial circulations recover spontaneously with different rates. The different stability behaviour is linked to the Atlantic freshwater budgets. In experiment C, the net atmospheric moisture export out of the Atlantic catchment area (>30°S, Arctic Ocean included) is 0.08 Sv greater than in experiment PD. The lack of a low-saline Bering Strait throughflow, owing to a lowered sea level, leads to a further reduction in the freshwater supply to the glacial North Atlantic (Prange et al., 2002). In experiments W and G, moisture exports out of the Atlantic are even higher than in experiment C (+0.17 Sv and +0.38 Sv, respectively, relative to experiment PD). As a result, the THC resides in the so-called 'thermohaline flow regime' (Rahmstorf, 1996) in all glacial experiments (Romanova et al., 2003). In this flow regime, freshwater is carried northward by the conveyor's upper limb into the regions of deep-water formation. Consequently, a circulation with reduced overturning is unstable, since net evaporation over the Atlantic and wind-driven oceanic salt transports would inevitably enhance North Atlantic salinities, driving convec-

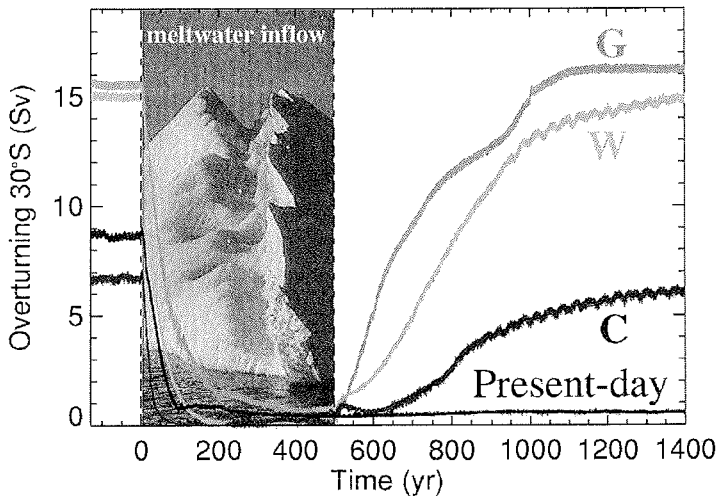

Fig.IV.3: *Temporal evolution of the Atlantic meridional overturning circulation (here: net export of North Atlantic deep water at 30° S) in the experiments C, W, G and PD. A 500-yr meltwater perturbation is applied at year 0. In experiment PD the circulation remains in the 'off' mode after termination of the meltwater input.*

tion and the THC. This mechanism works most efficiently in experiment G, where net evaporation is largest. By way of contrast, the present-day conveyor is driven by heat loss with freshwater forcing braking the overturning (so-called 'thermal flow regime'), thus allowing for multiple equilibria (Stommel 1961; Rahmstorf 1996).

Fig. IV.4 shows the response of Atlantic surface temperatures to the freshwater perturbation for the glacial and the present-day experiments. In experiment PD, the strongest cooling occurs in the northern North Atlantic and the Nordic Seas, where SSTs decrease by more than 5°C, consistent with other meltwater experiments for the present-day climate (e.g., Rahmstorf 1995; Manabe and Stouffer 1995; Schiller et al., 1997). In the glacial experiments, the cooling is restricted to lower latitudes. A salient temperature drop appears in the eastern North Atlantic off Portugal in experiments C and W. Alkenone data suggest that pronounced cooling off the Iberian peninsula in the order of 3-6°C is indeed a typical feature of Heinrich Events (Bard et al., 2000; Pailler and Bard, 2002; Rühlemann, unpubl.). This cooling can best be explained by looking at the flow anomalies induced by the freshwater input in the upper Atlantic (Fig. IV.2b). In both experiment C and experiment W a strong anomalous southward flow emerges in the eastern North Atlantic from Iceland to Cape Blanco, which is associated with anomalous advection of cold water from the North. In experiment G, the anomalous southward current in the eastern Atlantic is confined between latitudes 40°N and 20°N, reflecting a pure intensification of the Canary Current. The same holds for experiment PD (not shown).

In the South Atlantic, pronounced warming at about 40°S and off the coast of Namibia is detected for all climatic background states considered (Fig. IV.4). Both regional features are explored in the coupled AGCM/OGCM study of Lohmann (2003). The warming at 40°S is linked to an anomalous southward flow along the coast of South America which turns to the east at about 40°S. The strong warming off Namibia is associated with a reduced northward flow and more horizontal isotherms. Equatorial surface warming occurs only in experiment G (Fig. IV.4). The model results can be compared with palaeoceanographic data from the Atlantic Ocean. Some high-resolution marine sediment cores which provide information about SST

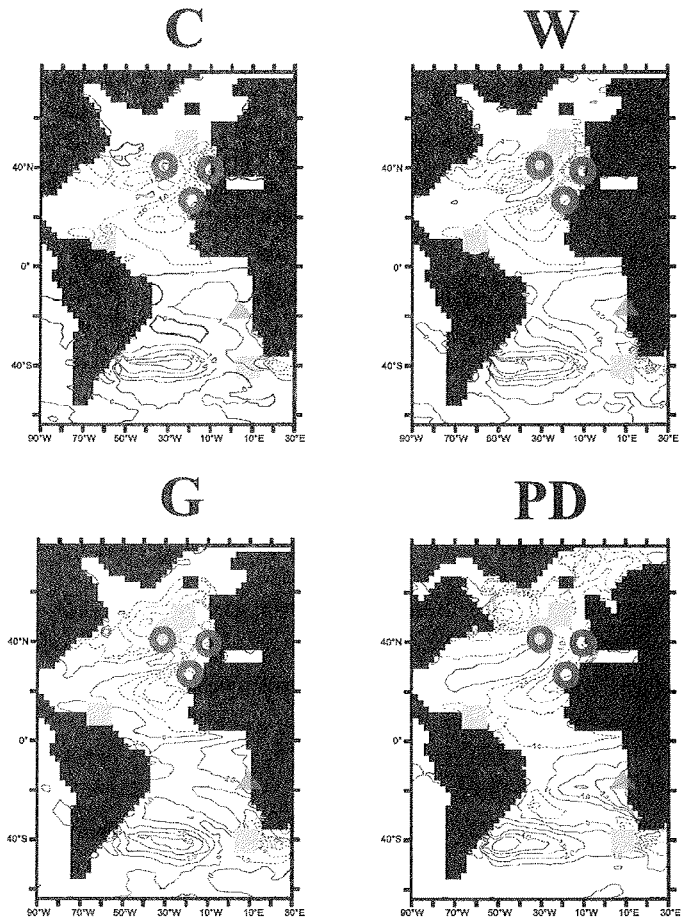

Fig.IV.4: *Atlantic SST response to the meltwater perturbation in experiments C, W, G and PD.Temperature anomalies relative to the unperturbed equilibria are plotted at the end of the meltwater period (i.e., at year 500). For comparison, temperature changes suggested by proxy data from marine sediment cores for Heinrich Event 1 are marked as follows: warming (triangles), temperature changes less than $\pm 0.5^{\circ}C$ (squares), cooling (light grey circles), very strong ($> 2^{\circ}C$) cooling (dark grey circles). See Table IV.1 for references (Cores SO 75-26KL, SU 81-18 and MD 992341 are represented by one circle).*

Core	Position	Method	Reference
BOFS 5K	51°N, 22°W	Faunal	Maslin et al. (1995)
SU 90-08	43°N, 30°W	Faunal	Paterne et al. (1999)
SU 90-03	41°N, 32°W	Faunal	Chapman and Shackleton (1998)
SO 75-26KL	38°N, 10°W	Faunal	Zahn (1997)
SU 81-18	38°N, 10°W	Alkenone	Bard et al. (2000)
MD 992341	37°N, 8°W	Alkenone	Rühlemann (unpublished)
15637-1	27°N, 19°W	Faunal	Kiefer (1998)
M 35003-4	12°N, 61°W	Alkenone	Rühlemann et al. (1999)
GeoB 1023-5	17°S, 11°E	Alkenone	Kim et al. (2002)
TN 057-21-PC2	41°S, 8°E	Alkenone	Sachs et al. (2001)

Table IV.1: *Some high-resolution marine sediment cores that provide information about SST changes during Heinrich Event 1 in the Atlantic Ocean (from north to south). Faunal and alkenone reconstructions are considered. The cores are marked in Fig. IV.4 by coloured circles.*

changes during Heinrich Event 1 (around 16 kyr BP) are compiled in Table IV.1 and marked in Fig. IV.4 by coloured circles. The data-model comparison reveals that the overall spatial signature of SST anomalies is captured much better in the glacial experiments than in experiment PD. In particular, note the behaviour of the three northernmost cores, BOFS 5K, SU 90-08 and SU 90-03, which indicates a reduced meridional SST gradient during the Heinrich Event in northern mid-latitudes (cf. Chapman and Maslin, 1999). This behaviour is captured only in experiments C and W.

IV.5 Conclusions

Our hybrid-coupled model approach has been successfully employed in previous palaeostudies (Prange et al., 2002; Knorr and Lohmann, 2003; Romanova et al., 2003; Rühlemann et al., 2003). It is a comparatively simplified climate model which

omits changes in atmosphere dynamics; that is, wind stresses remain unaffected during the perturbation experiments. Therefore, SST changes in our experiments are solely induced by variations in large-scale oceanic heat transports. We find that the SST response for present-day conditions is similar to experiments using coupled AGCM/OGCMs (e.g., Manabe and Stouffer, 1995; Lohmann, 2003). The main advantage of the hybrid-coupled approach is that palaeoceanographic reconstructions and modern observations can directly be 'assimilated' into the model. Our results reveal that the Atlantic SST response to meltwater perturbations strongly depends on the applied background climatology. Hence, simulations of Heinrich Events are challenging - not only because of many unknowns of the iceberg-meltwater forcing (magnitude, duration, location), but also because of uncertainties concerning the glacial 'basic state'. Nevertheless, all glacial experiments conducted capture important features of the Heinrich Event SST signature found in palaeoceanographic records, like an extreme cooling off Iberia.

Palaeoclimatic evidence shows that Heinrich Events had a strong impact on global climate during the last glacial period (e.g., Broecker and Hemming, 2001), probably even affecting the evolution of mankind. A recent study by d'Errico and Snchez Goi (2003) suggests that inhospitable environmental conditions during Heinrich Event 4 (around 39 kyr BP) favoured the persistence of the last Neanderthal populations in southern Iberia, where the replacement by anatomically modern humans took place only after the cold event. Our model experiments indicate that a breakdown of the present-day THC would induce even stronger climatic changes in the North Atlantic realm than did Heinrich Events during the ice age. Furthermore, our results suggest that the modern circulation can settle into a stable 'off' mode, whereas the glacial THC always recovered spontaneously as soon as anomalous freshwater inputs disappeared.

Acknowledgements *We thank Stefan Mulitza, Carsten Rühlemann and Mark Maslin for helpful suggestions. This research was funded by the Bundesministerium für Bildung und Forschung (BMBF) through DEKLIM and by the Deutsche Forschungsgemeinschaft as part of the DFG Research Center 'Ocean Margins' of the*

University of Bremen (No. RCOM0095).

Chapter V

The Relative Role of Oceanic Heat Transport and Orography on Glacial Climate

Vanya Romanova[1], Gerrit Lohmann[1,2,3], Klaus Grosfeld[1,3], Martin Butzin[4]

[1]Department of Physics, University of Bremen, 28334 Bremen, Germany
[2]DFG Research Center Ocean Margins (RCOM), University of Bre men, 28334 Bremen, Germany
[3]Alfred Wegener Institute for Polar and Marine Research, 27515 Bremerhaven, Germany
[4]Center of Marine Environmental Sciences, 28359 Bremen, Germany

---

Abstract

During the Last Glacial Maximum, the Earth's orography and oceanic heat transport contribute to a cooling in the North Atlantic. By using an atmospheric general circulation model of intermediate complexity, we investigate the sensitivity of the atmospheric temperature and circulation during glacial climate, focussing on the impact of the orography and different oceanic heat transports. The results show a strong dependence of the glacial Northern Hemisphere circulation pattern to the changed orography. The blocking effect of the elevated orography due to the Laurentide Ice Sheet over the North American continent forces a deflection of westerlies, their enhancement and

a southward displacement over the Atlantic. Independently, the glacial climate is influenced by the oceanic heat transport. The reduced oceanic heat transport on the glacial climate shows a 20-40% contribution for the total cooling relative to the present-day climate in the North Atlantic and polar regions. Finally, we find that the altered orography in the Northern Hemisphere and different oceanic heat transports result in a changed hydrological cycle, a reduction of the Hadley circulation and a southward shift of the Intertropical Convergence Zone in the boreal winter during glacial times.

V.1 Introduction

The Last Glacial Maximum (LGM) at about 21,000 years B.P. is the period when the most recent glaciation cycle was at its peak. This period is well captured by marine sediment cores, terrestrial climate records and ice-core data (e.g. Jouzel et al., 1987; Farrera et al., 1999; Mix et al., 1999; Alley and Clark, 1999; Bard, 1999; Clark et al., 2002). The abundance of LGM data allows to reconstruct global sea surface temperature (SST) fields and the sea-ice margins in the Atlantic Ocean. However, various SST reconstructions (e.g. CLIMAP 1981; GLAMAP 2000 - German Glacial Atlantic Ocean Mapping Project; Pflaumann et al., 2003; Mix et al., 2001; Sarnthein et al., 2003; Paul and Schäfer-Neth, 2003; Weinelt et al., 1996) differ in the constructing methodology and in the LGM definitions for time intervals, but all suppose climatic stability with maximum glacial sea level low stand.

The CLIMAP (1981) SST and sea-ice reconstruction is characterized with far to the south reaching sea-ice margins in Northern Hemisphere and general cooling of the surface waters, except for some areas in the tropical Pacific Ocean, where sea temperatures are higher than present-day values. An additional reduction of CLIMAP SSTs in the tropics (Lohmann and Lorenz, 2000) can provide for consistency with more actual paleo-data (Farrera et al., 1999) and snow lines (Lorenz and Lohmann, 2004). The CLIMAP (1981) reconstruction with applied additional tropical cooling at the surface boundary of an ocean model provokes weakening of the overturn-

ing circulation (Prange et al., 2002; Knorr and Lohmann, 2003). However, some new reconstructions give evidence for substantially reduced sea ice coverage with vast ice-free areas in the Nordic Seas (Weinelt et al., 1996; de Vernal and Hillaire-Marcel, 2000; Sarnthein et al., 2003; Paul and Schäfer-Neth, 2003). The GLAMAP 2000 (Pflaumann et al. 2003, Sarnthein et al., 2003; Paul and Schäfer-Neth, 2003) and Weinelt et al. (1996) SST reconstructions, taken as boundary conditions to an ocean general circulation model (OGCM), provoke even intensified overturning strength compared to the present-day simulation (Romanova et al., 2004; Prange et al., 2004), which maintains the warm temperatures in the Nordic Seas. To examine the atmospheric response to different oceanic background conditions, we use the corresponding heat transports, as obtained from an OGCM integrated under LGM conditions, to force an atmospheric general circulation model (AGCM).

During the LGM the orography over North American and European continents was altered due to the highly elevated Laurentide, Fennoscandian and Barents Sea Ice Sheets. Along with the modified thermal forcing, the changed orography over North America can strongly influence the atmospheric circulation causing splitting of the zonal flow and its deviation from the present-day circulation (Kutzbach and Wright, 1985; Manabe and Broccoli, 1985; Broccoli, 2000). As well, the blocked entrance of the Barents Sea and the bildup of continental ice on the Barents Sea shelf during LGM can influence the hydrological cycle over northwest Europe and have a significant impact over North Atlantic Ocean (Pflaumann et al., 2003).

The relative importance of thermal and orographic forcing for the extratropical stationary wave field in dependence of the strength of the zonal mean flow was investigated by several authors. Using an AGCM, Nigam et al. (1987), found that the orographical factor is two times bigger than the heating factor in the upper troposphere, and that their contributions are equal for the lower troposphere. Other authors (Valdes and Hoskins, 1989; Chen, 2000) found predominance of the thermal factor for maintaining the extratropical stationary wave structure in the lower troposphere. Held and Ting (1990) pointed out that the dominance of each factor depends mainly on the strength of the low-level midlatitude westerlies. Using a

coupled atmosphere-ocean climate model, Kim (2004) investigated the effect of the ice sheet topography and the change of CO_2concentration on the LGM climate. He found that the LGM climate cooling is more than half due to the reduction of the atmospheric CO_2.

This study, therefore, provides LGM simulations forced with oceanic heat transports, based on different glacial reconstructions, and concentrates on the sensitivity of the atmospheric circulation system to: i) different thermal forcing conditions; ii) large-scale orographic obstacles as the Laurentide Ice Sheet over North American continent; and iii) the glacial atmospheric CO_2reduction. Its objective aim is to decompose the effects of orographically and thermally induced responses and to assess the significance of each factor for the modified flow regime compared to the present-day conditions. The paper is organized as follows: the second section gives a description of the methodology and the experimental set-up, and the third section shows the results. The results are discussed in section 4, and the conclusions are given in sections 5.

V.2 Methodology

V.2.1 Boundary conditions

The present-day simulation is forced with SST and ice compactness taken from the Atmospheric Model Intercomparison Project (AMIP) (Phillips et al., 1995). The temperature fields represent climatological averages for the time period from 1979 to 1994. The CLIMAP (1981) SST and sea-ice extent reconstruction for the Last Glacial Maximum, based on foraminiferal assemblages, is taken as a boundary condition for simulating glacial conditions. The validity of CLIMAP reconstruction is strongly discussed, especially in the tropical areas (e.g. Farrera et al., 1999; Mix et al., 1999; Bard, 1999) indicating too warm SSTs. Hence, one experiment

is carried out forced with CLIMAP (1981) SSTs but additional cooling of 3°C in the tropics. This experiment aims to reduce the temperature discrepancies between marine and terrestrial proxy data for the LGM. The new reconstruction, GLAMAP 2000, provides SSTs and sea-ice margins for another boundary condition. In this reconstruction, the winter sea ice extent is similar to the CLIMAP summer sea ice margin and the Nordic Seas are ice-free during summer months. The average surface temperature in the Atlantic Ocean is by 0.7°C higher than in the CLIMAP reconstruction.

The glacial runs use glacial orography, land-sea and glacier masks (Peltier, 1994). The CO_2 concentration is fixed to 360 ppm for the present-day experiment and is reduced to 200 ppm for the glacial run according to observational values (e.g. Barnola et al., 1987; Keeling et al., 1996). The Earth's obliquity, orbital eccentricity and vernal equinox mean longitude of perihelion for the present day and glacial runs are taken for the years 2,000 year A.D. and 21,000 year B.P., respectively, and are calculated according to Berger (1978).

V.2.2 Ocean circulation model

The above mentioned SSTs and sea-ice cover are applied to the AGCM ECHAM3/T42 (Roeckner et al., 1992; Lohmann and Lorenz, 2000). The resulting monthly averaged surface air temperatures, surface freshwater fluxes and wind stresses serve as forcing fields for the OGCM LSG (Large Scale Geostrophic, Maier-Reimer et al., 1993). The ocean model integrates the momentum equations, including all terms except the nonlinear advection of momentum. It has a horizontal resolution of 3.5°x3.5° and 11 vertical levels. The advection scheme for the temperature and salinity is a third-order QUICK scheme (Leonard, 1979; Schäfer-Neth and Paul, 2001; Prange et al., 2003). Vertical diffusivity is explicitly prescribed ranging from 0.3 cm^2s^{-1} at the surface up to 3.2 cm^2s^{-1} in the abyssal ocean, as obtained from simulations of oceanic radiocarbon (Butzin et al., 2003). A heat

flux parameterization is applied, which allows for scale selective damping of surface temperature anomalies (Prange et al., 2003) and the free evolution of the SSS (sea surface salinity). The model includes a parameterization of overflow. The glacial sea level is reduced by 120 m, the Bering Strait is closed and the Barents Sea is ice covered, leading to a blocking of the ocean currents in these regions. The equilibrium states are obtained after 5500 years of model integration, initialized with present-day conditions and with an additional global salinity increase of 1 psu. The 10 years monthly averaged SST fields, as simulated by the ocean model, are applied to the bottom boundary of the AGCM PUMA.

V.2.3 Atmospheric circulation model

The atmospheric model used in the present study is PUMA (Portable University Model of Atmosphere) developed at the University of Hamburg (Fraedrich et al., 1998; Lunkeit et al., 1998). The dynamical core of PUMA is based on the multilayer spectral model proposed by Hoskins and Simmons (1975). It integrates the moist primitive equations formulated in terms of the vertical component of the absolute vorticity, the horizontal divergence, the temperature, the logarithm of the surface pressure and the specific humidity. The equations are solved using the spectral transform method (Orszag, 1970; Eliasen et al., 1970). The calculations are evaluated on a longitude/latitude T21 grid of 64 by 32 points, which corresponds approximately to 5.6° in Gaussian coordinates. Five equally spaced, terrain-following sigma levels are used in the vertical direction. The surface fluxes of moisture, heat and momentum are calculated with bulk formulas. Parameterizations for the land and soil temperatures, soil hydrology and river runoff are implemented in the model.

PUMA is classified as a model of intermediate complexity (Claussen et al., 2002) and it is designed to be comparable with comprehensive AGCMs like ECHAM (Roeckner et al., 1992). Previously, it was used for evaluation of stormtracks and baroclinic life cycles (e.g. Frisius et al., 1998; Franzke et al., 2000), for investigating the

atmospheric response during deglaciation (Knorr et al., 2005), and to simulate past climate states such as the LGM in comparision to full AGCM studies (Grosfeld et al., 2005).

The AGCM is coupled to a mixed layer (slab) ocean model. The mixed-layer temperature is calculated following the equation:

$$\frac{dT_{mix}}{dt} = \frac{Q_{atm} + Q_{ocean}}{\rho_w c_{\rho_w} h_{mix}}$$

where, ρ_w and c_{ρ_w} are the water density and the heat capacity, respectively. The mixed layer depth is fixed at 50 m. The atmospheric heat flux is the sum of the net short-wave and long-wave radiative energy fluxes, the sensible heat flux and the latent heat flux due to evaporation. The oceanic heat flux is monthly prescribed in the experimental set-up. The coupled system, forced with prescribed oceanic heat transport, allows prediction of the sea surface temperature. A simple thermodynamic sea ice model is implemented into the system.

V.2.4 Experimental set-up

To simulate the atmospheric present-day and glacial conditions, we perform numerical experiments using at first the PUMA with prescribed SSTs and sea-ice extend. The equilibrium states are obtained after 50 years integration. The present-day experiment using initially the AMIP forcing is denoted with AMIP, and the glacial simulations are indicated with: CLIMAP for the simulation with CLIMAP forcing; CLIMAPc for the simulation with CLIMAP and additional tropical cooling; and GLAMAP for the experiment with GLAMAP 2000 boundary conditions (Table V.1). To calculate the surface heat fluxes $-Q_{atm}$, monthly averages over the last ten modeled years from the experiments with prescribed surface boundary conditions are estimated. These fluxes are applied to the mixed layer ocean model. The heat flux from AMIP is used for five coupled experiments (Table V.1): a present-day experiment (hereafter called the control run); two glacial experiments with orography given by Peltier (1994), the first one with CO_2 equal to 200 ppm (Lau_200)

Prescribed surface temperatures	**Set-up**	**CO_2 (ppm)**	**Orbital parameters**	**Orography**	**Abbreviation**
AMIP	PD	360	2000 y A.D.	Present-day	***AMIP***
CLIMAP	LGM	200	21000 y B.P.	Peltier (1994)	***CLIMAP***
CLIMAP with tropical cooling	LGM	200	21000 y B.P.	Peltier (1994)	***CLIMAPc***
GLAMAP 2000	LGM	200	21000 y B.P.	Peltier (1994)	***GLAMAP***

AGCM+ML experiments with prescribed heat fluxes	**Set-up**	**CO_2 (ppm)**	**Orbital parameters**	**Orography**	**Abbreviation**
10 years averaged surface heat fluxes from exp. ***AMIP***	PD	360		Present-day	***control***
	LGM	200	21000 y B.P.	Peltier (1994)	***Lau_200***
	sensitivity exp.	360	21000 y B.P.	Peltier (1994)	***Lau_360***
	LGM	200	21000 y B.P.	½ Laurentide Ice Sheet	***halfLau_200***
	sensitivity exp.	360	21000 y B.P.	½ Laurentide Ice Sheet	***halfLau_360***
10 years averaged surface heat fluxes from exp. ***CLIMAP***	LGM	200	21000 y B.P.	Peltier (1994)	***LGM_CL***
10 years averaged surface heat fluxes from exp. ***CLIMAPc***	LGM	200	21000 y B.P.	Peltier (1994)	***LGM_CLc***
10 years averaged surface heat fluxes from exp. ***GLAMAP***	LGM	200	21000 y B.P.	Peltier (1994)	***LGM_GL***

Table.V.1: *Overview of numerical experiments and their set-up.*

and the second CO_2 equal to 360 ppm (Lau_360); and two experiments with implemented half height of the Laurentide Ice Sheet with 200 ppm (halfLau_200) and 360 ppm (halfLau_360) CO_2. To visualize the different orography used to force the sensitivity experiments as represented in the model grid, the surface geopotentials for the present-day, the half of the height and the full height of the Laurentide Ice Sheet are shown in Fig. V.1. The difference of the corresponding atmospheric patterns gives the isolated effect of the changed orographic forcing and the effect of changed atmospheric carbon dioxide concentration. The next three experiments (LGM_CL, LGM_CLc and LGM_GL) represent the glacial set-up, using heat fluxes taken from the glacial experiments with prescribed sea surface temperatures CLIMAP, CLIMAPc and GLAMAP, respectively. The latter climatological means, obtained through different thermal forcing, extract the effect of the different oceanic heating on the atmospheric circulation systems.

V.3 Results

V.3.1 The North Atlantic meridional overturning and the oceanic heat transport

The overturning circulations in the Atlantic Ocean as simulated with the OGCM LSG for the present-day simulation and the glacial experiments are shown in Fig. V.2. The maximum transport of the overturning cell is strongest for the present-day ocean and equal to 20 Sv (1 Sv=1x10^6m^{3}s^{-1}). The meridional overturning for the glacial experiments depends on the glacial reconstruction used as a boundary condition. The experiments forced with CLIMAP and GLAMAP 2000 reconstructions yield maximum overturning rates of about 18 Sv. These experiments differ in the location of the NADW (North Atlantic Deep Water) formation (Fig. V.2b and V.2d). The Nordic Seas are ice-free for the summer months in the GLAMAP 2000 reconstruction, which allows NADW to be formed further to the north (Fig. V.2d).

The experiment forced with the coldest boundary conditions - CLIMAP with additionally applied cooling in the tropics - gives 50% (around 10 Sv) reduction of the North Atlantic maximum overturning strength compared to the present-day simulation (Fig. V.2c). Along with the overturning rates, the meridional heat transports in the Atlantic basin differ in the four experiments. At 30°N, the oceanic heat transport is 0.5 PW (1 PW=10^{15} W) for the experiment performed with the coldest SST (CLIMAPc). The experiment forced with the original CLIMAP reconstruction (Fig. V.2b) has a meridional heat transport of 0.8 PW. The highest value is represented by the glacial experiment forced with GLAMAP 2000 at 0.9 PW. All glacial runs possess reduced heat transports compared to the present-day simulation (1.0 PW). The divergences of these oceanic heat transports, represented as Q_{ocean}, are taken as basis of the atmospheric simulations.

Along with the overturning rates, the meridional heat transports in the Atlantic basin differ in the four experiments. At 30°N, the oceanic heat transport is 0.5 PW (1 PW=10^{15} W) for the experiment performed with the coldest SST (CLIMAP with additionally applied tropical cooling). The experiment forced with the original CLIMAP reconstruction (Fig. V.1b) has a meridional heat transport of 0.8 PW. The highest value is represented by the glacial experiment forced with GLAMAP 2000 at 0.9 PW. All glacial runs possess reduced heat transports compared to the present-day simulation (1.0 PW). The divergence of these oceanic heat transports, represented as *Q_ocean*, are taken for basis of the atmospheric simulations.

V.3.2 Surface air temperatures

Mixed layer experiments versus prescribed SST experiments

Global mean surface air temperatures for the simulations with prescribed SSTs and for the experiments performed with a coupled mixed-layer ocean are shown in Fig. V.3. Lowering of global temperatures (of around 1°C) is found for the model

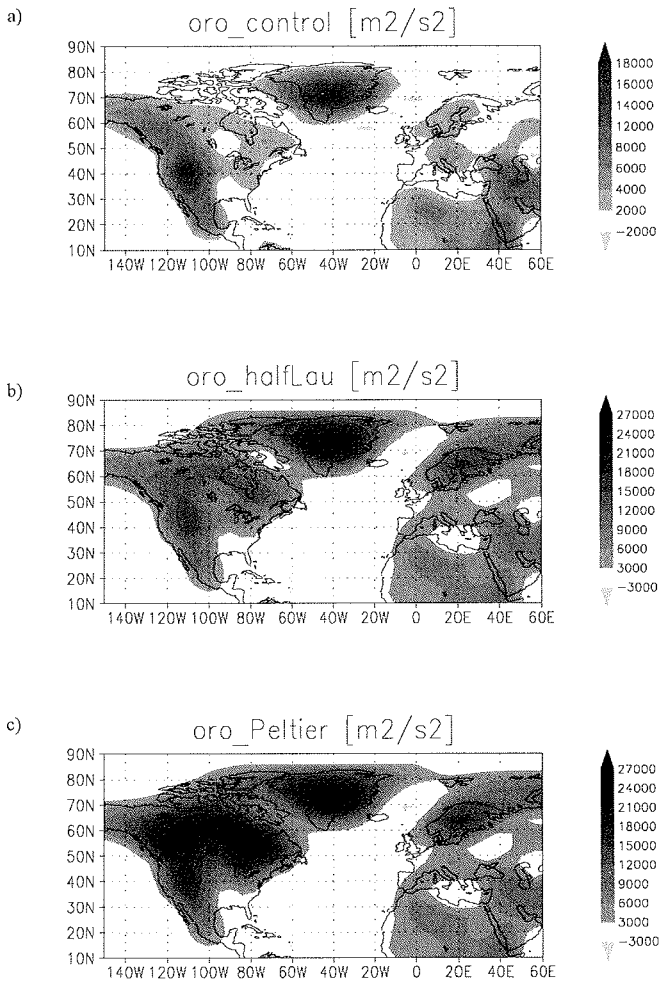

Fig.V.1: *Surface geopotential [m2/s2] for: a) the control run; b) the exp. with half of the height of the Laurentide Ice Sheet; c) the exp. with full height of the Laurentide Ice Sheet..*

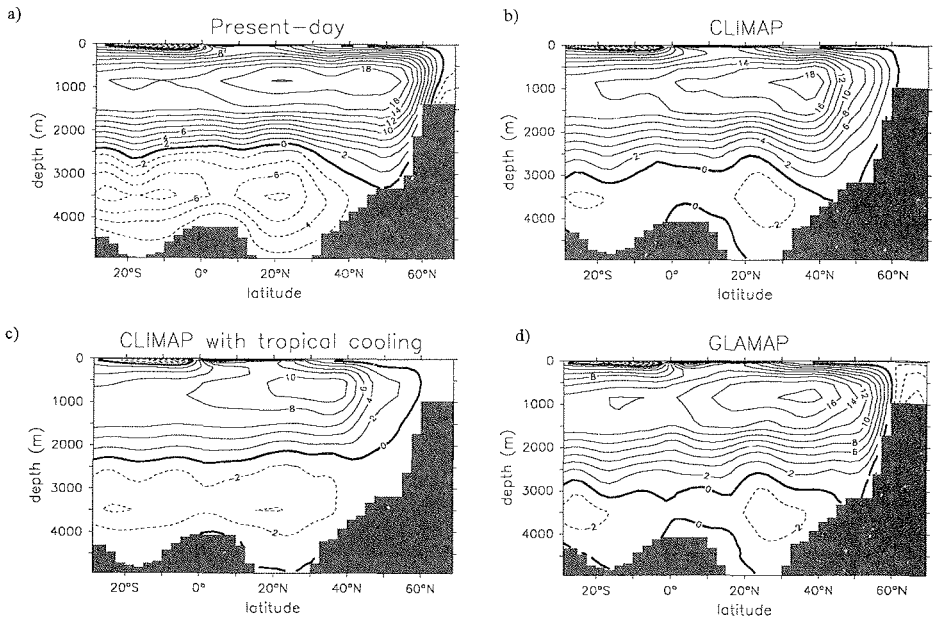

Fig.V.2: *Atlantic meridional overturning stream function for experiments a) present-day simulation; b) LGM exp. forced with the CLIMAP reconstruction (LGM_CL); c) LGM exp. forced with the CLIMAP reconstruction with additionally applied tropical cooling (LGM_CLc); and d) LGM exp. forced with the GLAMAP 2000 reconstruction (LGM_GL). Units are in Sv 1 Sv=1.*$10^6 m^3 s^{-1}$.

runs performed with the coupled model, compared to the experiments forced with prescribed SSTs. The spatial surface temperature patterns and the surface heat fluxes for the experiments with prescribed SST are very similar to the respective ones performed with the mixed layer ocean (not shown). Since the discrepancies in the SSTs are small, we presume that the slab ocean representation yields an adequate heat balance to assure a stable climatological forcing. In the further discussion, we therefore consider only the experiments performed with PUMA coupled to a mixed layer ocean.

The global surface temperature lowering as a result of the reduction of CO_2 from

the present-day value of 360 ppm to 200 ppm is around 0.5°C (Fig. V.3), compare exp.: 1) Lau_360 and Lau_200; and 2) halfLau_360 and half_Lau_200). A similar reduction (0.3°C) of the global surface temperature is provoked by the change of the orography from half of the height of the Laurentide Ice Sheet to full height of the Laurentide Ice Sheet (Fig. V.3, compare exp.: 1) halfLau_360 and Lau_360; and 2) halfLau_200 and Lau_200).

Comparing the SAT of the glacial experiments (Lau_200, LGM_CL, LGM_CLc and LGM_GL) to the present-day experiment, a global temperature lowering is found (Fig. V.3), which is a consequence of the combined effect of the glacial experimental set-up, orbital parameters, glacial ice sheets, and reduced CO_2. The difference between the glacial experiments in the SAT values is solely due to the difference in the oceanic heating. The highest value of the global SAT is found for experiment Lau_200, forced with a present-day heat transport but glacial set-up, and the lowest value for experiment LGM_CLc, forced with the heat transport resulting from the experiment with CLIMAP with additional cooling in the tropics (CLIMAPc).

Comparison of the modeled present-day climate to data

To validate the present-day simulation we use an extended SST data set after Kaplan et al. (1981). The data set represents 145 years of analyzed global SST anomalies (with regards to normals of 1951-1980) on a 5°x5°grid. The monthly SST anomalies were added to the AMIP climatology (Phillips et al., 1995) and the averaged DJF temperatures are plotted in Fig. V.4b. As the SST spatial pattern of the control run (Fig. V.4a) is similar to the SST pattern over the observational period, our heat flux forced climate simulation can be taken as an adequate representation of the present-day climate. The averaged SST differences between the model and the observational data are 0.64°C, 0.07°C and 0.58°C for the Atlantic, Pacific and Indian oceans, respectively.

		Tropics 30°S-30°N (°C)	Midlatitudes 30°N-60°N (°C)	Polar regions 60°N-90°N (°C)
Global	*Lau_200– control*	–2.14	–9.20	–18.98
	Lau_360– control	–0.79	–6.89	–16.93
	HalfLau_200– control	–1.80	–9.08	–17.54
	HalfLau_360– control	–0.52	–6.63	–15.33
	LGM_CL– control	–3.46	–13.55	–24.62
	LGM_CLc– control	–6.20	–15.14	–26.01
	LGM_GL– control	–2.69	–11.80	–22.96
Atlantic	*Lau_200– control*	– 2.17	– 8.78	– 19.33
	Lau_360– control	– 0.84	– 6.89	– 17.37
	HalfLau_200– control	– 2.06	– 8.45	– 17.57
	HalfLau_360– control	– 0.80	– 6.59	– 16.13
	LGM_CL– control	– 3.59	– 13.29	– 24.85
	LGM_CLc– control	– 6.18	– 14.55	– 26.57
	LGM_GL– control	– 3.32	– 11.17	– 23.14
Pacific	*Lau_200– control*	– 2.00	– 7.69	– 11.59
	Lau_360– control	– 0.76	– 5.11	– 9.35
	halfLau_200– control	– 1.90	– 6.90	– 10.94
	halfLau_360– control	– 0.74	– 4.80	– 8.50
	LGM_CL– control	– 3.06	– 14.04	– 18.99
	LGM_CLc– control	– 5.52	– 14.65	– 19.66
	LGM_GL– control	– 2.08	– 11.74	– 17.18

Table.V.2: *Annual mean surface air temperatures (SAT) anomalies with respect to the control run calculated over different global latitudinal belts and over the Atlantic and Pacific Oceans.*

Spatial temperature differences

The spatial pattern of the SAT differences between experiments Lau_200, halfLau_200, Lau_360 and halfLau_360 and the control run are shown in Fig. V.5. Strong cooling of –16°C is found over North American continent, which is provoked only from the half of the height of the Laurentide Ice Sheet and the ice albedo (Fig. V.5c). Simulating a climate with the full height of the Laurentide Ice Sheet adds another –4°C to the North American cooling (Fig. V.5a), thus the temperature is reduced to –20°C. The estimates of the SAT anomalies relative to the present-day climate in different latitudinal belts (Table V.2) show the effect of CO_2 reduction which is comparable to the effect of the elevation increase of the Laurentide Ice Sheet to its maximum height.

All glacial simulations exhibit strong continental cooling in the midlatitudes in the Northern Hemisphere (for all simulations the values are about: Europe –10°C, Siberia –15°C, North America –20°C and Greenland –30°C; not shown). The differences between the experiments appear mainly in the tropics. The coldest experiment LGM_CLc exhibits a decrease of the tropical zonal mean SAT of around –6°C compared to the control run, whereas the experiments LGM_CL and LGM_GL show a decreases of 3°C only (Table V.2). The spatial SAT anomalies relative to the glacial experiment forced with present-day oceanic heat transport (Fig. V.6a,c) show positive anomalies of around 1°C in the tropical regions for the experiments LGM_CL and LGM_GL.

V.3.3 Consequences of different SST forcings on the atmospheric circulation

The global sea level pressure (SLP) pattern over the Northern Hemisphere is relatively well captured in the present-day experiment (control run) (Fig. V.7a). The model simulates the bipolar pressure structure in the North Atlantic, however, its

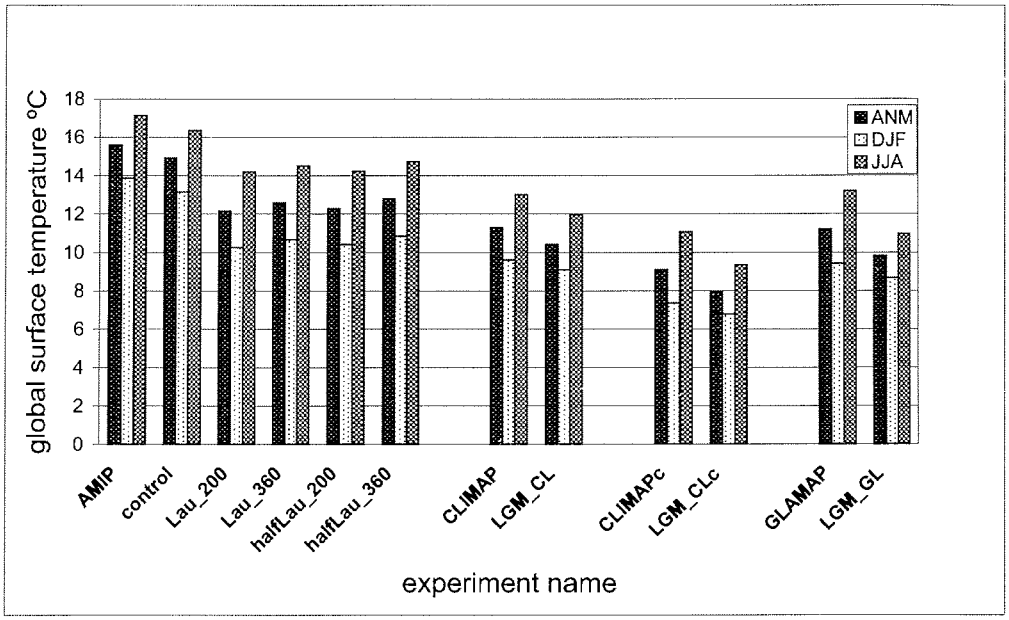

Fig.V.3: *Annual mean, summer and winter global surface air temperatures averaged over a period of 25 years of integration for the different experiments (AMIP, CLIMAP and GLAMAP forced with prescribed SST, and control, Lau_200, Lau_360, halfLau_200, halfLau_360, LGM_CL, LGM_CLc and LGM_GL performed with PUMA coupled to a slab ocean, Table V.1).*

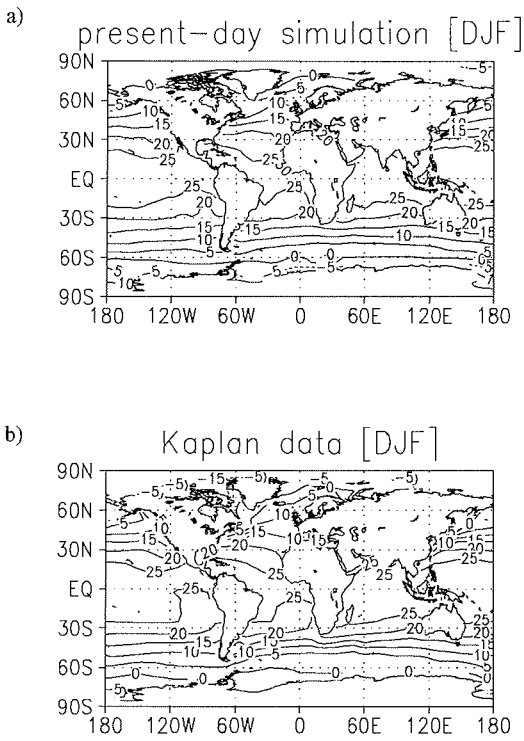

Fig.V.4: *Sea surface temperature a) control run (averaged over a period of 25 years); b) Kaplan et al. (1998) data set.*

strength is slightly underestimated in the present-day experiment. Its deepening appears not as strong as the observational data, due to the coarse model resolution. The Azores High, the Aleutian Low and the Siberian High are well captured by the model, giving a reasonable climatology (Fig. V.7a). The glacial SLP distributions in experiments Lau_200 (Fig. V.7b), LGM_CLc (Fig. V.7d), LGM_CL, and LGM_GL (both not shown) differ from the present day pattern due to the higher glacier elevation, affecting especially the orography over North America. A high-pressure center is situated over the North American continent, which is in contrast to present-day conditions. The Icelandic Low is deepened and shifted to the south-eastern part of the North Atlantic. Thus, the meridional pressure gradient structure is strengthened and dislocated from the present-day configuration. A strong ridge in the sea level isobars is located along the eastern coast of North America, indicating strong advection of warm air from the tropics. The high pressure center over the elevated orography of the North American continent is located oppositely to the Siberian High, and the Aleutian Low is situated against the Icelandic Low pressure. The regular alternation of the highs and lows under glacial conditions provide a wavelike structure of the pressure formations, a feature which is lacking in the present-day climatology. In Fig. V.7c, the sea level pressure field is shown for experiment halfLau_200, experiencing only half of the height of Laurentide Ice Sheet. The zonal pressure structure in this case is already disturbed and the anomalous high isobaric center over the North American continent is already formed.

The annual mean present-day and glacial surface wind patterns in the Northern Hemisphere are shown in Figs. V.8a,b. Enhanced westerlies over the Atlantic Ocean caused by the enhanced strength of the pressure gradient between Icelandic Low and Azores High are representative for the simulated glacial set-ups (Fig. V.8b for experiment Lau_200) compared to the control run (Fig. V.8a). The atmospheric flow, originating from the Pacific Ocean, turns to the north and is tending to overpass the glacier's orography along with the barotropic vorticity balance. After entering the American continent, the flow sets southward in anticyclonic rotation. Over central North America it turns to a cyclonic circulation and enters the Atlantic Ocean, where it is strengthened by the enhanced pressure gradient. The axes of the

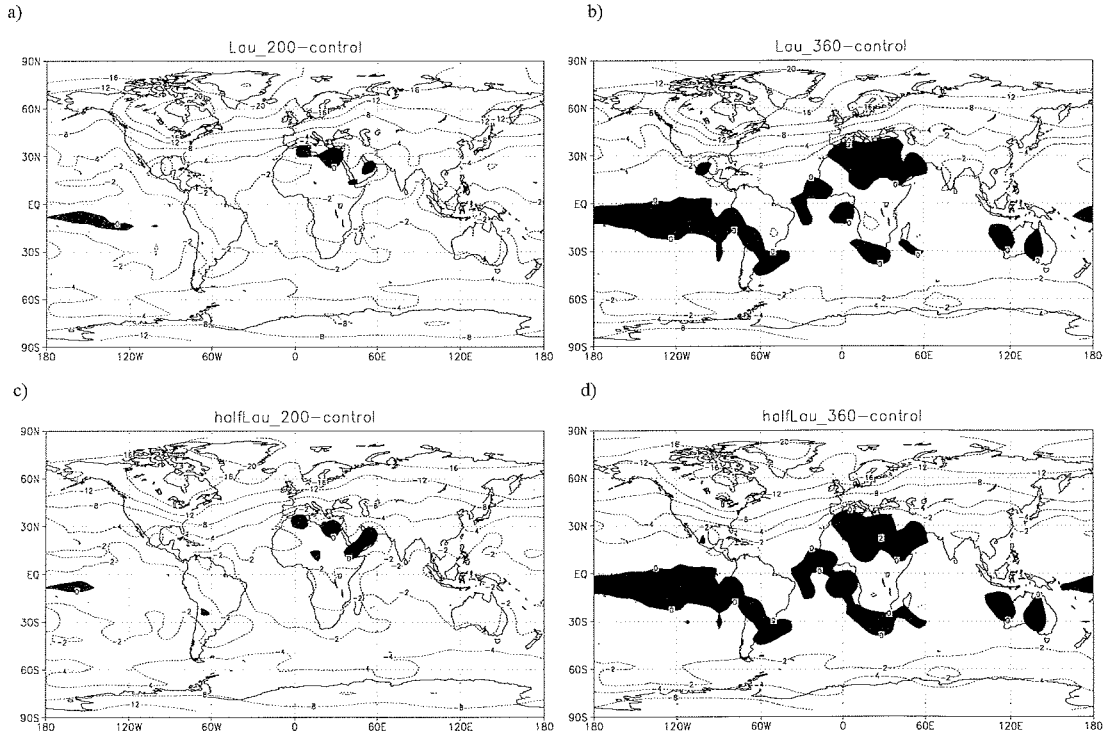

Fig.V.5: *Spatial pattern of the annual mean surface air temperatures anomalies between the experiments: a) Lau_200–control; b) Lau_360–control; c) halfLau_200–control; d) halfLau_360–control. (Contour intervals:* $1^\circ C$ *when* $SAT > 0^\circ C$; $2^\circ C$ *for* $0^\circ C > SAT > -4^\circ C$; *and* 4° *for* $-4^\circ C > SAT$*).*

westerlies over the Atlantic are oriented in southwest-northeast direction and shifted to the south. In the control run, the axes of the westerlies stay clearly zonal and are located more to the north.

The surface circulation over North America depends on the height of the Laurentide Ice Sheet (Fig. V.8c, exp. halfLau_200). The westerlies also divert their trajectories due to the blocking effect of the orography in experiment halfLau_200, but not as pronounced as in the glacial experiments. Their strengthening in the North Atlantic is in between the present-day and the glacial one.

V.3.4 The zonal mean precipitation

To assess different representations of the Hadley circulation and the Intertropical Convergence Zone (ITCZ) for the different glacial reconstructions, the zonal mean precipitation is calculated. The boreal summer and winter zonal mean precipitation values as a function of the latitude are shown in Fig. V.9a,b. The region of maximum precipitation in the boreal summer for the present-day simulation is situated in the Northern Hemisphere, while in boreal winter it is located in the Southern Hemisphere. All the year round it stays close to the equator. The modeled JJA precipitation is in a good agreement with the summer climatological estimates of Jaeger (1976) (Fig. V.9b). The winter precipitation profiles of the control run are consistent over the Northern Hemisphere and equatorial region (Fig. V.9a), but differ substantially over the Southern Ocean. The precipitation maximum at 60°S could be due to uncertainties in the measured data and/or it can not be reproduced by the model due to its coarse resolution. Under glacial conditions, more pronounced seasonality is detected. In the boreal summer the precipitation maximum has shifted deeper to the north and in boreal winter deeper to the south. In the temperate latitudes of the Northern Hemisphere the influence of the Laurentide Ice Sheet is seen, leading to a distinct decrease in glacial precipitation.

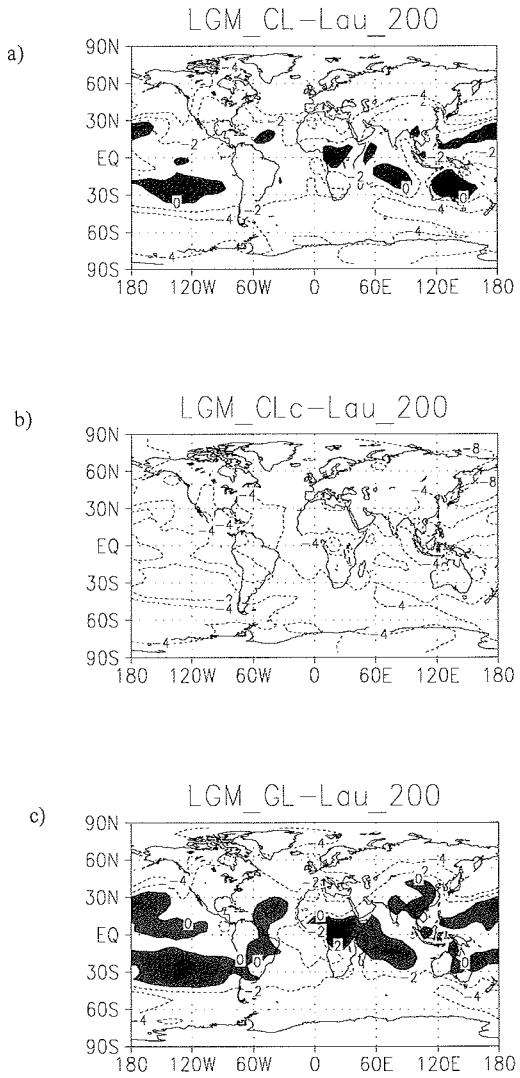

Fig.V.6: *Spatial pattern of annual mean surface air temperatures anomalies between LGM exp. forced with three different oceanic heat flux patterns and the LGM exp. forced with present-day heat fluxes: a) LGM_CL-Lau_200; b) LGM_CLc-Lau_200; c) LGM_GL-Lau_200. (Contour intervals: 1° C when SAT > 0° C; 2° C for 0° C> SAT > −4° C; and 4° for −4° C> SAT).*

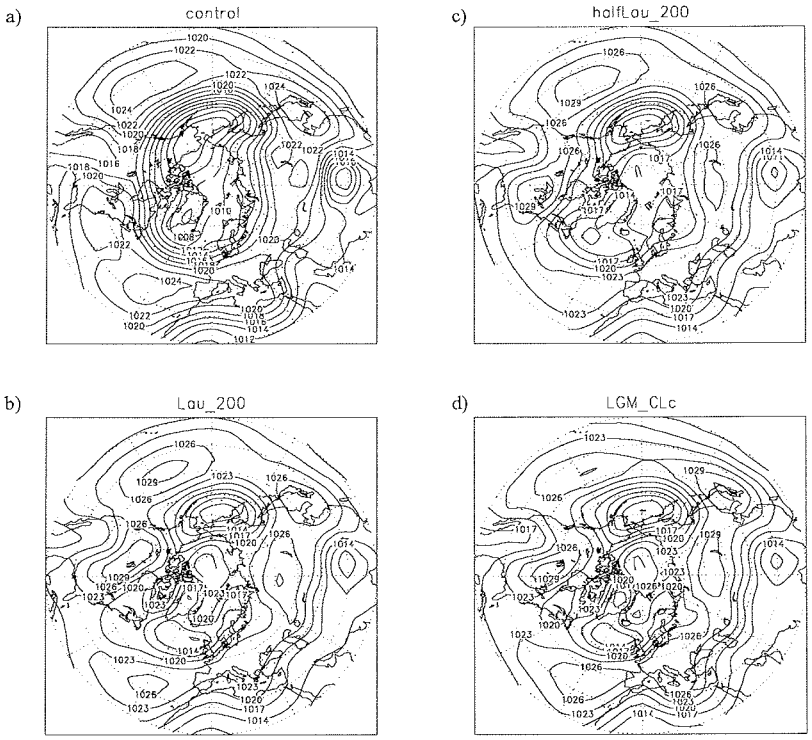

Fig.V.7: *Annual mean sea level pressure for a) the control run; b) Lau_200; c) halfLau_200 and d) LGM_CLc experiments. Units are hPa. The fields are averaged over 25 years of integration.*

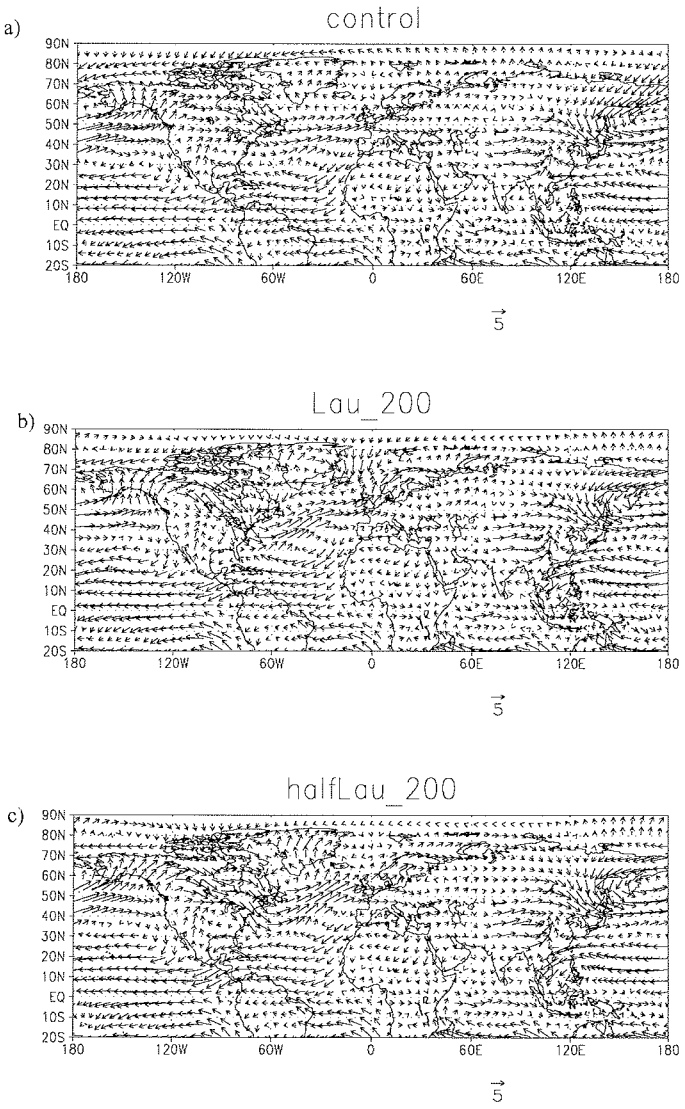

Fig.V.8: *Surface wind field for a) control run; b) Lau_200 and c) halfLau_200 experiments. The fields are averaged over 25 years of integration. Units are* ms^{-1}.

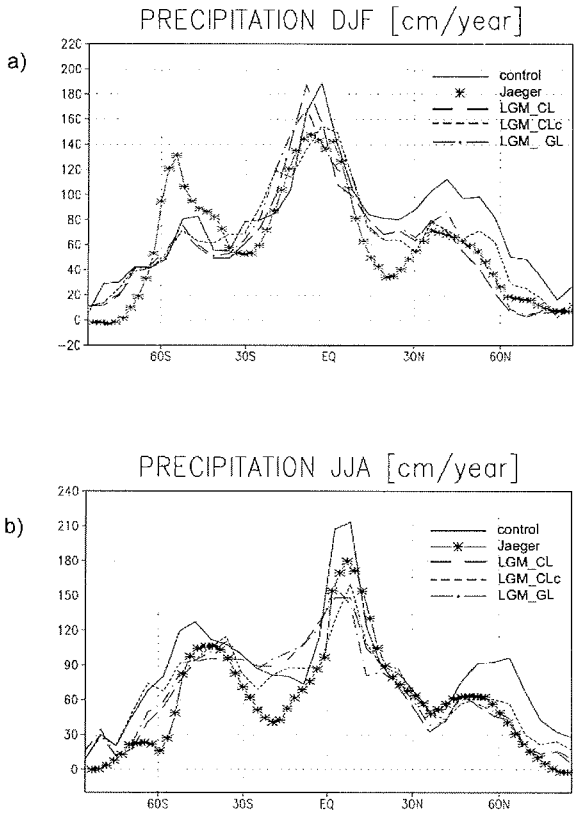

Fig.V.9: *Zonal mean precipitation obtained from the control run and from the experiments LGM_CL, LGM_CLc and LGM_GL, compared with climatological estimates of Jaeger (1976): a) for winter and b) summer seasons. The fields are averaged over 50 years of integration. Units are cm/year.*

V.4 Discussion

The different glacial reconstructions provide different steady states of the ocean circulation with a definite overturning strength. The forcing 'CLIMAP with tropical cooling' produces a weak Atlantic overturning circulation relative to that under present-day conditions. The lowered tropical energy release to the atmosphere, resulting from the imposed tropical cooling in this experiment (LGM_CLc), reduces the capability of the atmosphere to export heat to the north. Thus, the atmospheric circulation leads to a uniform cooling of the globe in experiment LGM_CLc (about 7°C compared to control run, Fig. V.2), and the weak oceanic heat transport in the North Atlantic allows the occurrence of ice formation far to the south. The glacial simulations LGM_CL and LGM_GL, using the oceanic heat transport generated by the ocean experiments with a stronger overturning circulation, are associated with ice-free conditions in the Nordic Seas during summer. The increase of the SAT mainly in the tropical Pacific Ocean is an effect of the high tropical temperatures in the CLIMAP and GLAMAP 2000 reconstructions. The latter is implicitly connected with the enhanced evaporative conditions and water vapour export from the Atlantic Ocean (Lohmann and Lorenz, 2000). The composed effect of changed land ice sheets, oceanic heat transport and hydrology during glacial times affect the tropics by displacing the ITCZ to the south, as shown by coupled and uncoupled model studies (Lohmann, 2003; Chiang et al., 2003). Reduced zonal mean precipitation in all glacial simulations prompt for a weaker Hadley circulation and deeper shifts of the ITCZ towards both sides of the equator (Fig. V.9).

The altered orography during the LGM induces completely different glacial SLP patterns compared to present-day. A new high-pressure center is located over northern North America, which is related to the elevations of the glaciers and appears to be a robust feature for the LGM climate. Thus, a stable wavelike distribution of the SLP is established over the Northern Hemisphere. This leads to excitation of stationary waves, as a bifurcation of the flow occurs from a relatively zonal flow for the present-day to a wavelike structure under LGM conditions (Cook and Held, 1988).

The westerlies from the Pacific Ocean tend to overpass the glaciers from the north, which is in agreement to other model results (e.g., Kutzbach and Wright, 1985; Manabe and Broccoli, 1985). The splitting of the flow in the luff side of the Laurentide Ice Sheet, followed by a southward displacement of a part of the flow, is weakly represented in our simulations, which is a result of the low horizontal resolution of the model. Along with the modified glacial pressure structure in the North Atlantic, the westerlies at the surface are enhanced and displaced to the south. Simulating LGM with an AGCM coupled to a mixed layer ocean, Marsiat and Valdes (2000) found stronger westerlies over the whole atmospheric column and the highest speed over the Atlantic ocean.

The flow deflection in the glacial experiments in the Northern Hemisphere is caused by the diabatic heating and/or orography and transients. The zonal asymmetries in the transient eddy vorticity fluxes play a minor role in maintaining the climatological stationary eddies (Held et al., 2002). Therefore, their contribution for the steady atmospheric state is not considered in this study. A separation of the thermally induced climatological changes from the orographically provoked diversion of the atmospheric flow is carried out through applying different thermal boundary conditions to the mixed layer model keeping the same orography. The analysis of the experimental results shows that the thermal heating, as given through different LGM reconstructions, could contribute from 17% to 40% for the midlaltitude and polar cooling (Table V.2).

Regarding the orographic influence onto the climate, experiment halfLau_200, performed with half of the height of the Laurentide Ice Sheet and the same heat flux forcing as in experiment Lau_200, shows that the effect is already large enough to excite a planetary wave and an anticyclonic formation which is found over the ice sheet. The temperature over the North American continent is lowered by 80% relative to the whole cooling provoked by the 'full' height of the Laurentide Ice Sheet. Therefore, the atmospheric response to the half of the land boundary conditions is not half lowered than the 'full' orography, which points to a non-linear behavior of the climate system to orographic changes.

V.5 Summary and conclusions

We performed AGCM simulations for present day and glacial climates using different oceanic background states and orography. The reference climate is based on present-day SSTs (Phillips et al., 1995), whereas the glacial background climate was derived from different reconstructions based on CLIMAP (1981), CLIMAP SST with additional cooling in the tropics (Lohmann and Lorenz, 2000), and the new reconstruction GLAMAP 2000 (Sarnthein et al., 1996; Paul and Schäfer-Neth, 2003). The oceanic heat transports for present-day and glacial climates are derived from OGCM simulations.

Our experiments aim to systematically analyze the role of the oceanic heat transport and orography for the glacial climate. Since coupled models show mutually inconsistent results (Hewitt et al. 2001, Kitoh 2001, Shin et al. 2003), our admittedly simplified approach provides another perspective to understand the glacial climates.

We find that the elevated North American continent provokes a more wavelike Northern Hemisphere atmospheric circulation relative to a situation when the Laurentide Ice Sheet was absent. The situation is not qualitatively different from a sensitivity experiment where the height of the Laurentide Ice Sheet was reduced. In the glacial experiments, the surface flow over the North Atlantic is enhanced and displaced southward. This flow characteristics is independent of the CO_2 concentration and appears to be robust for the glacial climate. In our first set of experiments, the oceanic heat transport is fixed to present-day conditions. Along with the wavelike Northern Hemisphere atmospheric circulation, the equatorial Pacific Ocean is warmed while the North Atlantic is cooled. Caused by a southward shift of the thermal equator during glacial times, a southward shift of the ITCZ is detected for the boreal winter season. The southward shift of the ITCZ during glacial times affects the interbasin water vapor transport which is important for the large-scale THC under glacial and present day conditions (Lohmann and Lorenz, 2000; Lohmann, 2003).

Additional to the orographic forcing, significant changes of the Northern Hemisphere circulation are induced by the glacial background climate. Assessing, separately, the relative contribution of the ocean circulation and the Laurentide Ice Sheet upon the North Atlantic climate, it is found that the changes of the orography and albedo caused even only with half height of the Laurentide Ice Sheet induce strong temperature changes of about −16°C, whereas a reduced glacial ocean circulation with about half of present day strength induces an additional cooling of about −4°C, only. We conclude therefore, that the strength of the oceanic thermohaline circulation is of secondary importance for the North Atlantic climate relative to the orography and albedo effects induced by the Laurentide Ice Sheet.

In our experiments we have neglected feedbacks connected with the dynamics of the ice sheet and with asynchronous development of the American, Fennoscandian, and Barents Sea Ice Sheets. However, the experiment with half of the height of the Laurentide Ice Sheet can represent a transient state of the glacial continental ice cover and the associated atmospheric reaction. Our study emphasizes the importance of reconstructing the extent and height of the continental ice sheets and including dynamical ice sheets in model experiments, rather than investigating the changes of the oceanic heat transport.

Acknowledgements *We gratefully acknowledge the suggestions and recommendations of M. Prange and F. Lunkeit. We also thank the reviewers for the suggestions and constructive comments which helped to improve the manuscript. This work has been funded through German Ministry for Education and Research (BMBF) within DEKLIM project Climate Transitions.*

Chapter VI

Simulation of extreme climates: effect of land albedo, CO_2, orography, and oceanic heat transport.

Vanya Romanova[1], Gerrit Lohmann[1,2,3], Klaus Grosfeld[1,2]

[1]Department of Physics, University of Bremen, Klagenfurterstr., 28334 Bremen, Germany

[2]Alfred Wegener Institute for Polar and Marine Research, 27515 Bremerhaven, Germany

[3]DFG Research Center Ocean Margins (RCOM), University of Bremen, 28334 Bremen, Germany

---

Abstract

Using an atmospheric general circulation model of intermediate complexity coupled to a sea ice - slab ocean model, we perform a number of sensitivity experiments under present-day orbital conditions and geographical distribution to assess the possibility that land albedo, atmospheric CO_2, orography and oceanic heat transport may cause an ice-covered Earth. Changing only one boundary or initial condition, the model produces open water solutions. Using a proper combination of these varied

forcing parameters a full Earth's glaciation is obtained. We demonstrate, that the most significant factor leading to an ice-covered Earth instability is the high land albedo in combination with initial temperatures set equal to the freezing point. Oceanic heat transport and orography play only a minor role for climate instability. The extremely low concentrations of CO_2 also appear to be insufficient to provoke a runaway ice-albedo feedback, but the strong deviations in surface air temperatures in the Northern Hemisphere point to the existence of a strong nonlinearity in the system. Finally, we argue that the initial condition determines whether the system can go into completely ice covered state, indicating for multiple equilibria, as known from simple energy balance models.

VI.1 Introduction

Investigations of glacial carbonate deposits suggest a sequence of extreme Neoproterozoic climate events (600-800 million years ago). Paleolatitude indicators and paleomagnetic data (Hoffman, et al. 1998; Schmidt and Williams, 1995; Sohl et al., 1999; Evans et al., 2000) imply widespread equatorial glaciation at sea level. It was hypothesised that the Earth was completely ice covered (Kirschvink, 1992; Hoffman et al., 1998; Kirschvink et al., 2000; Hoffman and Schrag, 2002). Still, the question remains, whether the Earth was completely ice covered ('hard snowball' Earth) or some tropical ocean areas remained ice free ('slushball' Earth), and which mechanism drove the climate system into the glaciated state and which allowed the escape from it.

The 'snowball' Earth hypothesis provoked the interest of many climate modellers (e.g., Crowley and Baum, 1993; Jenkins and Frakes, 1998; Hyde et al., 2000; Chandler and Sohl, 2000; Crowley et al., 2001; Poulsen et al., 2001; Donnadieu et al., 2002; Lewis et al., 2003; Donnadieu et al., 2004; Bendtsen, 2002; Stone and Yao, 2004) to simulate an ice covered Earth. Using different types of models, from simple Energy Balance Models (EBM) (Budyko, 1969; Sellers, 1969) to coupled ocean atmospheric general circulation models (OAGCM) (e.g., Poulsen et al, 2001), the role of solar insolation, Earth's rotation rate and high obliquity (Longdoz and Francois,

1997; Jenkins and Frakes, 1998; Jenkins, 2000) has been investigated. Furthermore, the influence of various paleogeography and continental geometries (Poulsen et al., 2002; Donnadieu et al., 2004) during Neoproterozoic era has been analysed.

Such extreme climates in the Earth's history provide the motivation to investigate under what conditions the climate system is susceptible to irreversible changes. Fraedrich et al. (1999) used a general circulation model to investigate the land-albedo effect of homogeneous vegetation extremes - global desert and global forest. It was found that the dominant signal is related to changes in the hydrological cycle and that the altered water and heat balance at the surface has a potential impact on regional climate. Wyputta and McAvaney (2001) showed that during the Last Glacial Maximum (LGM) the land albedo increased with 4% due to vegetation changes. In addition to this, the influence of the mountain chains and highly elevated glaciers with strong ice albedo feedback leads to large climate anomalies and an alteration of the atmospheric circulation and precipitation patterns (Lorenz et al., 1996; Lohmann and Lorenz, 2000; Romanova et al., 2004). The increase of the oceanic heat transport is also considered to be a crucial factor to prevent Earth's glaciation. For example, Poulsen et al. (2001) investigated the role of the oceanic heat transport in 'snowball' Earth simulations and concluded that it could stop the southward advance of glaciers, such that a 'snowball' Earth could not occur. Moreover, the atmospheric CO_2 level could also lead to a climate instability and a runaway sea-ice albedo mechanism (Poulsen, 2003). The magnitude of the atmospheric greenhouse gas concentrations, causing glaciation, is still under intense debate (e.g. Chandler and Sohl, 2000; Donnadieu et al., 2004).

In this study, we are interested in the sensitivity of the climate to changes of the land albedo, orography, oceanic heat transport and CO_2 concentration. Using an AGCM of intermediate complexity we investigate the climate response to some extreme configurations of the boundary conditions. Therefore, we perform experiments with different land albedo values and investigate scenarios, in which the land is completely covered with oak forests, glaciers or deserts. We have chosen sensitivity experiments with extreme orographical and oceanic heat transport forcings, and with respect to

the 'snowball' Earth hypothesis, we vary the CO_2 concentrations to some extreme values.

The paper is organized as follows: in Section 2 the model is briefly described and the experiments are outlined, Section 3 reviews and analyses the results, and in Section 4 the results are discussed and conclusions are given.

VI.2 Methodology

VI.2.1 Model Design

The atmospheric general circulation model (AGCM) used in our study is PUMA (Portable University Model of the Atmosphere) developed in Hamburg (Friedrich, 1998; Lunkeit et al., 1998). It is based on the primitive equations transformed into dimensionless equations of the vertical component of absolute vorticity, the horizontal divergence, the temperature, the logarithm of the surface pressure and the specific humidity. The equations are solved using the spectral transform method (Orszag, 1970; Eliasen et al., 1970), in which the variables are represented by truncated series of spherical harmonics with wave number 21. The calculations are evaluated on a longitude/latitude grid of 64 by 32 points, which corresponds approximately to a 5.6° resolution in Gaussian grid. In the vertical direction five equally spaced, terrain-following sigma levels are used. The land and soil temperatures, soil hydrology and river runoff are parameterized in the model.

PUMA is classified as a model of intermediate complexity (Claussen et al., 2002) and it is designed to be comparable with comprehensive AGCMs like ECHAM (Roeckner et al., 1992). Previously, it was used to study stormtracks and baroclinic life cycles (e.g. Frisius et al., 1998; Franzke et al., 2000) and to investigate multidecadal atmospheric response to the North Atlantic sea surface temperatures (SST) forcing

Sensitivity experiments		**CO2**	**Orography**	**Abbreviation**
AMIP (prescribed at the surface)		360	Present-day	***Exp_prescr***
10 years averaged surface heat fluxes from exp. ***Exp_prescr***		360	Present-day	***Exp_slab*** ***(control run)***
Albedo	albedo land - 0.2 albedo ocean - 0.069	360	Present-day	***Exp_alb02***
	albedo land - 0.8 albedo ocean - 0.069			***Exp_alb08***
	albedo land: 0.8 initial temp: - 1.9° C heat transport: zero			***Exp_IP*** (ice-planet)
Sensitivity toward initial and boundary conditions	albedo land: 0.8 initial temp: - 1.9° C **heat transport: PD**	360	Present-day	***ExpIP_HfPD***
	albedo land: 0.8 **initial temp: PD** heat transport: zero			***ExpIP_iniTempPD***
	albedo land: free initial temp: - 1.9° C heat transport: zero			***ExpIP_albfree***
	Initial state ***Exp_IP*** Albedo land: free Heat transport: zero			***ExpIP_iniIP***
CO_2 - 1 ppm		1	Present-day	***Exp_1***
CO_2 - 10 ppm		10	Present-day	***Exp_10***
CO_2 - 50 ppm		25	Present-day	***Exp_25***
CO_2 - 200 ppm		200	Present-day	***Exp_200***
CO_2 - 720 ppm		720	Present-day	***Exp_720***
CO_2 - 1440 ppm		1440	Present-day	***Exp_1440***
Zero orography		360	Zero	***Exp_flat***
Glacial orography		360	(Peltier 1994)	***Exp_glac***
Zero heat transport		360	Present-day	***Exp_zero***

Table.VI.1: *Overview of numerical experiments and their set-up.*

(Grosfeld et al., 2004) as well as to simulate glacial climates (Romanova et al., 2004).

PUMA is coupled to a mixed layer ocean model, which allows the prognosis of the sea surface temperatures (SST). The mixed layer ocean is forced with the oceanic heat transport and its depth is fixed at 50 m. A simple zero layer thermodynamic sea ice model is also included. The temperature gradient in the sea ice is linear and eliminates the capacity of the ice to store heat. Sea ice is formed if the ocean temperature drops below the freezing point (–1.9°C), and melts whenever the ocean temperature increases above this point. The albedo for sea ice, glaciers and snow-covered areas is a linear function of the surface temperature. The minimum and maximum albedo for sea ice is 0.5 and 0.7, respectively, that for glaciers is 0.6 and 0.8, and that for snow varies from 0.4 to 0.8. The albedo of water is set at 0.069.

VI.2.2 Model set-up

To initialise the control run, a spin-up run (Exp_prescr, Table VI.1) is performed with prescribed SSTs and sea ice margins. The values of the global SST are taken to be equal to the climatological mean for the time period between 1979 and 1994 from the Atmospheric Model Intercomparison Project (AMIP) (Phillips et al., 1995). The CO_2 concentration is fixed at 360 ppm. The orography and land-sea masks are set to present-day conditions. An equilibrium state of the spin-up run is obtained after 50 model years. The calculated 10 years monthly averaged total surface heat fluxes from Exp_prescr are taken to be equal to the oceanic heat fluxes, which serve as a forcing for the mixed layer ocean model. Thus, the oceanic heat transport is prescribed for the coupled simulations and is taken to be the same for all sensitivity studies described below, except for those which investigate the impact of zero oceanic heat transport. The maximum value of the oceanic heat transport is 1.0 PW at 30°N (Butzin et al., 2004; Romanova et al., 2004) and represents a realistic value for present-day conditions (Macdonald and Wunsch, 1996). The simulation, forced with the present-day heat transport, is called the 'control run' (Exp_slab, Table VI.1).

For all experiments, the Earth's orbital parameters are taken for the year 2000 A.D., and are calculated according to Berger (1978).

There are four groups of sensitivity experiments (Table VI.1):

1. The first group of experiments includes sensitivity studies related to variations of the surface albedo. In Exp_alb02 the land albedo is fixed to 0.2, corresponding to a warmer than present-day Earth, in which all the continents are being forested. In Exp_alb08, the land albedo is set to 0.8, corresponding to all continents being completely covered by glaciers. One experiment is performed to simulate Earth's complete glaciation. In this experiment, called 'Ice Planet' simulation (abbr. Exp_IP), the land albedo is fixed to 0.8, the oceanic heat transport is set to zero and the initial SST field is uniformly set to −1.9 °C, the freezing temperature of seawater.

2. The second group of experiments investigates the influence of different initial and boundary conditions in the 'Ice Planet' simulation. Only one initial or boundary condition is changed in each experiment. In ExpIP_HfPD the oceanic heat transport is changed to that of present-day (same as control run). In experiment ExpIP_iniTempPD the initial surface temperature field is set to that from AMIP data; and in ExpIP_albfree the albedo is free to develop. An additional experiment ExpIP_iniIP is performed, starting from a planet covered with snow (with intermediate snow albedo of 0.6), zero heat transport and an initial temperature equal to the freezing point. This experiment is run for 6 months and then the surface albedo is allowed to develop.

3. The third group of experiments is performed to investigate the sensitivity of the climate system to carbon dioxide concentration. The experiments are run under present-day boundary conditions with different atmospheric CO_2 values. The highest concentration is taken to be 4 times the present-day value of 360 ppm and the lowest is 1 ppm, corresponding to a 'clear' atmosphere. In between these values, simulations are carried out with CO_2 concentrations of 10, 25, 200 and 720 ppm (abbreviated Exp_1440, Exp_720, ... Exp_1; Table VI.1).

4. The fourth group of experiments investigate the sensitivity of the system related to orography and oceanic heat transport. In experiment Exp_flat, the orography is taken to be zero and in the experiment Exp_glac the orography is the glacial one as given by Peltier (1994). In the experiment Exp_zero, zero oceanic heat transport is applied to the mixed layer model (Table VI.1).

The experiments are integrated over 50 years, when they reach the equilibrium state. All results shown represent averages over the last 25 years of integration.

VI.3 Results and analyses

VI.3.1 Sensitivity related to changes of the land albedo

The annual mean spatial pattern of the absolute values of the surface air temperatures (SAT) results for the control run, for the experiments with prescribed surface albedo of 0.2 and 0.8 and for the ice-planet simulation are shown in Fig. VI.1. The grey shading indicates the sea-ice coverage. A slight decrease of the land albedo to 0.2 (Exp_alb02, Fig. VI.1b) compared to the present-day simulation (control run, Fig. VI.1a) leads to a global warming of around 1°C (Table VI.2) and a retreat of the sea-ice margin. Especially in high latitudes, the SAT increases and the sea ice retreats along the Antarctic coast. Contrary, a drastic increase of the albedo over the land to 0.8 (Fig. VI.1c), results in a decrease of the global annual mean SAT to about 18°C (Table VI.2) and the temperature at the equator of the Atlantic Ocean is less than 15°C (Fig. VI.1c). Sea-ice is formed closer to the equator as its margin reaches 40°N and 50°S. The experiment Exp_IP shows a full Earth glaciation. The global temperature falls to approximately –50°C, and over the Antarctica it reaches –80°C (Fig. VI.1d). The calculated globally averaged surface albedo and the planetary albedo (Table VI.2) show that the planetary albedo is larger with 82% and 158% than the surface albedo in the control run and Exp_alb02, due to the high

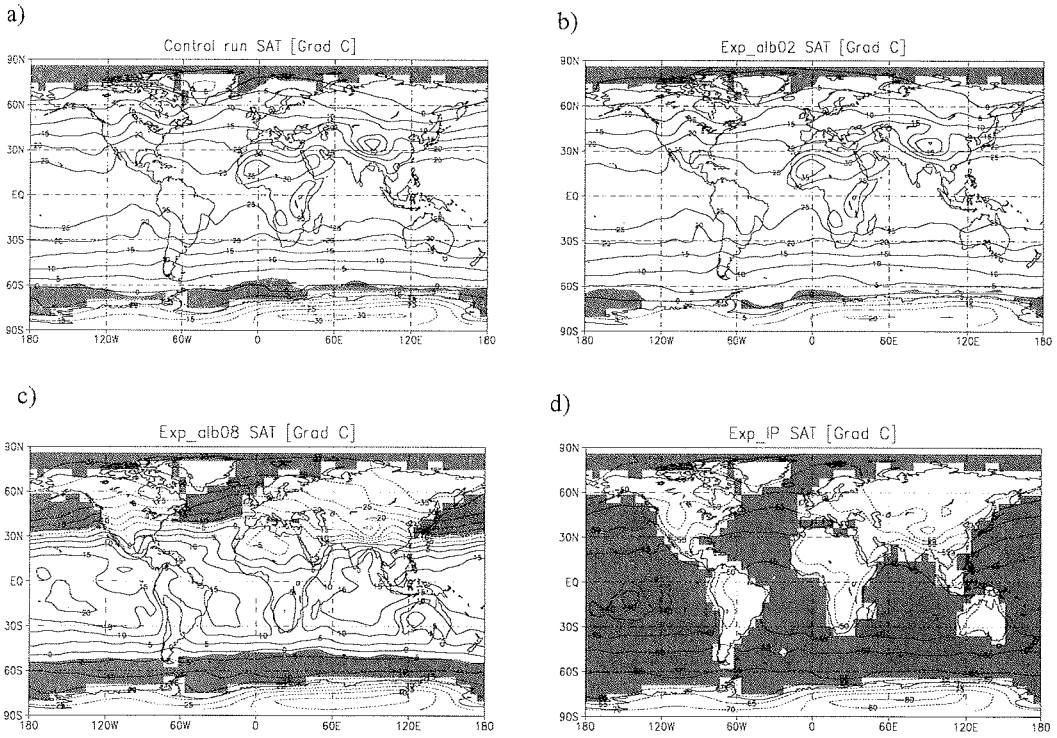

Fig.VI.1: *Spatial pattern of the annual mean surface air temperatures averaged over a period of 25 years of integration for experiments a) control run; b) Exp_alb02; c) Exp_alb08; and d) Exp_IP. The grey shading indicates the annual mean sea-ice cover.*

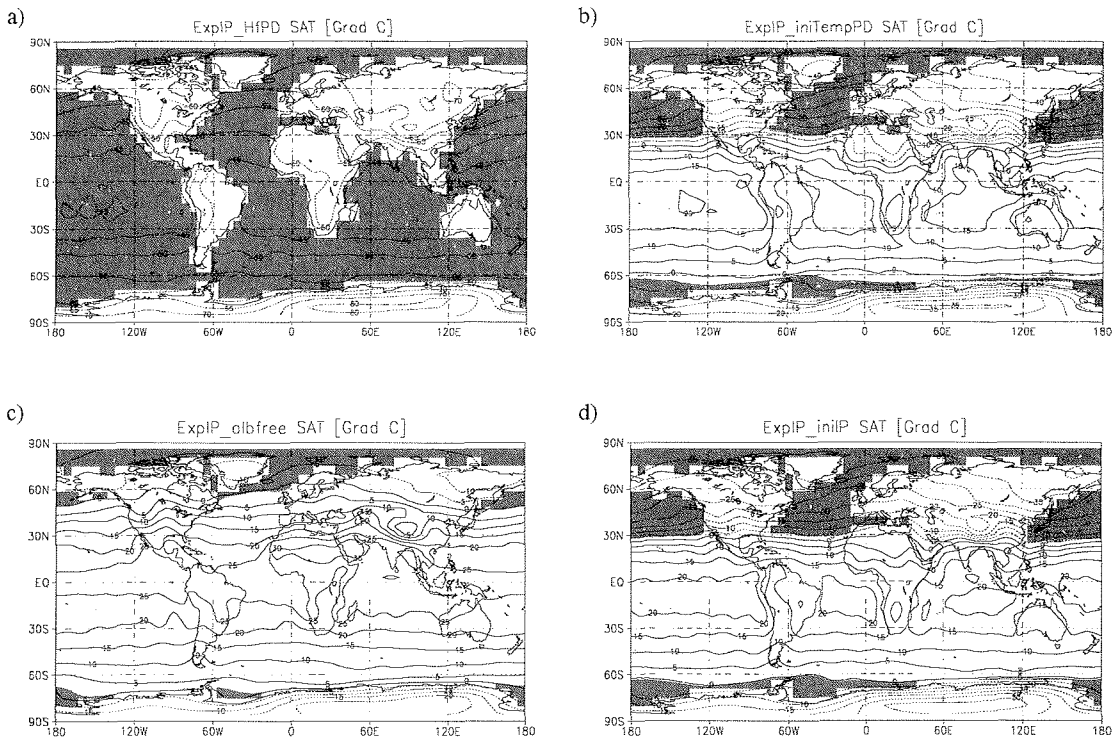

Fig.VI.2: *As in Fig. VI.1, but for experiments a) ExpIP_HfPD; b) ExpIP_iniTempPD; c) ExpIP_albfree; and d) ExpIP_iniIP.*

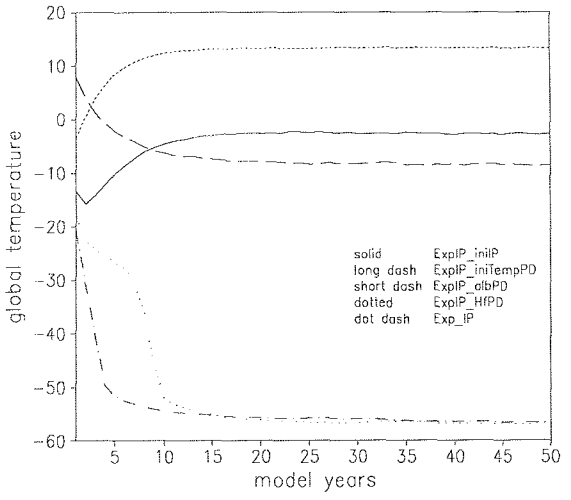

Fig.VI.3: *Time series of global average surface temperature for ExpIP_HfPD, ExpIP_iniTempPD, Ex pIP_albfree, ExpIP_iniIP and Exp_IP.*

rates of evaporation and cloud formation. In experiment Exp_alb08 it is only 5%. On contrast to this, in the ice planet simulation (Exp_IP) the surface albedo is larger (approximately 6%) than the planetary albedo.

VI.3.2 Sensitivity of the Ice Planet simulations

To isolate the effect and determine the importance of each boundary and initial conditions, sensitivity experiments of the Ice Planet simulation are performed, holding only one of the boundary conditions constant the same as in the case of the control run. Changing the heat transport to present-day values, the model simulation does not generate any considerable change in the SAT pattern (Fig. VI.2a). The temperatures increase slightly with approximately 5°C but the earth remains ice covered in the equilibrium state, which is reached about 5 years later than in the Exp_IP (Fig. VI.3). If the initial temperature is set to present-day (AMIP) values, the planet does not end in a full glaciation, although a strong sea-ice formation in

Exp. name	Global Temperature (°C) ANM	DJF	JJA	Planetary Albedo (%)	Surface Albedo (%)
control	17.00	15.84	18.36	31	17
Exp_alb02	18.33	17.21	19.65	31	12
Exp_alb08	-0.36	-1.26	1.10	41	39
Exp_IP	-50.58	-49.20	-52.11	69	73
ExpIP_HfPD	-50.84	-49.61	-52.23	69	73
ExpIP_iniTempPD	-1.02	-2.76	1.21	42	38
ExpIP_albfree	16.14	14.66	17.15	32	18
ExpIP_iniIP	2.94	1.23	5.17	39	33
Exp_1	-7.06	-6.73	-6.76	40	39
Exp_10	0.15	-0.50	1.35	37	33
Exp_25	7.61	6.84	8.97	33	26
Exp_200	14.25	13.03	15.85	32	20
Exp_720	19.35	18.20	20.76	32	15
Exp_1440	21.64	20.54	22.99	32	13
Exp_glac	13.96	12.54	15.80	33	23
Exp_flat	18.23	17.02	19.70	31	16
Exp_zero	16.19	14.75	17.96	32	17

Table.VI.2: *Annual mean, DJF and JJA surface air temperatures (SAT) and globally averaged surface and planetary albedo.*

the Northern Hemisphere occurs and the global temperature is almost 20°C lower compared to control run (Table VI.2 and Fig. VI.3). Leaving the land albedo free in ExpIP_albfree, the global temperature increase to about 16°C (Fig. VI.2c) and the spatial temperature pattern tends to resemble the control run. An increase of the temperature (of about 10°C) also occurs in the experiment ExpIP_iniIP, in which the land albedo was released free to develop after 6 months of the Ice Planet integration (Fig. VI.2d, Fig. VI.3). The relation between the surface and planetary albedo in the last two sensitivity experiments is similar to the present-day conditions (the planetary albedo is larger than the surface albedo), characterised by an evaporation regime and cloud formation (Table VI.2).

The decrease of temperature in the first two sensitivity experiments shows that

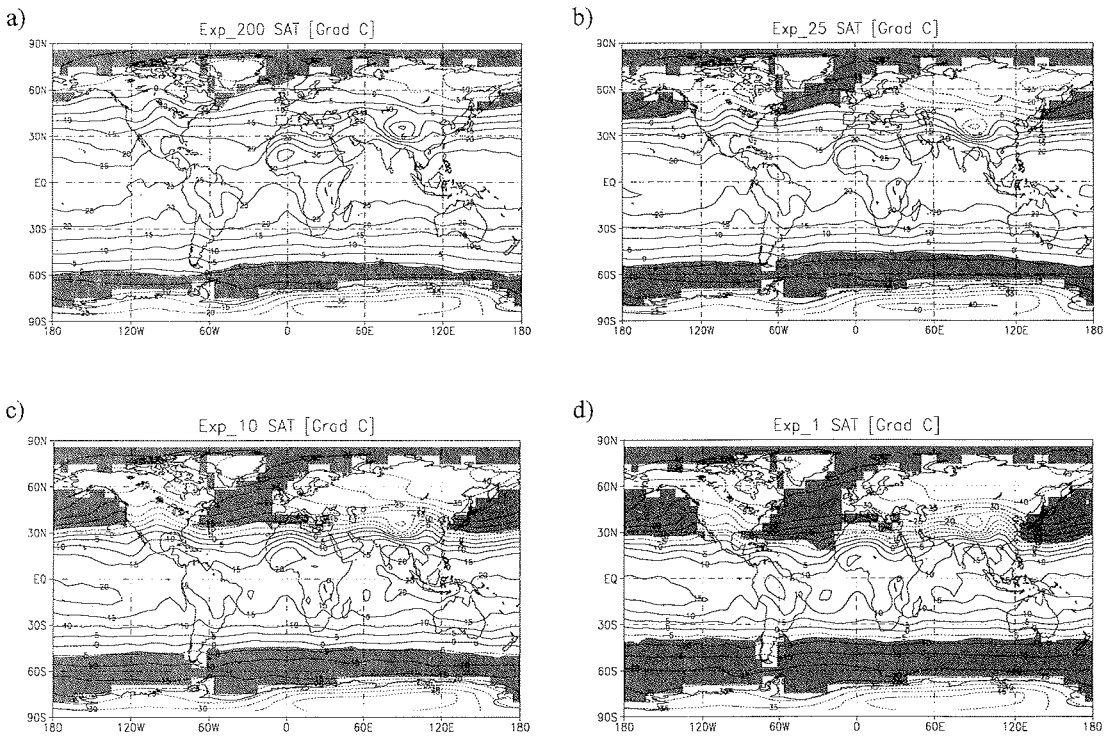

Fig.VI.4: *As in Fig. VI.1, but for experiments a) Exp_200; b) Exp_25; c) Exp_10; and d) Exp_1.*

the oceanic heat transport and the initial temperature are not sufficient to prevent the global cooling. The global glaciation occurs independently of the oceanic heat transport. On contrast to this, the increased land albedo provokes the planet's warming and appears to be the most important factor for the change of the climate system.

VI.3.3 Sensitivity of the climate system to CO_2 concentration

A fourfold increase of CO_2 concentration relative to present-day values, results in a more than 4°C increase of the global temperature, and a two fold increase of the CO_2 concentration provokes a 2°C global warming (Table VI.2). Reduction of CO_2 to 1 ppm results in a global cooling of 25°C compared to the control run, yielding an annual mean SAT of –7°C in Exp_1. In Fig. VI.4 the SAT and the sea-ice margin evolution for experiments with CO_2 concentration of 200, 25, 10 and 1 ppm are shown. Reduction of CO_2 cools the planet, sea-ice is formed closer to the equator, and the positive ice-albedo feedback is initiated. Nevertheless, the reduction of CO_2 under present-day geography and orbital conditions is not sufficient to cause a full glaciation of the planet.

VI.3.4 Orography and oceanic heat transport

In Fig. VI.5 the spatial SAT pattern of the experiments investigating the role of orography and ocean heat transport are shown. Applying zero orography (Exp_flat), the simulation shows global warming of 1°C (Table VI.2). In Fig. VI.5a it is shown that, the warming is not uniformly altered. Over land, the impact is more obvious, as the temperature anomaly can reach up to 8°C in the Himalayas Massive and around 22°C in the Antarctic. Warming also occurs over the Pacific and almost over the entire Atlantic. Still, cooling is noted in some areas of the North Atlantic and the whole Southern ocean (up to –2°C).

The experiment, forced with glacial orography (Peltier, 1994) and present-day heat transport generates cooling (globally about 3°C Fig. VI.5b). Strong North American, North Atlantic, and Eurasian cooling of –16°C to –20°C is due to the highly elevated Laurentide Ice Sheet, influencing generally the atmospheric circulation pattern (Romanova et al., 2004). Along with a global cooling, an equatorial Pacific warming is found, a feature similar to that in the CLIMAP (1981) reconstruction of

the Last Glacial Maximum. To investigating the role of the oceanic heat transport separately, we carried out an experiment, in which all boundary conditions are set equal to those in the control run and only the ocean heat transport was reduced to zero. This experiment Exp_zero shows warming in the Southern Hemisphere (SH) and cooling in the Northern Hemisphere (NH). This see-saw effect is due to a changed ocean heat redistribution. When the meridional oceanic heat transport is prohibited, the SH warms up and the heat exchange between the hemispheres is sharply reduced. A surplus of heat is found in the SH and a lack of it in the NH.

VI.3.5 Zonal mean SAT anomalies

An overview of the zonally averaged temperature anomalies relative to the control run is shown for all experiments in Fig. VI.6. The first panel represent the temperature anomalies for Exp_glac, Exp_flat and Exp_zero. Strong midlatitude and polar region cooling in the NH and SH, due to the extended glacial ice sheets, is found in Exp_glac. The see-saw effect between the NH and SH characterises the results of Exp_zero and an overall warming except in the Southern Ocean is found in Exp_flat. On the second panel (Fig. VI.6b) the SAT anomalies for the experiments with changed albedo are displayed. Exp_alb02 shows a small increase of the temperature (around 1°C) relative to the present-day simulation, except for the Antarctic, where the sharp change of surface reflectivity from glaciers (0.8) to forest (0.2) yields a warming of nearly 10°C; Exp_alb08 exhibits strong, zonal cooling up to −30°C in mid and high northern latitudes, indicating the opposite effect than in Exp_alb02 for the Antarctic; and in Exp_IP the temperature anomaly can reach −70°C in the equatorial and tropical latitudes. The third panel visualizes the climate instability in the NH due to the reduction of CO_2 and the consequential positive ice-albedo feedback. The extreme experiment Exp_1 exhibits very strong anomalies, up to −40°C SAT in the subtropics in the NH.

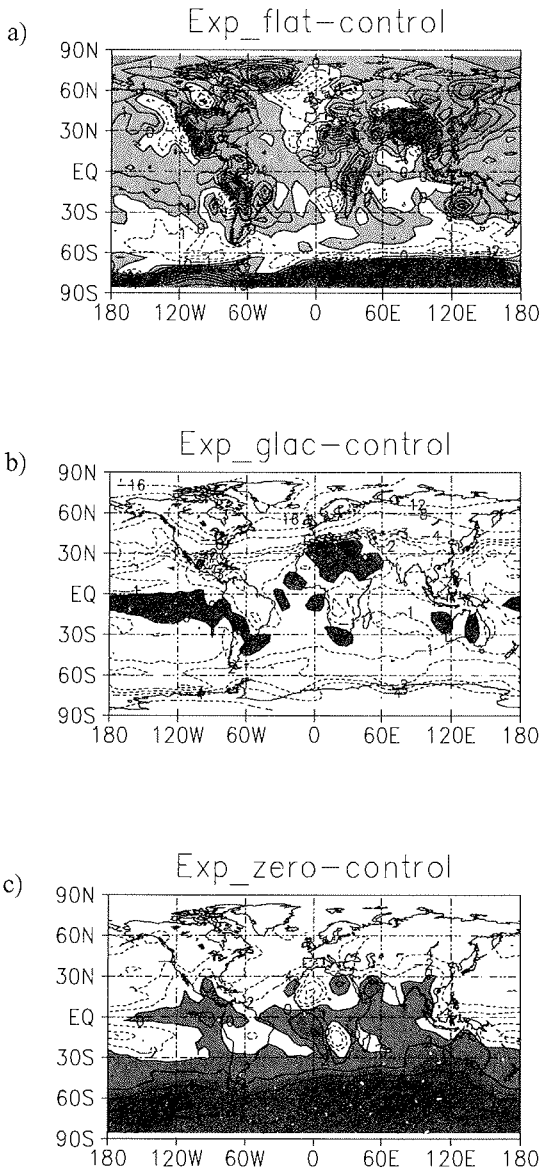

Fig.VI.5: *Annual mean surface air temperatures anomalies: a) Exp_flat–control run; b) Exp_glac–control run; and c) Exp_zero–control run. The grey shading indicates the positive anomalies. Contour interval is: 2° C when SAT > 0° C; 1° C when 0° C> SAT > −4° C; and 4° C when −4° C> SAT.*

VI.3.6 Zonal mean precipitation

To assess the Hadley circulation and the Intertropical Convergence Zone (ITCZ) for different sensitivity experiments the averaged zonal mean precipitation is calculated. The zonal mean boreal winter and summer values for the sensitivity experiments are shown in Fig. VI.7. The maximum precipitation in boreal winter for the present-day simulation is situated in the SH, while in the boreal summer it is located in the NH. The experiments investigating the effect of the orography (Fig. VI.7a,b) Exp_flat and Exp_glac show seasonal magnitude deviations from the present-day values. In Exp_flat the maximum precipitation during boreal winter is reduced, while in Exp_glac it is enhanced. The opposite tendency is found in boreal summer, Exp_flat shows an increase in precipitation and experiment Exp_glac produces a decrease. The land elevation in the NH results in pronounced seasonality in the equatorial region. As the orography is higher, the ITCZ is strengthened in boreal winter and is suppressed in boreal summer. The absence of heat transport in Exp_zero increases the maximum precipitation in both seasons, compared to the control run.

The precipitation in the land albedo experiment Exp_alb02 is similar to the present-day's one, except in the region of Antarctic, where the drastic change of the albedo produces a peak in precipitation in winter (Fig. VI.7cd). In Exp_alb08 the precipitation maximum is strongly shifted to the SH (around 15°S) and located in the belt of all-years SAT maximum. The magnitude is 20% less than the present-day value. A decreases in precipitation occurs in the midlatitudes of the NH and SH due to the extensive ice-coverage and negative surface temperatures. The ice-covered planet in Exp_IP prohibits precipitation the whole year round.

The experiment with a fourfold present-day CO_2 concentration shows a decrease in the precipitation during boreal winter and an increase during boreal summer (Fig. VI.7e,f). The tendency is the same as in Exp_flat (described earlier), whereas the experiment with CO_2 equal to 200 ppm exhibits the tendency of Exp_glac - an increase in the precipitation during boreal winter and decrease during boreal

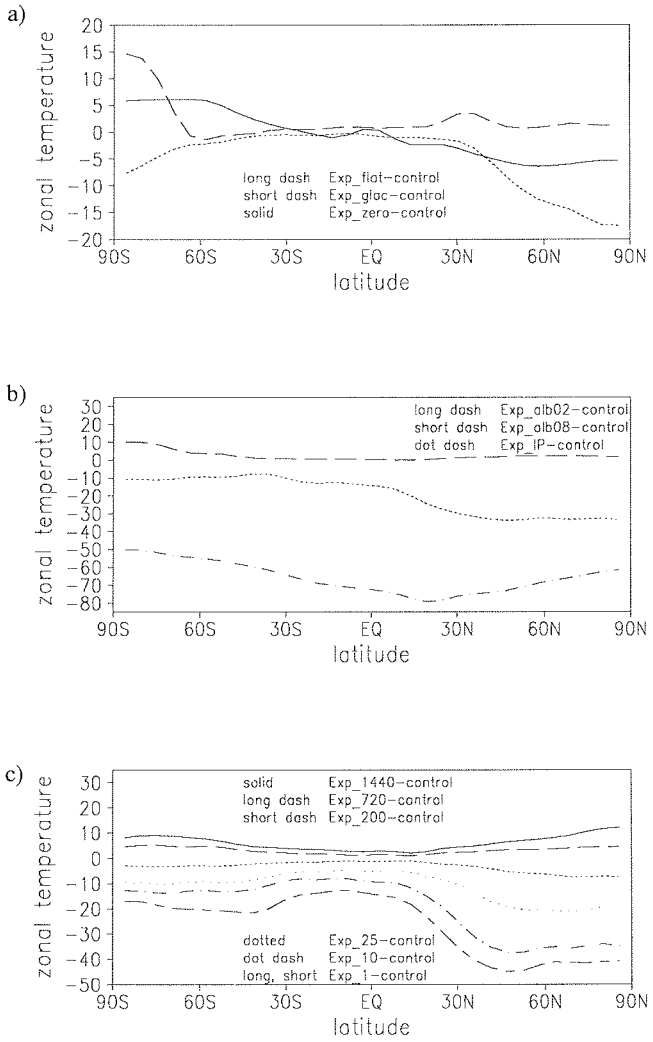

Fig.VI.6: *Zonal mean of the global surface temperature anomalies relative to the control run: a) effect of orography and oceanic heat transport; b) changed land albedo and Ice Planet simulation; and c) different CO_2 concentrations in the atmosphere. Units are ° C.*

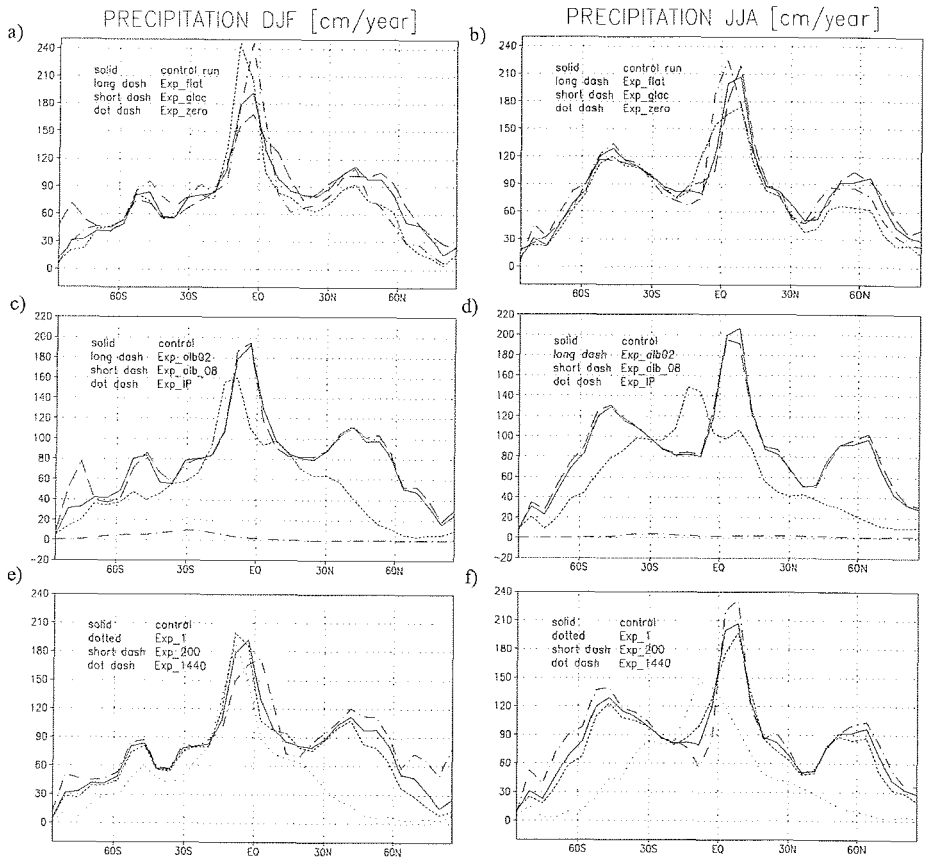

Fig. VI.7: *The DJF and JJA zonal mean precipitation for control run (solid line) and a,b) the experiments investigating the effect of orography and oceanic heat transport; c,d) experiments with changed land albedo and Ice Planet simulation; and e,f) experiments with different CO_2 concentrations.*

summer. Therefore, glacial orography and the reduction of CO_2 act in the same direction. Both change the ITCZ and Hadley circulation in equatorial and tropical latitudes. In experiment Exp_1, an instability occurs due to the sea-ice albedo feedback and the precipitation is considerably lowered, as its maximum does not experience seasonality and is always located in the SH, tending to the same result as in Exp_IP.

VI.4 Discussions and Conclusions

Motivated by recent attempts to simulate Neoproterozoic glaciations with climate models (e.g. Jenkins and Smith, 1999; Hyde at al., 2000; Chandler and Sohl, 2000; Poulsen et al., 2001; Lewis et al., 2003; Dounadieu et al., 2004), we investigate the sensitivity of the climate to some extreme boundary and initial conditions and combinations of extreme parameters under present-day insolation and continental distributions. Examining the influence of each factor, we assess the role of the land-albedo, the influence of high and low CO_2 concentration levels, the importance of the orography and of the oceanic heat transport.

The experiments with only one parameter changed, show equilibrium states, in which the equatorial ocean remains ice-free. Using a combination of extreme boundary and initial conditions, like zero oceanic heat transport, high land-albedo and the initial temperature uniformly set to a value equal to the freezing point, a 'snowball' Earth under present-day orbital parameters and CO_2 concentration can be attained. Further investigation of the experiments with a combination of two of the mentioned extreme boundary conditions, shows that the dominant factor for the decrease of temperature in the ice planet simulation is the land albedo. If the land-albedo is a variable parameter, independently of the zero oceanic heat transport or the low initial temperature field, the temperatures increase and tend to reach the values of the control run. Interestingly, the present-day oceanic heat transport, alone is not able to produce ice-free equatorial oceans. A full glaciation is delayed but

successfully reaches the ice-planet equilibrium (Fig. VI.3). Even though the heat transport of the present-day climate seems not to be appropriate with respect to ice-covered oceans (Poulsen et al., 2001; Lewis et al., 2003), its role appears to be negligible compared to continental surface properties. Using a two dimensional coupled climate model, Dounadieu et al. (2004) concluded that the dynamic oceanic process cannot prevent the onset of the ice-albedo instability in a Neoproterozoic simulation. Another factor prohibiting the formation of an ice-covered planet is the high initial temperature field (set to present-day values). Although the global temperature falls approximately 20°C the sea-ice cover advance is restricted up to 30°N and 60°S. The asymmetrical distribution of the sea-ice lines is more sensitive to the paleogeography differences than to the change of other parameters, e.g. the orbital insolation (Poulsen et al., 2002). Releasing the land albedo after the 20-th year of the ice planet simulation (not shown) does not infer any change in the climate system, due to the very low temperatures, which force the land and ice albedo to attain their maximal values. Thus, the ice planet simulation reaches a stable climate and only an external influence can lead to change of this stable state (e.g. increase of carbon dioxide due to strong volcanic activity and lack of chemical weathering).

Does the orography matter in the initiation of extreme climate? The LGM reconstruction of the orography (Peltier, 1994), including the highly elevated Laurentide Ice Sheet, reduces the global temperature by 3°C. The influence of changed orography predominates in the contribution to the Northern Hemispheric cooling, but it is of no importance to the tropics. Thus the altered orography is more important in regional sense, than in global. Jenkins and Frakes (1998) introduced a 2 km north-south mountain chain on the super continent in their model set up, and showed that the orogeny could not be considered as a factor for the global glaciation. But it can redistribute the humidity over sea-ice and thus, change the hydrological cycle (Donnadieu et al., 2003). However, the climate system responses nonlinearly to linear change of the height of the ice-sheet (Romanova et al., 2004), which points to the existence of a threshold, over which a runaway albedo feedback could be initiated. Further investigation of the sensitivity of the climate system with respect to enlargement of the Laurentide ice sheet could be of interest when searching for this

threshold.

The experiments control run, Exp_alb02, Exp_flat, Exp_1440 showed a planetary albedo larger than the surface albedo (in some cases more than 150%), due to the strong evaporation over the ice-free oceans and cloud formation. In the experiments (Exp_alb08, ExpIP_iniTempPD and Exp_1), in which the absolute global temperature is around 0°C and which are characterised by cold climatic conditions and ice-free equatorial and tropical latitudes, the global surface and planetary albedo tend to be in the same order. However, these cold climates (Exp_alb08 and Exp_1) could exhibit an intense equatorial precipitation maxima and a strong Hadley circulation due to the sharp temperature gradients from the equator to the edge of the sea-ice margin, which works against the positive ice-albedo feedback (Bendtsen, 2002). The hydrological cycle and the ITCZ are rather sensitive to the change of the surface temperature in the tropics and to the strength of the Atlantic overturning (Lohmann and Lorenz, 2000; Lohmann, 2003). Interestingly, in the ice-planet experiments Exp_IP and ExpIP_iniIP, the estimates of the global planetary albedo appear smaller than the global surface albedo. On a completely glaciated Earth, the processes of evaporation, cloud formation and precipitation are strongly suppressed or even do not exist, thus the ratio between the incident and reflected short wave radiation on the surface is higher than the ratio between the incident and reflected/scattered short wave radiation on the top of the atmosphere. The loss of energy in the atmosphere could be due to the process of water vapour absorption, where the water vapour is provided only by the process of sublimation.

Investigating the Neoproterozoic glaciations, many authors search for a CO_2 threshold value. Different simulations show a sensitivity of the minimum CO_2 level to continental configurations (Poulsen et al., 2002; Donnadieu et al., 2004), Earth's rotation rate and obliquity (Jenkins and Smith, 1999; Jenkins, 2000), solar luminosity (Crowly et al., 2001) oceanic heat transport (Poulsen et al., 2001) or an increase of the albedo (Lewis et al., 2003). Our experiments, however, demonstrate that the reduction of atmospheric CO_2 alone is not sufficient to provoke global glaciation under present-day insolation. Nevertheless, a strong nonlinearity occurs in the NH

at a CO_2 concentration of 25 ppm and the temperature anomaly, relative to the present-day simulation, can reach –40°C at 1 ppm. Our simulations show that the initial condition of the system is important when simulating a 'snowball' Earth. Indeed, a hysteresis of the climate system is found with respect to a change of the infrared forcing (Crowley et al., 2001) and solar constant (Stone and Yao, 2004). We suppose similar climate behaviour to a slow change of the CO_2 concentration and a snow cover we will address this question in our further research.

Acknowledgements *We gratefully acknowledge the suggestions and recommendations of Dr. Frank Lunkeit and thank Prof. Klaus Fraedrich for providing us with the model code. We thank also Dr. Michai Dima and Dr. Katrin Vosbeck for the improvement of the manuscript. This work has been funded by the German Ministry for Education and Research (BMBF) within DEKLIM project 'Climate Transitions'.*

CHAPTER VII

SUMMARY

The geological data prompt for abrupt climate changes in the Earth's history. Climate models of different complexity are used to understand the underlying mechanisms for the scientist search for the clues, that could provide answers to the observed climate transitions. In this thesis, the sensitivity of the climate system with respect to different boundary conditions, the climate stability regimes and the connected thresholds are investigated.

The sensitivity and stability analysis of the present-day and glacial ocean circulations related to freshwater pulse and slow perturbations showed the existence of thresholds and hysteresis behavior of the THC. It is found that the glacial quasi-equilibrium hysteresis is less pronounced compared to the present-day one, and multiple equilibria exist only when an anomalous freshwater input is applied. These results, produced with a 3D ocean general circulation model are in consistence with the study of Ganopolski and Rahmstorf (2001), who used a coupled system with a zonally averaged ocean model. In spite of, the different model approaches the results are in consistence. The present-day circulation is attributed to 'thermal regime' in which the freshwater forcing breaks the overturning and multiple equilibria exist. The glacial circulation belongs to the 'thermohaline regime', in which only one stable equilibria exists. However, this stable glacial state, during the deglaciation phase, can easily be shifted into the regime of bi-stability, where the conveyor is prone to transitions.

The North Atlantic fresh water balance plays a crucial role for the stability of the ocean circulation and, hence, for the glacial climate. Analyzing the hydrological budget in the Atlantic catchment area, a linear dependence between the net evaporation over the basin and the 'critical' freshwater input is found, which causes the breakdown of the conveyor. Thus, the vulnerability of the ocean circulation strongly depends on the background climatic state associated with a specific Atlantic hydrol ogy. The warm climatic states (forced with GLAMAP 2000 reconstruction and the reconstruction given by Weinelt et al. (1996)), which are associated with a stronger than present-day overturning circulation and higher evaporative rates over the Atlantic, exhibit higher stability than the cold climatic background state, (forced with CLIMAP (1981) with tropical cooling), which shows a reduced THC compared to present-day and lower evaporative rates over the basin. The higher rates of evaporation over the Atlantic determine a larger water vapor transport from the Atlantic to the Pacific Oceans (Lohmann and Lorenz, 2000). The water vapor loss conditions the freshwater inflow in the Atlantic basin and thus determines the predominance of the type of the circulation - 'thermal' or 'haline'. It is found that when the 'haline' factor predominates, the circulation is more stable.

The pulse meltwater perturbations in the North Atlantic on the obtained oceanic glacial states are performed to simulate the effect of Heinrich Events. The experiments show that all glacial states recover after a relaxation time period, which depends on the climatic background state and the present-day climate is settled into a stable conveyor 'off' mode (shutdown of the THC). This confirms the monostable behavior of the glacial state and the location of the present-day equilibrium in the bi-stable regime on the hysteresis map. Usage of the equilibriums of the glacial states as a background for a meltwater pulse experiments aiming to simulate a Heinrich event, seems more appropriate, than using the present-day climatic state. That is deducted by the data-model comparison, which shows that the SST anomalies are better captured in the glacial experiments than in the analogous present-day experiment.

The heat transports of the present-day and glacial oceanic background states, de-

rived as described above, are used to force an AGCM to investigate the surface air temperatures (SAT), atmospheric circulations and precipitation patterns. Moreover, sensitivity experiments with applied different height of the Laurentide Ice Sheets are performed to study the separate effects of the oceanic heat transport and the role of the orography in connection with ice-albedo feedback. The highly elevated and largely expanded Laurentide Ice Sheet (as given by Peltier, 1996) is responsible for the wave-like structure of the atmospheric flow in the Northern hemisphere, a fea ture lacking in the simulation, in which the Laurentide Ice Sheet is absent. The experiment with reduced Laurentide Ice Sheet's height shows qualitatively the same result. The flow over North Atlantic is enhanced and displaced to the south only due to the orographycal forcing. Assessing, separately, the relative contribution of the oceanic circulation and the Laurentide Ice Sheet upon the North Atlantic climate, it is found that the changes in orography and albedo induce 80% contribution for the reduction of the temperature, and the reduced oceanic heat transport contributes only with 20%. Therefore, the altered orography is of primary importance for the Northern Hemispheric cooling.

The precipitation patterns of the present-day and glacial simulations showed reduction of the ITCZ and its southward displacement in boreal winter for all glacial simulations compared to the present-day simulation, primary due to the reduced oceanic heat transport. The role of the heat transport predominates in the tropics (its contribution is 70-80%), whereas the influence of changed orography in the Northern Hemisphere in the tropics is negligible.

Analyzing the role of orography on the glacial climate and ascertaining its importance for the climate in the North Atlantic, a question rises to what extent other boundaries, e.g., land albedo or CO_2 reduction, and the initial boundary conditions could affect the climate. Selecting and applying several extreme boundary conditions, as land albedo set to the maximum albedo of the glaciers, zero oceanic heat transport and the initial temperature set to the freezing point, a global Earth's glaciation is simulated. Evidences for such extreme events, called 'snowball' Earth, are found in the paleomagnetic observations of equatorial carbonate deposits in the

Neoroterozoic era (Hoffman et al. 1998).

Investigating the importance of each forcing parameter separately, it is found that the dominant cause for the lowering of the temperature (to -50°C at the equator) is the fixed high land albedo. When the land albedo is free to develop, despite of the zero oceanic heat transport and the low initial temperatures, the system settles in a state similar to the present-day simulation. Therefore, we conclude that the change of land-albedo is a factor of primary importance for the changes of the climate system.

The attempts to find a CO_2 threshold level for the Earth's glaciations failed in our experimental set-up. The reduction of CO_2 concentration, alone is not sufficient to provoke a global glaciation under present-day insolation and present-day continental distribution. However, strong nonlinear response, occur in the Northern Hemisphere showing that the system is close to a state of irreversible like changes.

The analyses of a large number of numerical experiments and the conclusions drawn on them show the strong vulnerability of the climate system to the Earth's hydrology, changes of CO_2 concentration and the land albedo. These climatic variables, to a certain extent, are under humans control and could be kept in the limits, beyond which the changes are possible. Therefore, this branch of climate research appears also of great importance with respect to the governmental and human concern for the future.

REFERENCES

Aagaard, K., Carmack, E.C., 1989. The role of sea ice and other fresh water in the Arctic circulation. J. Geophys. Res. 94, 14,485-14,498.

Adkins, J.F., McIntyre, K., Schrag, D.P., 2002. The salinity, temperature and $\delta^{18}O$ content of the glacial deep ocean. Science 298, 1769-1773.

Alley, R. B., Clark, P.U., 1999. The deglaciation of the northern hemisphere: A global perspective. Annual Reviews of Earth and Planetary Sciences 27, 149-182.

Bard, E., 1999. Ice age temperatures and geochemistry. Science 284, 1133-1134.

Bard, E., Rostek F., Turon, J.L., Gendreau, S., 2000. Hydrological impact of Heinrich events in the subtropical Northeast Atlantic. Science 289, 1321-1324.

Barnola, J.M., Raynaud, D., Korotkevich, Y.S., Lorius, C., 1987. Vostok ice core provides 160,000 year record of atmospheric CO_2Nature 329, 408-14.

Bendtsen, J., 2002. Climate sensitivity to changes in solar insolation in a simple coupled model. Clim. Dyn. 18, 595-609.

Berger, A.L., 1978. Long term variations of daily insolation and quaternary climatic changes. J. Atmos. Scie. 35(12), 2362-2367.

Bickert, T., Mackensen, A., 2003. Last Glacial to Holocene changes in South Atlantic deep water circulation. in The South Atlantic in the Quaternary Reconstruction ofmaterial budget and current systems. Wefer G, Mulitza S, Rathmeyer V. Springer, Berlin Heidelberg, pp 599-620.

Boyle, E.A., Keigwin, L.D., 1987. North Atlantic thermohaline circulation during the past 20,000 years linked to high-latitude surface temperature. Nature 330, 35-40.

Boyle, E.A., 1992. Cadmium and δ^{13}C paleochemical ocean distribution during the stage 2 glacial maximum. Ann. Rev. Earth Planet Sci. 20, 245-287.

Boyle, E.A., 1995. Last Glacial Maximum North Atlantic Deep Water: on, off, or somewhere in between? Phil. Trans. Roy. Soc. London B 348, 243-253.

Broccoli, A.J., 2000. Tropical cooling at the Last Glacial Maximum: An atmosphere-mixed layer ocean model simulation. Journal of Climate 13, 951-976.

Broecker, W., Bond, G., Klas, M., Clark, E., McManus, J., 1992. Origin of the North Atlantic's Heinrich events. Clim. Dyn. 6, 265-273.

Broecker, W.S., Hemming, S., 2001. Climate swings come into focus. Science 294, 2308-2309.

Bryan, F., 1986. High-latitude salinity effects and interhemispheric thermohaline circulations. Nature 322, 302-304.

Budyko, M.I., 1969. The effect of solar radiation variations on the climate of the Earth, Tellus 21, 611-619.

Butzin, M., Prange, M., Lohmann, G., 2003. Studien zur ^{14}C-Verteilung im glazialen Ozean mit einem globalen Ozeanzirkulationsmodell. Terra Nostra 6, 86-88.

Calov, R., Ganopolski, A., Petoukhov, V., Claussen, M., Greve, R., 2002. Large-scale instabilities of the Laurentide ice sheet simulated in a fully coupled climate-system model. Geophys. Res. Let. 29, 2216, doi:10.1029/2002GL016078.

Chandler, M.A., Sohl, L.E., 2000. Climate forcings and the initiation of low-latitude ice sheets during Neoproterozoic Varanger glacial interval. J. Geophys. Res. 105, 20,737-20,756.

Chapman, M.R., Shackleton, N.J., 1998. Millennial-scale fluctuations in North Atlantic heat flux during the last 150,000 years. Earth Planet. Sci. Lett. 159, 57-70.

Chapman, M.R., Maslin, M.A., 1999. Low-latitude forcing of meridional temperature and salinity gradients in the subpolar North Atlantic and the growth of glacial ice sheets. Geology, 27, 875-878.

Chapman, M.R., Shackleton, N.J., 1999. Global ice-volume fluctuations, North Atlantic ice-rafting events, and deep-ocean circulation changes between 130 and 70 ka. Geology 27, 795-798.

Chappell, J., 2002. Sea level changes forced ice breakouts in the Last Glacial cycle: new results from coral terraces. Quat. Sci. Rev. 21, 1229-1240.

Chen, P., 2000. Thermally forced stationary waves in a quasigeostrophic system. J. Atmos. Scie. 58, 1585-1594.

Chiang, J.C.H., Biasutti, M., Battisti, D.S., 2003. Sensitivity of the Atlantic ITCZ to Last Glacial Maximum boundary conditions. Paleoceanography 18, doi: (10.1029/2003PA000916).

Clark, P.U., Pisias, N.G., Stocker, T.F., Weaver, A.J., 2002. The role of the thermohaline circulation in abrupt climate change. Nature 415, 863-869.

Claussen, M., Mysak, L.A., Weaver, A.J., Crucifix, M., Fichefet, T., Loutre, M.F., Weber, S.L., Alcamo, J., Alexeev, V.A., Berger, A., Calov, R., Ganopolski, A., Goosse, H., Lohmann, G., Lunkeit, F., Mokhov, I.I., Petoukhov, V., Stone, P., Wang, Z., 2002. Earth system models of intermediate complexity: Closing the gap in the spectrum of climate system models. Clim. Dyn. 18, 579-586.

CLIMAP project members, 1981. Seasonal reconstructions of the Earth surface at the Last Glacial Maximum. Geological Society of America, Map and Chart Series, MC-36,18 maps, Boulder, Colorado.

Cook, K.H., Held, I.M., 1988. Stationary waves of the ice age climate. J Clim 1, 807-819.

Crowley, T.J., Baum, S.K., 1993. Effects of decreased solar luminosity on Late Precambrian ice extent. J. Geophys. Res. 98, 16723-16732.

Crowley, T.J., Hyde, W.T., Peltier, W.R., 2001. CO_2 levels required for deglaciation of a 'Near Snowball' Earth. Geophys. Res. Lett. 28, 283-286.

Crucifix, M., Tulkens, P., Berger, A., 2001. Modeling abrupt climatic change during the last glaciation. In. Seidov, D., Haupt, B.J., Maslin, M. (Eds.). The oceans and rapid climate change - Past, present and future, 117-134. Geophys. Monogr. 126, American Geophysical Union, Washington, DC.

Dansgaard, W., Johnsen, S.J., Clausen, H.B., Dahl-Jensen, D., Gundestrup, N.S., Hammer, C.U., Hvidberg, C.S., Steffensen, J.P., Sveinbjrnsdottir, A.E., Jouzel, J. and Bond, G., 1993. Evidence for general instability of past climate from a 250-kyr ice-core record. Nature 364, 218-220.

de Vernal, A., Hillaire-Marcel, C., 2000. Sea-ice cover, sea-surface salinity and halo-/thermocline structure of the northwest North Atlantic: modern versus full glacial conditions. Quat. Sci. Rev. 19, 65-68.

d'Errico, F., Snchez Goi, M.F., 2003. Neandertal extinction and the millennial scale climatic variability of OIS 3. Quat. Sci. Rev. 22, 769-788.

Donnadieu, Y., Ramstein, G., Fluteau, F., Besse, J., Meert, J., 2002. Is high obliquity a plausible cause for Neproterozoic glaciations? Geophys. Res. Lett. 29, 10.1029/2002GL015902.

Donnadieu, Y., Fluteau, F., Ramstein, G., Ritz, C., Besse, J., 2003. Is there a conflict between the Neoproterozoic glacial deposits and snowball Earth interpretation: an improved understanding with numerical modeling. Earth Plan. Sci. Lett. 208, 101-112.

Donnadieu, Y., Ramstein, G., Fluteau, F., Roche, D., Ganopolski, A., 2004. The impact of atmospheric and oceanic heat transports on the sea-ice-albedo instability during the Neoproterozoic. Clim. Dyn. 22, 293-306.

Duplessy, J.C., Labeyrie, L., Juillet-Leclerc, A., Maitre, F., Duprat, J., Sarnthein, M., 1991. Surface salinity reconstruction of the North Atlantic Ocean during the last glacial maximum. Oceanologica Acta 14, 311-324.

Eliasen, E., Machenhauer, B., Rasmussen, E., 1970. On a numerical method for integration of the hydrodynamical equations with a spectral representation of the horizontal fields. Report No. 2, Institute for Theoretical Meteorology, University of Copenhagen, 37 pp.

Evans D.A.D., Li Z.X., Kirschvink J.L., Wingate M.T.D., 2000. A high-quality mid-Neoproterozoic paleomagnetic pole from South China, with implications for ice ages and the breakup configuration of Rodinia. Precambrian Res. 100 1-3, 313-334.

Fanning, A.F., Weaver A.J., 1997. Temporal-geographical meltwater influences on the North Atlantic conveyor: Implications for the Younger Dryas. Paleoceanography 12, 307-320.

Farrera, I., Harrison, S. P., Prentice, I. C., Ramstein, G., Guiot, J., Bartlein, P. J., Bonnefille, R., Bush, M., Cramer, W., von Grafenstein, U., Holmgren, K., Hooghiemstra, H., Hope, G., Jolly, D., Lauritzen, S.-E., Ono, Y., Pinot, S., Stute, M., Yu, G., 1999. Tropical climates at the Last Glacial Maximum: a new synthesis of terrestrial palaeoclimate data. I. Vegetation, lake-levels and geochemistry. Clim. Dyn. 15, 823-856.

Fraedrich K., Kirk E., Lunkeit F., 1998. Portable University Model of the Atmosphere. Deutsches Klimarechenzentrum, Tech. Rep. 16, 377 pp.

Franzke, C., Fraedrich, K., Lunkeit, F., 2000. Low frequency variability in a simplified atmospheric global circulation model: Storm track induced 'spatial resonance'. Quat. J. Royal Met. Society 126, 2691-2708.

Frenz, M., Heinrich, R., 2003. Carbonate dissolution revealed by silt grain-size distributions: comparison of Holocene and Last Glacial Maximum sediments from the pelagic South Atlantic. Sedimentology: submitted.

Frisius, T., Lunkeit, F., Fraedrich, K., James, I.N., 1998. Storm-track organization and variability in a simplified atmospheric global circulation model (SGCM). Quat. J. Royal Met. Society 124, 1019-143.

Ganopolski, A., Rahmstorf, S., Petoukhov, V., Claussen, M., 1998. Simulation of modern and glacial climates with a coupled global climate model. Nature 391, 351-356.

Ganopolski, A., Rahmstorf, S., 2001. Simulation of rapid glacial climate change in a coupled climate model. Nature 409, 153-158.

Gordon, A.L., 1986. Interocean exchange of thermocline water. J. Geophys. Res. 91, 5037-5046.

Grootes, P.M., Stuiver, M., White, J.W.C., Johnsen, S., Jouzel, J., 1993. Comparison of oxygen isotope records from the GISP2 and GRIP Greenland ice cores. Nature 366, 552-554.

Grosfeld, K., Lohmann, G., Romanova, V., Lunkeit, F., Fraedrich, K., Atmospheric simulations using a GCM of intermediate complexity: present day and last glacial maximum experiments (in preparation).

Heinrich, H., 1988, Origin and consequences of cyclic ice rafting in the northeast Atlantic Ocean during the past 130,000 years. Quat. Res. 29, 142-152.

Held, I.M., Ting, M., 1990. Orographic and thermal forcing of stationary waves: the importance of the mean low-level wind. J. Atm. Scie. 47, 697-706.

Held, I.M., Ting, M., Wang, H., 2002. Northern winter stationary waves: theory and modeling. J. Climate 15, 2125-2144.

Hewitt, C.D., Broccoli, A.J., Mitchell, J.F.B., Stouffer, R.J., 2001. A coupled model study of the last glacial maximum: Was part of the North Atlantic relatively warm?. Geophys. Res. Lett. 28, 1571-1574.

Hoffman, P.F., Kaufman, A.J., Halverson, G.P., Scharg, D.P., 1998. A Neoproterozoic snowball earth. Science 281, 1342-1346.

Hoffman, P.F., Schrag, D.P. 2002. The snowball Earth hypothesis: testing the limits of global change. Terra Nova 14, 129-155.

Hoskins, B.J., Simmons, A.J., 1975. A multi-layer spectral model and the semi-implicit method. Quat. J. Royal Met. Society 101, 637-655.

Hyde, W.T., Crowley, T.J., Baum, S.K., Peltier, W.R., 2000. Neoproterozoic 'snowball Earth' simulations with a coupled climate/ice-sheet model. Nature 405, 425-429.

IPCC, 2001. Climate Change 2001, The Scientific Basis. Contribution of Working group I to the Third Assessment Report of the Intergovernmental Panel on Climate Change. Houghton, J.T., Ding, J., Griggs, D.J., Noguer, M., van der Linden, P.J., Dai, X., Maskell, K., Johnson, C.A., (eds.). Cambridge University Press. Cambridge, United Kingdom and New York, N.Y., USA, 881 pp.

Jaeger, L., 1976. Monatskarten des Niederschlags fr die ganze Erde. Ger. Weather Serv. Rep. 139, Offenbach.

Jenkins, G.S., Frakes, L.A. 1998. GCM sensitivity test using increased rotation rate, reduced solar forcing and orography to examine low latitude glaciation in the Neoproterozoic. Geophys. Res. Lett. 25, 3525-3528.

Jenkins, G.S. 1999. Examining the sensitivity of Earth's climate to removal of ozone, landmasses and enhanced ocean heat transport in the GENESIS global climate model. Glob. Plan. Change 20, 257-279.

Jenkins, G.S., Smith, S.R. 1999. GCM simulation of Snowball Earth conditions during the late Proterozoic. Geophys. Res. Lett. 26, 2263-2266.

Jenkins, G.S. 2000. Global climate model high-obliquity solutions to the ancient climate puzzles of the Faint Young Sun Paradox and low altitude Proterozoic Glaciation. J. Geophys. Res. 105, 7357-7370

Jouzel, J., Lorius, C., Petit, J.R., Genthon, C., Barkov, N.J., Kotlyakov, V.M., Petrov, V.M., 1987. Vostok ice-core: a continuous isotope temperature record over the last climatic cycle (160,000 years). Nature 329, 403-408.

Kaplan, A., Cane, M., Kushnir, Y., Clement, A., Blumenthal, M., Rajagopalan B., 1998. Analyses of global surface temperatures 1856-1991. J. Geophys. Res., 103,18567-18589.

Keeling, C.D., Chin, J.F.S., Whorf, T.P., 1996. Increased activity of northern vegetation inferred from atmospheric CO_2 measurements. Nature 382, 146-149.

Keigwin, L.D., Lehman, S.J., 1994. Deep circulation change linked to Heinrich Event 1 and Younger Dryas in a mid-depth North Atlantic core. Paleoceanography 9, 185-194.

Kiefer, T., 1998. Produktivitt und Temperaturen im subtropischen Nordatlantik, zyklische und abrupte Vernderungen im spten Quartr. Berichte-Reports, Geol.-Palont. Inst. Univ. Kiel 90, Kiel, Germany, 127 pp.

Kim, J.-H., Schneider, R.R., Müller, P.J., Wefer, G., 2002. Interhemispheric comparison of deglacial sea-surface temperature patterns in Atlantic eastern boundary currents. Earth Planet. Sci. Lett. 194, 383-393.

Kim, S.J., 2004. The effect of atmospheric CO_2 and ice sheet topography on LGM climate. Clim. Dyn., 10.1007/s00382-004-0412-2.

Kirschvink, J.L., 1992. Late proterozoic low-lattitude global glaciation: the Snowball Earth. In The Proterozoic biosphere, Schopf, J.W.; Klein, C,; Cambridge UK, pp 51-52.

Kirschvink, J.L., 1992. Late proterozoic low-lattitude global glaciation: the Snowball Earth. In The Proterozoic biosphere, Schopf JW, Klein C, Cambridge UK, pp 51-52.

Kirschvink, J.L., Gaidos, E.J., Bertani, E., Beukes, N.J., Gutzmer, J., Maepa, L.N., Steinberger, R.E., 2000. Paleoproterozoic snowball Earth: Extreme climatic and geochemical global change and its biological consequences. PNAS 97, 1400-14005.

Kitoh, A., Murakami, F.S., Koide, H., 2001. A simulation of the Last Glacial Maximum with a coupled atmosphere-ocean GCM. Geoph. Res. Lett. 28, 2221-2224.

Knorr, G., Lohmann G., 2003: Southern Ocean Origin for Resumption of Atlantic Thermohaline Circulation during Deglaciation. Nature 424, 532-536.

Knorr, G., Grosfeld, K., Lohmann, G., Lunkeit, G., Fraedrich, K., 2005, Atmospheric response to abrupt changes in the thermohaline circulation during deglaciation. Geochmistry, Geophysics, Geosystems, (in revision).

Kutzbach, J.E., Wright, H.E., 1985. Simulation of the climate of 18,000 BP: Results from the North American/North Atlantic/European sector and comparison with the geologic record. Quat. Sci. Rev. 4, 147-187.

Latif, M., Roeckner, E., Mikolajewicz, U., Voss, R., 2000. Tropical stabilization of the thermohaline circulation in a Greenhouse warming simulation. J. Clim. 13, 1809-1813.

Lautenschlager, M., Mikolajewicz, U., Maier-Reimer, E., Heinze, C., 1992. Application of ocean models for the interpretation of the atmospheric general circulation model experiments on the climate of the Last Glacial Maximum. Paleoceanography 7, 769-782.

Leonard, B. P., 1979. A stable and accurate convective modellingprocedure based on quadratic upststream interpolation. Comput. Methods Appl. Mech. Eng., 19, 59-98.

Lewis, J.P., Weaver, A.J., Johnston, S.T., Eby, M., 2003. Neoproterozoic 'snowball Earth': Dynamic sea ice over a quiescent ocean. Paleoceanography 18, 10.1029/2003PA000926

Lohmann, G., Gerdes, R., Chen, D., 1996. Sensitivity of the thermohaline circulation in coupled oceanic GCM-atmospheric EBM experiments. Clim. Dyn. 12, 403-416.

Lohmann, G., Gerdes, R., Chen, D., 1996b. Stability of the thermohaline circulation in a simple coupled model. Tellus 48A, 465-476.

Lohmann, G., Lorenz, S. 2000. On the hydrological cycle under paleoclimatic conditions as derived from AGCM simulations. J. Geophys. Res. 105, 17417-17436.

Lohmann, G., 2003. Atmospheric and oceanic freshwater transport during weak Atlantic overturning circulation. Tellus 55 A, 438-449.

Longdoz, B., Francois, L.M., 1997. The Faint young sun climatic paradox: Influence of the continental configuration and of the seasonal cycle on the climatic stability. Glob. Plan. Change 14, 97-112

Lorenz, S., Grieger, B., Helbig, Ph., Herterich K., 1996. Investigating the sensitivity of the atmospheric general circulation model ECHAM 3 to paleoclimatic boundary conditions. Geol. Rundsch. 85, 513-524.

Lorenz, S., Lohmann, G., 2004. Reconciling glacial snow lines with tropical sea surface temperatures. Geochem. Geophys. Geosyst., accepted.

Lunkeit, F., Bauer, S.E., Fraedrich, K., 1998. Storm tracks in a warmer climate: Sensitivity studies with a simplified global circulation model. Clim. Dyn. 14, 813-826.

Macdonald, A.M., Wunsch, C., 1996. An estimate of global ocean circulation and heat fluxes. Nature 382, 436-439.

Maier-Reimer, E., Mikolajewicz, U., 1989. Experiments with an OGCM on the cause of the Younger Dryas. Tech Rep 39, Max-Planck-Inst for Meteorol, Hamburg, pp 13.

Maier-Reimer, E., Mikolajewicz, U., Hasselmann, K., 1993. Mean circulation of the Hamburg LSG OGCM and ist sensitivity to the thernmohaline surface forcing. J. Phy. Oceanography 23, 731-757.

Manabe, S., Broccoli, A.J., 1985. The influence of continental ice sheets on the climate of an ice age. Journal of Geophysical Research 90, 2167-2190.

Manabe, S., Stouffer R.J., 1988. Two stable equilibria of a coupled ocean-atmosphere model. J. Climate 1, 841-866.

Manabe, S., Stouffer, R.J., 1995. Simulation of abrupt climate change induced by freshwater input to the North Atlantic Ocean. Nature 378, 165-167.

Marchitto, T.M., Oppo, D.W., Curry, W.B., 2002. Paired benthic foraminiferal Cd/Ca and Zn/Ca evidence for a greatly increased presence of Southern Ocean Water in the glacial North Atlantic. Paleoceanography 17, 1038,doi:10.1029/2000PA000PA000598.

Marotzke, J., 1990. Instabilities and multiple equilibria of the thermohaline circulation. Ber. Inst. Meeresk. Kiel 194, 126 pp.

Marsiat, I., Valdes, P.J., 1999. Sensitivity of the Northern Hemisphere climate of the Last Glacial Maximum to sea surface temperatures. Clim. Dyn. 17, 233-248.

Maslin, M.A., Shackleton, N.J., Pflaumann, U., 1995. Surface water temperature, salinity and density changes in the northeast Atlantic during the last 45,000 years: Heinrich events, deep water formation, and climatic rebounds. Paleoceanogr. 10, 527-544.

McManus, J.F., Francois, R., Gherardi, J.M., Keigwin, L.D., Brown-Leger, S., 2004. Collapse and rapid resumption of Atlantic meridional circulation linked to deglacial climate changes. Nature 428, 834-837.

Mikolajewicz, U., Maier-Reimer, E., 1994. Mixed boundary conditions in ocean general circulation models and their influence on the stability of the model's conveyor belt. J. Geophys. Res. 99, 22633-22644.

Milankovitch, M., 1941. Canon of insolation and the Ice-Age Problem. Royal Serbian Academy, Belgrade.

Mix, A.C., Morey, A.E., Pisias, N.G., Hostetler, S.W., 1999. Foraminiferal faunal estimates of paleotemperature: circumventing the no-analog problem yields cool ice age tropics. Paleoceanography 14, 350-359.

Mix, A.C., Bard E., Schneider, R., 2001. Environmental processes of the ice age: land, oceans, glaciers (EPILOG). Quat. Sci. Rev. 20, 627-657.

Nigam, S., Held I.M., Lyons, S.W. 1987. Linear simulation of the stationary eddies in a GCM. Part I: The "no-mountain" model. J. Atmos. Sci., 43, 2944-2961.

Orszag, S.A., 1970. Transform method for calculation of vector-coupled sums: Application to the spectral form of the vorticity equation. J.Atm. Scie. 27, 890-895.

Pailler, D., Bard, E., 2002. High frequency paleoceanographic changes during the past 140,000 years recorded by the organic matter in sediments of the Iberian Margin. Palaeogeogr., Palaeoclim., Palaeoecol. 181, 431-452.

Paterne, M., et al., 1999. Hydrological relationship between the North Atlantic Ocean and the Mediterranean Sea during the past 15-75 kyr. Paleoceanogr. 14, 626-638.

Paul, A., Schäfer-Neth, C., 2003. Modeling the water masses of the Atlantic Ocean at the Last Glacial Maximum. Paleoceanography 18, No. 3, 1058, doi:10.1029/2002PA000783.

Peltier, W.R., 1994. Ice age paleotopography. Science 265, 195-201.

Pflaumann, U., Sarnthein, M., Chapman, M., d'Abreu, L., Funnell, B., Huels, M., Kiefer, T., Maslin, M., Schulz, H., Swallow, J., van Kreveld, S., Vautravers, M., Vogelsang, E., Weinelt, M., 2003. Glacial North Atlantic: Sea-surface Pflaumann, U., Sarnthein, M., Chapman, M., d'Abreu, L., Funnell, B., Huels, M., Kiefer, T., Maslin, M., Schulz, H., Swallow, J., van Kreveld, S., Vautravers, M., Vogelsang, E., Weinelt, M., 2003. Glacial North Atlantic: Sea-surface conditions reconstructed by GLAMAP 2000, Paleoceanography 18(3), 1065, doi:10.1029/2002PA000774.conditions reconstructed by GLAMAP 2000, Paleoceanography 18(3), 1065, doi:10.1029/2002PA000774.

Phillips, T.J., Anderson, R., Brsius, M., 1995. Hypertext summary documentation of the AMIP models. UCRL-MI-116384, Lawrence Livermore National Laboratory, Livermore, CA.

Poulsen, C.J., Pirrehumbert, R.T., Jacob, R.L. 2001. Impact of ocean dynamics on the simulation of the Neoproterozoic 'snowball Earth'. Geophys. Res. Lett. 28, 1575-1578.

Poulsen, C.J., Jacob, R.L., Pierrehumbert, R.T., Huynh, T.T., 2002. Testing paleogeographic controls on a Neoproterozoic snowball Earth. Geophys. Res. Lett. 29, 10.1029/2001GL014352.

Poulsen, C.J. 2003. Absence of runaway ice-albedo feedback in the Neoproterozoic, Geology 31, 473-476.

Prange, M., Lohmann, G., Gerdes, R., 1997. Sensitivity of the thermohaline circulation for different climates - investigations with a simple atmosphere-ocean model. Palaeoclimates 2, 71-99.

Prange, M., Romanova V., Lohmann G., 2002. The glacial thermohaline circulation: stable or unstable? Geophys. Res. Lett. Vol. 29, No. 21, 2028, doi:10.1029/2002GL015337.

Prange, M., Lohmann, G., Paul, A., 2003. Influence of vertical mixing on the thermohaline hysteresis: Analyses of an OGCM. J. Phys. Oceanography 33(8), 1707-1721.

Prange, M., Lohmann, G., Romanova, V., Butzin, M., 2004. Modelling tempospatial signatures of Heinrich Events: Influence of the climatic background state. Quat. Sci. Rev. 23, 521-527.

Rühlemann, C., Mulitza, S., Lohmann, G., Paul, A., Prange, M., Wefer, G., 2004. Intermediate-depth warming in the tropical Atlantic related to weakened thermohaline circulation: combining paleoclimate and modeling data for the last deglaciation. Paleoceanography 19, doi:1029/2003PA 0000948 .

Rahmstorf, S., 1995. Bifurcations of the Atlantic thermohaline circulation in response to changes in the hydrological cycle. Nature 378, 145-149.

Rahmstorf, S., Willebrand, J., 1995. The role of temperature feedback in stabilizing the thermohaline circulation. J. Phys. Oceanogr. 25, 787-805.

Rahmstorf, S., 1996. On the freshwater forcing and transport of the Atlantic thermohaline circulation. Clim. Dyn. 12, 799-811.

Rind, D., Peteet, D., Broecker, W., McIntyre, A., Ruddiman, W., 1986. The impact of cold North Atlantic sea surface temperatures on climate: Implications for the Younger Dryas cooling (11-10Ka). Clim. Dyn. 1, 3-33.

Rind, D., deMenocal, P., Russell, G., Sheth, S., Collins, D., Schmidt, G.A., Teller, J., 2001. Effects of glacial meltwater in the GISS coupled atmosphere-ocean model: Part I: North Atlantic Deep Water response. J Geophys. Res. 106, 27335-27354.

Roeckner, E., Arpe, K., Bengtsson, L., Brinkop, S., Dmenil, L., Esch, M., Kirk, E., Lunkeit, F., Ponater, M., Rockel, B., Sausen, R., Schlese, U., Schubert, S., Windelband, M., 1992. Simulation of the present-day climate with ECHAM model: Impact of model physics and resolution. Tech Rep 93, Hamburg, Max-Planck Inst for Meteorol, Hamburg, Germany, pp 171.

Romanova, V., Prange, M., Lohmann, G., 2004. Stability of the glacial thermohaline circulation and its dependence on the background hydrological cycle. Clim. Dyn. 22, 527-538.

Rooth, C., 1982. Hydrology and ocean circulation. Prog. Oceanogr. 11, 131-149.

Rutberg, R.L., Hemming, S.R., Goldstein, S.L., 2000. Reduced North Atlantic Deep Water flux to the glacial Southern Ocean inferred from neodymium isotope ratios. Nature 405, 935-938.

Sachs, J.P., Anderson, R.F., Lehman, S.J., 2001. Glacial surface temperatures of the southeast Atlantic Ocean. Science 293, 20772079.

Saenko, O., Gregory, J.M., Weaver, A.J., Eby, M., 2002. Distinguishing the influence of heat, freshwater, and momentum fluxes on ocean circulation and climate. Clim. Dyn. 15, 3686-3697.

Sagan, C., Chyba, C., 1997. The Early Faint Sun Paradox: organic shielding of ultraviolet-labile greenhous gases. Science 279, 12217-12221.

Sakai, K., Peltier, W.R., 1997. Dansgaard-Oeschger oscillations in a coupled atmosphere-ocean climate model. J. Climate 10, 949-969.

Sarnthein, M., Gersonde, R., Niebler, S., Pflaumann, U., Spielhagen, R., Thiede, J., Wefer, G. Weinelt, M., 2003. Overview of Glacial Atlantic Mapping (GLAMAP 2000). Paleoceanography 18, 1030, doi:10.1029/2002PA000769.

Schäfer-Neth C., Paul, A., 2001. Circulation of the glacial Atlantic: A synthesis of global and regional modeling. In: The Northern North Atlantic: A Changing Environment, Schaefer P., Ritzrau W., Schlueter M., Thiede J., Springer Berlin, pp 446-462.

Schäfer-Neth, C., Paul A., 2003 The Atlantic Ocean at the last glacial maximum: 1. Objective mapping of the GLAMAP sea-surface conditions. In: Wefer G., Mulitza S., and Ratmeyer V. (eds) The South Atlantic in the Late Quaternary: Material Budget and Current Systems, Springer, Berlin, 531-548.

Schiller, A., Mikolajewicz, U., Voss, R., 1997. The stability of the North Atlantic thermohaline circulation in a coupled ocean-atmosphere general circulation model. Clim. Dyn. 13, 325-347.

Schmidt P.W., G.E. Williams G.E., 1995. The Neoproterozoic climatic paradox; equatorial palaeolatitude for Marinoan Glaciation near sea level in South Australia. Earth Planet. Sci. Lett. 134 1-2, 107-124.

Schmittner, A., Clement, A.C., 2002. Sensitivity of the thermohaline circulation to tropical and high latitude freshwater forcing during the last glacial-interglacial cycle. Paleoceanography 17: 10.1029/2000PA000591.

Schmittner, A., Yoshimori, M., Weaver, A.J., 2002. Instability of glacial climate in a model of the ocean-atmosphere-cryosphere system. Science 295, 1489-1493.

Schulz, M., 2002. On the 1470-year pacing of Dansgaard-Oeschger warm events. Paleoceanography 17, doi 10.1029/2000PA000571.

Schulz, M., Paul, A.,Timmermann, A., 2002. Relaxation oscillators in concert: A framework for climate change at millennial timescales during the late Pleistocene. Geophys. Res. Lett., 29 (24), 10.1029/2002GL016144.

Sellers, W.D., 1969. A climate model based on the energy balance of the earth atmosphere system, J. Appl. Meteorol. 8, 392-400.

Shin, S., Liu, Z., Otto-Bliesner, B.L., Brady, E.C., Kutzbach, J.E., Harrison, S.P., 2003. A simulatiopn of the Last Glacial Maximum climate using the NCAR-CCSM. Clim. Dyn. 20, 127-151.

Sima, A., Paul, A., Schulz, M. 2004. The Younger Dryas - an intrinsic feature of late Pleistocene climate change at millennial timescales. Earth Planet. Sci. Lett. 222, 741-750.

Sohl, L.E., Christie-Blick, N., Kent, D.V., 1999. Paleomagnetic polarity reversals in Marinoan (ca. 600 Ma) glacial deposits of Australia: implications for the duration of low-latitude glaciation in Neoproterozoic time. Geol. Soc. Am. Bull. 111 8, pp. 1120-1139.

Stocker, T.F., Wright, D.G., 1991. Rapid transitions of the ocean's deep circulation induced by changes in surface water fluxes. Nature 351,729-732.

Stocker, T.F., 1998. The seesaw effect. Science 282, 61-62.

Stommel, H., 1961. Thermohaline convection with two stable regimes of flow. Tellus 13, 224-230.

Stone, P.H., Yao, M.S., 2004. The ice-covered Earth instability in a model of intermediate complexity. Clim. Dyn., 10.1007/s00382-004-0408-y.

Valdes, P.J., Hoskins, B.J., 1989. Linear stationary wave simulations of the time-mean climatological flow. J. Atmos. Sci. 46, 2509-2527.

Volbers, A.N.A., Henrich, R., 2002. Present water mass calcium carbonate corrosiveness in the eastern South Atlantic inferred from ultrastructural breakdown of Globigerina bulloides in surface sediments. Marine Geology 186, 471-486.

Weaver, A.J., Eby, M., Fanning, A.F., Wiebe, E.C., 1998. Simulated influence of carbon dioxide, orbital forcing and ice sheets on the climate of the Last Glacial Maximum. Nature 394, 847-853.

Weinelt, M., Sarnthein, M., Pfaumann, U., Schulz, H., Jung, S., Erlenkeuser, H., 1996. Ice-free Nordic Seas during the Last Glacial Maximum? Potential sites of deepwater formation. Palaeoclimates 1, 283-309.

Winguth, A.M.E., Archer, D., Maier-Reimer, E., Mikolajewicz, U., Duplessy J.C., 1999. Sensitivity of paleonutrient tracer distributions and deep-sea circulation to glacial boundary conditions. Palaeoceanography 14, 304-323.

Wyputta, U., McAvaney B.J. 2001. Influence of vegetation changes during the Last Glacial Maximum using the BMRC atmospheric general circulation model. Clim. Dyn. 17, 923-932

Yu, E.F., Francois, R., Bacon, M.P., 1996. Similar rates of modern and last glacial ocean thermohaline circulation inferred from radiochemical data. Nature 379, 689-694.

Zahn, R., 1997. North Atlantic thermohaline circulation during the last glacial period: Evidence for coupling between meltwater events and convective instability. GEOMAR Report 63, Kiel, Germany, 133 pp.

Acknowledgments

This work was carried out at the Geoscience and Physic/Elektrotechnic Department of Bremen University, and was funded by the German Federal Ministry of Education and Research through Climate Research Program DEKLIM - Climate Transitions and Alfred-Wegener-Institut für Polar- und Meeresforschung.

I would like to thank my supervisor, Prof. Dr. Gerrit Lohmann, for giving me an opportunity to work in this project, for his encouragement throughout the work and for his interesting ideas. Many thanks to Prof. Dr. Micheal Schulz for being my reviewer. A special thanks go to Dr. Matthias Prange and Dr. Klaus Grosfeld for the countless number of discussions, for the comments and suggestions that helped to improve my understanding in the research field. Many thanks to Dr. Andreas Manschke for the excellent computer support.

I would like to say thanks to the whole 'palmod' group: Dr. Martin Butzin, Dr. Michai Dima, Dr. André Paul, Dr. Norel Rimbu, Dr. Christian Schäfer-Neth, Dr. Xavier Giraud, Dr. Duane Thresher, Adriana Sima, Leslie Sütterlin, Svetlana Zech, and Lisa Könnecke, the people, who created a cozy working environment and for the coffee breaks full of humor.

Finally, I wish to thank my family for the understanding and the extreme support.

„Berichte zur Polarforschung"
Eine Titelübersicht der Hefte 1 bis 376 (1981 - 2000) erschien zuletzt im Heft 413 der nachfolgenden Reihe „Berichte zur Polar- und Meeresforschung". Ein Verzeichnis aller Hefte beider Reihen sowie eine Zusammenstellung der Abstracts in englischer Sprache finden Sie im Internet unter der Adresse:
http://www.awi-bremerhaven.de/Resources/publications.html

Ab dem Heft-Nr. 377 erscheint die Reihe unter dem Namen:
„Berichte zur Polar- und Meeresforschung"

Heft-Nr. 377/2000 – „Rekrutierungsmuster ausgewählter Wattfauna nach unterschiedlich strengen Wintern" von Matthias Strasser

Heft-Nr. 378/2001 – „Der Transport von Wärme, Wasser und Salz in den Arktischen Ozean", von Boris Cisewski

Heft-Nr. 379/2001 – „Analyse hydrographischer Schnitte mit Satellitenaltimetrie", von Martin Losch

Heft-Nr. 380/2001 – „Die Expeditionen ANTARKTIS XI/1-2 des Forschungsschiffes POLARSTERN 1998/1999", herausgegeben von Eberhard Fahrbach und Saad El Naggar.

Heft-Nr. 381/2001 – „UV-Schutz- und Reparaturmechanismen bei antarktischen Diatomeen und *Phaeocystis antarctica*", von Lieselotte Riegger.

Heft-Nr. 382/2001 – „Age determination in polar Crustacea using the autofluorescent pigment lipofuscin", by Bodil Bluhm.

Heft-Nr. 383/2001 – „Zeitliche und räumliche Verteilung, Habitatspräferenzen und Populationsdynamik benthischer Copepoda Harpacticoida in der Potter Cove (King George Island, Antarktis)", von Gritta Veit-Köhler.

Heft-Nr. 384/2001 – „Beiträge aus geophysikalischen Messungen in Dronning Maud Land, Antarktis, zur Auffindung eines optimalen Bohrpunktes für eine Eiskerntiefbohrung", von Daniel Steinhage.

Heft-Nr. 385/2001 – „Actinium-227 als Tracer für Advektion und Mischung in der Tiefsee", von Walter Geibert.

Heft-Nr. 386/2001 – „Messung von optischen Eigenschaften troposphärischer Aerosole in der Arktis" von Rolf Schumacher.

Heft-Nr. 387/2001 – „Bestimmung des Ozonabbaus in der arktischen und subarktischen Stratosphäre", von Astrid Schulz.

Heft-Nr. 388/2001 – „Russian-German Cooperation SYSTEM LAPTEV SEA 2000: The Expedition LENA 2000", edited by Volker Rachold and Mikhail N. Grigoriev.

Heft-Nr. 389/2001 – „The Expeditions ARKTIS XVI/1 and ARKTIS XVI/2 of the Research Vessel 'Polarstern' in 2000", edited by Gunther Krause and Ursula Schauer.

Heft-Nr. 390/2001 – „Late Quaternary climate variations recorded in North Atlantic deep-sea ostracodes", by Claudia Didié.

Heft-Nr. 391/2001 – „The polar and subpolar North Atlantic during the last five glacial-interglacial cycles", by Jan. P. Helmke.

Heft-Nr. 392/2000 – „Geochemische Untersuchungen an hydrothermal beeinflußten Sedimenten der Bransfield Straße (Antarktis)", von Anke Dählmann.

Heft-Nr. 393/2001 – „The German-Russian Project on Siberian River Run-off (SIRRO): Scientific Cruise Report of the Kara-Sea Expedition 'SIRRO 2000' of RV 'Boris Petrov' and first results", edited by Ruediger Stein and Oleg Stepanets.

Heft-Nr. 394/2001 – „Untersuchung der Photooxidantien Wasserstoffperoxid, Methylhydroperoxid und Formaldehyd in der Troposphäre der Antarktis", von Katja Riedel.

Heft-Nr. 395/2001 – „Role of benthic cnidarians in the energy transfer processes in the Southern Ocean marine ecosystem (Antarctica)", by Covadonga Orejas Saco del Valle.

Heft-Nr. 396/2001 – „Biogeochemistry of Dissolved Carbohydrates in the Arctic", by Ralph Engbrodt.

Heft-Nr. 397/2001 – „Seasonality of marine algae and grazers of an Antarctic rocky intertidal, with emphasis on the role of the limpet *Nacilla concinna* Strebel (Gastropoda: Patellidae)", by Dohong Kim.

Heft-Nr. 398/2001 – „Polare Stratosphärenwolken und mesoskalige Dynamik am Polarwirbelrand", von Marion Müller.

Heft-Nr. 399/2001 – „North Atlantic Deep Water and Antarctic Bottom Water: Their Interaction and Influence on Modes of the Global Ocean Circulation", by Holger Brix.

Heft-Nr. 400/2001 – „The Expeditions ANTARKTIS XVIII/1-2 of the Research Vessel 'Polarstern' in 2000" edited by Victor Smetacek, Ulrich Bathmann, Saad El Naggar.

Heft-Nr. 401/2001 – „Variabilität von CH_2O (Formaldehyd) - untersucht mit Hilfe der solaren Absorptionsspektroskopie und Modellen" von Torsten Albrecht.

Heft-Nr. 402/2001 – „The Expedition ANTARKTIS XVII/3 (EASIZ III) of RV 'Polarstern' in 2000", edited by Wolf E. Arntz and Thomas Brey.

Heft-Nr. 403/2001 – „Mikrohabitatansprüche benthischer Foraminiferen in Sedimenten des Südatlantiks", von Stefanie Schumacher.

Heft-Nr. 404/2002 – „Die Expedition ANTARKTIS XVII/2 des Forschungsschiffes 'Polarstern' 2000", herausgegeben von Jörn Thiede und Hans Oerter.

Heft-Nr. 405/2002 – „Feeding Ecology of the Arctic Ice-Amphipod *Gammarus wilkitzkii*. Physiological, Morphological and Ecological Studies", by Carolin E. Arndt.

Heft-Nr. 406/2002 – „Radiolarienfauna im Ochotskischen Meer - eine aktuopaläontologische Charakterisierung der Biozönose und Taphozönose", von Anja Nimmergut.

Heft-Nr. 407/2002 – „The Expedition ANTARKTIS XVIII/5b of the Research Vessel 'Polarstern' in 2001, edited by Ulrich Bathmann.

Heft-Nr. 408/2002 – „Siedlungsmuster und Wechselbeziehungen von Seepocken (Cirripedia) auf Muschelbänken (*Mytilus edulis* L.) im Wattenmeer", von Christian Buschbaum.